3-D HUMANOID GAIT SIMULATION USING AN OPTIMAL PREDICTIVE CONTROL

A MASTER THESIS SUBMITTED TO
THE GRADUATE SCHOOL OF NATURAL AND APPLIED SCIENCES
OF
MIDDLE EAST TECHNICAL UNIVERSITY

BY

GÖKHAN ÖZYURT

IN PARTIAL FULFILLMENT OF THE REQUIREMENTS
FOR
THE DEGREE OF MASTER OF SCIENCE
IN
MECHANICAL ENGINEERING

AUGUST 2005

Approval of the Graduate School of Natural and Applied Sciences

Prof. Dr. Canan ÖZGEN
Director

I certify that this thesis satisfies all the requirements as a thesis for the degree of Master of Science.

Prof. Dr. Kemal İDER
Head of Department

This is to certify that we have read this thesis and that in our opinion it is fully adequate, in scope and quality, as a thesis for the degree of Master of Science.

Prof. Dr. Kemal ÖZGÖREN
Supervisor

Examining Committee Members

Prof. Dr. Reşit SOYLU	(METU, ME)	
Prof. Dr. Kemal ÖZGÖREN	(METU, ME)	
Prof. Dr. Kemal İDER	(METU, ME)	
Asst. Prof. Dr. Buğra KOKU	(METU, ME)	
Prof. Dr. Kemal LEBLEBİCİOĞLU	(METU, EE)	

I hereby declare that all information in this document has been obtained and presented in accordance with academic rules and ethical conduct. I also declare that, as required by these rules and conduct, I have fully cited and referenced all material and results that are not original to this work.

Name, Last Name : Gökhan ÖZYURT

Signature:

ABSTRACT

3-D HUMANOID GAIT SIMULATION USING AN OPTIMAL PREDICTIVE CONTROL

ÖZYURT, Gökhan

M.S., Department of Mechanical Engineering

Supervisor : Prof. Dr. M. Kemal ÖZGÖREN

August 2005, 129 pages

In this thesis, the walking of a humanoid system is simulated applying an optimal predictive control algorithm. The simulation is built using Matlab and Simulink softwares. Four separate physical models are developed to represent the single support and the double support phases of a full gait cycle. The models are three dimensional and their properties are analogous to the human's. In this connection, the foot models in the double support phases include an additional joint which connects the toe to the foot. The kinematic relationships concerning the physical models are formulated recursively and the dynamic models are obtained using the Newton – Euler formulation.

The computed torque method is utilized at the level of joints. In the double support phase, the redundancy problem is solved by the optimization of the actuating torques. The command accelerations required to control the gait are obtained by applying an optimal predictive control law.

The introduced humanoid walker achieves a sustainable gait by tuning the optimization and prediction parameters. The control algorithm manages the

tracking of the predefined walking pattern with easily realizable joint accelerations. The simulation is capable of producing all the reaction forces, reaction moments and the values of the other variables. During these computations, a three dimensional view of the humanoid walker is animated simultaneously. As a result of this study, a suitable simulation structure is obtained to test and improve the mechanical systems which perform bipedal locomotion. The modular nature of the simulation structure developed in this study allows testing the performance of alternative control laws as well.

Keywords: Bipedal locomotion, humanoid walking, gait simulation, optimal predictive control.

ÖZ

EN İYİ ÖNGÖRÜLÜ BİR DENETİM KULLANILARAK ÜÇ BOYUTLU İNSANSI YÜRÜYÜŞ BENZETİMİ

ÖZYURT, Gökhan

Yüksek Lisans, Makina Mühendisliği Bölümü

Tez Yöneticisi: Prof. Dr. M. Kemal ÖZGÖREN

Ağustos 2005, 129 sayfa

Bu tezde, bir en iyi öngörülü denetim algoritması uygulanarak insansı bir sistemin yürüyüş benzetimi yapılmıştır. Benzetim, Matlab ve Simulink yazılımları kullanılarak oluşturulmuştur. Tam bir yürüyüş döngüsünün tek destek ve çift destek evrelerini temsil etmek amacıyla dört ayrı fiziksel model geliştirilmiştir. Modeller üç boyutludur ve özellikleri insanınkilerle benzer şekildedir. Bu bağlamda, çift destek evrelerindeki ayak modelleri, ayak parmaklarını ayağa bağlayan ilave bir eklem içermektedir. Fiziksel modellerle ilgili kinematik ilişkiler yenilemeli olarak ifade edilmiş ve dinamik modeller Newton – Euler formülasyonu kullanılarak elde edilmiştir.

Eklemler düzeyinde, "hesaplanan tork yöntemi" kullanılmıştır. Çift destek evresindeki artıksıllık sorunu, eyletim torklarının eniyilenmesi ile çözülmüştür. Yürüyüşü denetlemek için gereken komut ivmeleri ise en iyi öngörülü denetim uygulanarak oluşturulmuştur.

Tanıtılan insansı yürüyücü, eniyileme ve öngörme parametreleri ayarlanarak, sürdürelebilir bir yürüyüşü başarmıştır. Denetim algoritması, önceden belirlenmiş

yürüyüş biçiminin rahatça gerçekleştirilebilir eklem ivmeleri ile izlenmesini başarıyla sağlamaktadır. Benzetim, bütün tepki kuvvetlerini, tepki momentlerini ve diğer değişkenlerin değerlerini ortaya koyabilmektedir. Bu çalışmanın bir sonucu olarak, iki bacaklı hareket gerçekleştiren mekanik sistemlerin sınanması ve geliştirilmesi için uygun bir benzetim yapısı elde edilmiştir. Bu çalışmada geliştirilen benzetim yapısının birimsel niteliği, başka denetim kurallarının başarımlarını da sınamaya izin vermektedir.

Anahtar Kelimeler: İki bacaklı hareket, insansı yürüyüş, yürüyüş benzetimi, en iyi öngörülü denetim.

to my parents

ACKNOWLEDGEMENTS

I would like to express my sincere thanks to my supervisor Prof. Dr. M. Kemal Özgören for his helpful guidance, understanding and support throughout the study.

I am grateful to my colleagues Asst. H. Müjde Sarı and Asst. İbrahim Sarı for their encouragements and valuable support whenever I was in need.

The greatest thanks go to my family. This thesis would not have been possible without their patience and endless love.

TABLE OF CONTENTS

LIST OF SYMBOLS

a_i : Length of the ith link (m)

$\bar{a}_{O_i}$: Acceleration vector of the ith link's origin (m/s^2)

$\bar{a}_i$: Acceleration vector of ith link's mass center (m/s^2)

$\bar{b}^{(i)}$: Column matrix representation of a vector ($\vec{b}$) resolved in the ith frame. No superscript means the resolution frame is the earth frame.

c_i : Length between the ith link mass center and the origin of the ith frame (m)

$\hat{C}^{(i,j)}$: Transformation matrix converting components from the jth frame to the ith frame

$F_{i,j}$: Reaction force transmitted to the jth body from the ith body (N)

h : Total height of the humanoid body (m)

$\hat{J}_i$: Centroidal inertia matrix of the ith body expressed in its own frame

$\bar{\ell}_{i,j}$: Position vector from ith link's mass center to jth frame's origin

m : Total mass of the humanoid body (kg)

m_i : Mass of the ith body

$M_{i,j}$: Reaction moment transmitted to the jth body from the ith body (Nm)

$\bar{p}_{O_i}$: Position vector from point O_o (earth frame origin) to point O_i (m)

$\bar{p}_i$: Position vector from point O_o to the ith link's mass center (m)

T_i : Actuating torque at the ith joint (Nm)

$\bar{u}_1$: Column matrix representation of the unit vector along x-direction

$\bar{u}_2$: Column matrix representation of the unit vector along y-direction

$\bar{u}_3$: Column matrix representation of the unit vector along z-direction

$\bar{v}_{O_i}$: Velocity vector of the ith link's origin (m/s)

$\bar{v}_i$: Velocity vector of ith link's mass center (m/s)

$\bar{\alpha}_i$: Angular acceleration of the ith link (rad/s^2)

θ_i : Angular displacement of the ith joint (rad)

$\dot{\theta}_i$: Angular velocity of the ith joint (rad/s)

$\ddot{\theta}_i$: Angular acceleration of the ith joint (rad/s^2)

$\bar{\omega}_i$: Angular velocity of the ith link (rad/s)

$(\vec{\ })$: Vector

$(\bar{\ })$: Column matrix

$(\hat{\ })$: Square matrix

$(\tilde{\ })$: Cross product matrix generated from $(\bar{\ })$.

$(\dot{\ })$: Time derivative

LIST OF TABLES

TABLES

LIST OF FIGURES

FIGURES

CHAPTER 1

INTRODUCTION

1.1 Motivation

Human gait and bipedal locomotion have been investigated by many scientists for decades. Many researchers from different branches of science have carried out numerous studies on this challenging subject. Parallel to these studies, in the last twenty years, many developments have been realized in the bipedal walking machines and several humanoid robots have been manufactured. Both in the design and also in the improvement of these robots, simulation has been widely used as a powerful technique to answer “what if” questions. Also, the gait simulations help us for a better understanding of how humans walk normally or pathologically. Another application area of human gait simulation studies comes out in the design and pre-test stages of lower limb orthotic and prosthetic devices.

Since, it is the basic concept of the thesis, the general definition of simulation should be stated first of all. According to Robert E. Shannon, simulation is defined as the process of designing a model of a real system and conducting experiments with this model for the purpose of understanding the behavior of the system and /or evaluating various strategies for the operation of the system [1].

As expressed in the above definition; a model which resembles the human body is designed at the beginning of a gait simulation study. Then, a control algorithm is incorporated to imitate the human gait. Later, the control algorithm and the model are tested by many simulational experiments. They are modified to accomplish the objectives of the simulation study. Finally, the outcomes are obtained to use for various purposes.

Maybe, the most interesting one of these purposes is the humanoid robot projects. The advances in technology seem to make humanoid robots a part of every day

life. However, it is obvious that the definition of humanoid robots has to be done before talking about them. There are two points of view:

1. The first is to call a robot a ‘humanoid robot’ if he looks humanoid, which means that he has a structured body similar to a human being: An upright body with two legs (preferable with knee joints and the right proportions) and two arms, hands with five fingers and a head on top of all.
2. The other, more academic point of view is to define a robot as ‘humanoid’, if he can act like a human being. The emphasis here lays more on the possible actions of a robot, and less on his outer appearance and structure. If he can achieve typical ‘humanoid’ tasks in a normal ‘humanoid’ environment, he can be called humanoid, no matter how many arm joints he has or how many legs he uses [2].

As it is remarked in the second paragraph, a humanoid robot has to act like a human being. Probably, the most typical human act is the bipedal locomotion. It can be defined as the ability to translate the body by two legs and maintain a rhythmic stepping. Bipedal walking in a humanoid style makes humanoid robots more advantageous than other mobile robots.

The world’s infrastructure has been designed to be human-accessible. Stairways, ladders and devices proportional to average human size are all put in place to make humans’ lives more comfortable [3]. Especially, wheeled robots are helpless in these kinds of situations. For instance, they are unable to step over obstacles or move on uneven surfaces contrary to bipedal walkers.

All these reasons make humanoid gait simulation an attractive and ongoing research area. In the future, by the rapidly growing capabilities of computers, more complicated models are going to be established and new control strategies are going to be performed in these simulations.

1.2 Description and Phases of Human Gait

In order to simulate bipedal walking and applying it on a mechanical model; first, the normal human gait should be examined and its determinants should be

identified. The term, gait, is used as the manner of walking, rather than the motion itself. The human gait is a cyclic motion and the basic components of the gait cycle are stance and swing. The entire period during which the foot is on the ground is the stance phase. The swing phase begins when the foot is lifted from the floor until the heel contacts again with the ground. The normal gait cycle is illustrated in Figure 1.1.

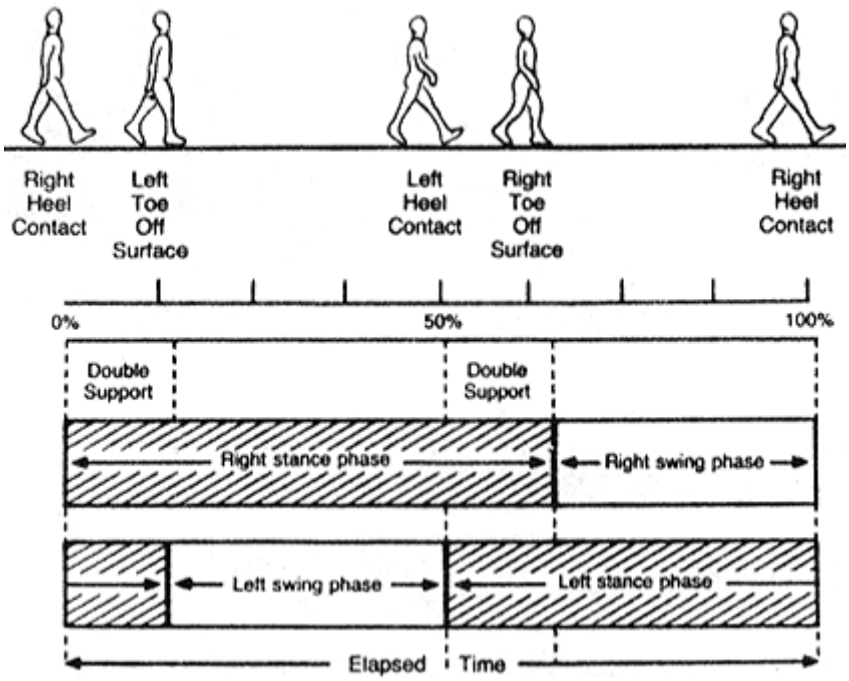

Figure 1.1 The normal gait cycle [4]

The elapsed time to complete a gait cycle is divided into 100 equal parts and the gait events are designated by this percentage. As seen in the Figure 1.1, the right heel contact with the ground is assigned as 0 percent and the next contact of the same heel is assigned as 100 percent. Each gait cycle consists of two periods of the single support phase and two periods of the double support phase. The gait cycle, can be further broken down into eight sub-phases. In Figure 1.2, these sub-phases are illustrated.

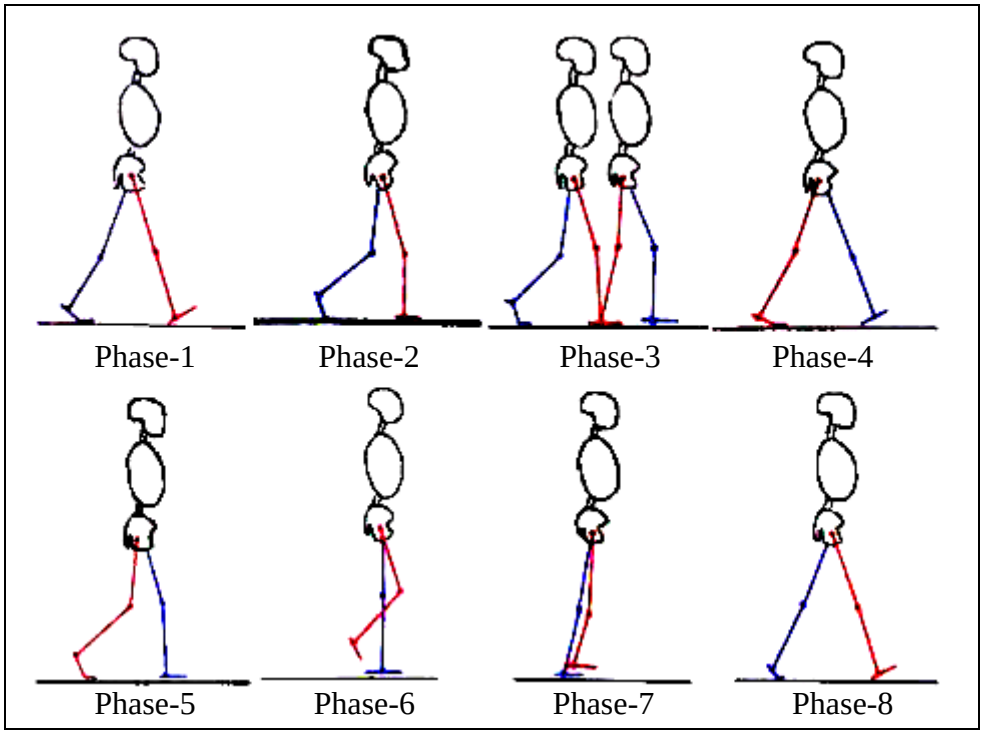

Figure 1.2 The phases of human gait [5]

Phase-1 Initial Contact: This is the moment when the red foot just touches the floor. Normally, the heel is the first part of the foot to touch the ground. The hip is flexed, the knee is extended, and the ankle is dorsiflexed to neutral. Meanwhile, the blue leg is at the end of terminal stance.

Phase-2 Loading Response: This is the double stance period which begins when the foot contacts the floor and continues until the other foot is lifted for swing. Body weight is transferred onto the red leg. The blue leg is in the pre-swing phase.

Phase-3 Mid Stance: This phase is the first half of the single support interval. It begins with the lifting of the blue foot and continues until body weight is aligned over the supporting foot. The red leg advances over the red foot by ankle dorsiflexion while the hip and knee extend. The blue leg advances in its mid-swing phase.

Phase-4 Terminal Stance: This part of the human gait begins when the red heel rises and continues until the heel of the blue foot hits the ground. Body weight progresses beyond the red foot as increased hip extension puts the leg in a more trailing position.

Phase-5 Pre-Swing: This is the second double stance interval in the gait cycle. It begins with the initial contact of the blue foot and ends with red toe-off. Ground contact by the blue leg causes the red leg to increase ankle plantar flexion, increase knee flexion, and decrease hip extension. Transfer of body weight from ipsilateral to opposite limb takes place.

Phase-6 Initial Swing: It begins when the foot is lifted from the floor and ends when the swinging foot is opposite the stance foot. The red leg is advanced by increased hip flexion and increased knee flexion. The ankle only partially dorsiflexes to ensure ground clearance. The blue leg is in mid-stance.

Phase-7 Mid Swing: This phase continues from the end point of the initial swing and continues until the swinging limb is in front of the body and the tibia is vertical. Advancement of the red leg is accomplished by further hip flexion. The knee is allowed to extend in response to gravity while the ankle continues dorsiflexion to neutral. The blue leg is in late mid-stance.

Phase-8 Terminal Swing: It begins when the tibia is vertical and ends when the foot touches the floor. Limb advancement is completed by knee extension. The hip maintains its flexion and the ankle remains dorsiflexed to neutral [5].

1.3 Previous Studies on Humanoid Gait

In many universities and research centers, scientists have been involved in the humanoid gait subject. While, some of them have studied on a specific part of the problem, some have introduced full simulations and even produced prototypes of humanoid walkers. Therefore, this survey covers not only the humanoid gait simulation studies but also the more specific ones which are related or contributing to the area of humanoid gait. In addition, some prominent humanoid robots which can realize walking in a human like style are also presented.

In the literature, the simulations of normal human gait or the simulations of bipedal robots differ by many attributes they have. Some of these attributes are the models, the methods or the goals of the simulations. The number of segments which constitute the simulation model, the degree of freedom and the complexity increases according to the resemblance to the ones of a human being. In this sense, researchers have tried many alternatives. Skelly and Chizeck presented a 3-dimensional computer model of sustained bipedal walking. In this study, it is intended to be used as a development tool for walking controllers. The direct dynamic simulation has 8 segments, 19 degrees of freedom and is driven by prescribed joint moment and stiffness trajectories. Limited feedback in the form of a proportional-derivative controller provides upper body stability and allows walking to be sustained indefinitely. The foot is approximated by an ellipsoid and foot-to-floor contact is modeled by a spring and damper activated by the penetration of the foot into the floor [6].

Figure 1.3 Simulation of bipedal walking by M.M.Skelly and C.J.Chizeck

In another study, Gilchrist and Winter used a nine-segment 3-dimensional model, including a two part foot. In this computer simulation, the resultant joint moments of a gait analysis were used as driving moments. The system description, initial conditions and driving moments were taken from an inverse dynamics analysis of

a normal walking trial. Torsional, linear springs and dampers were used at the hip joints to keep the trunk vertical. The knee and ankle joints were also limited to prevent nonphysiological motion. Dampers at other joints were required to ensure a smooth and realistic motion [7].

In one of the gait simulations, the model was built in ADAMS environment. For the gait stabilization, a simple closed loop control algorithm was introduced. The net torques (generated in the way that enables realization of the gait patterns) are applied to a mechanical system and the direct problem of dynamics is solved [8].

Figure 1.4 Superimposed frames from stable walk animation [8]

In order to reduce the complexity of the biped simulations, 2-dimensional models are preferred instead of 3-dimensional ones [9], [10], [11]. In the University of New Hampshire a biped simulator, called WALK, was developed incorporating a model of this kind. This simulator is designed to facilitate the evaluation of bipedal walking algorithms. Also, a neural network algorithm was applied on the model [12].

In some of the studies, the muscles and the skeleton of human being was included in the simulation models. Günther and Ruder proposed a 2-dimensional, eleven-segment musculoskeletal model of the human body. Human walking was synthesized by numerical integration of the coupled muscle-tendon and rigid body dynamics [13].

In another study, the body was modeled as a 10-segment, 23 degree-of-freedom (dof) articulated linkage. As in the above study, each leg was actuated by 24 muscles. The head, arms, and torso (HAT), was modeled as a single rigid body and actuated by six stomach and back muscles. Each foot was modeled using two segments: a hind foot and the toes. The interaction between each foot and the ground was modeled by using five spring-damper units distributed under the sole of the foot [14]. The foot model and particularly the interaction between the ground and the foot are the key features of the gait simulations. The performance of the simulations and the closeness of the results to the ideal are directly related to these features. Moreover, they determine the shape of transitions between the phases of gait.

As in the present thesis study; some researchers have applied optimal control algorithms on the simulations. This is performed in several ways like optimizing the gait pattern, energy or stability [15]. In this connection; Granata, Brogan and Sheth proposed a bipedal walking control algorithm that simultaneously solves for movement trajectory and joint torques. In the technique they used, a constraint-based space-time optimization algorithm was utilized to compute the optimal movements and torques [16].

Another example of this kind of studies was achieved by Denk and Schmidt. In this study, corresponding control torques allowing straight ahead walking with pre–swing, swing, and heel–contact phases are derived by dynamic optimization using a direct collocation approach. The computed torques minimize an energy based, mixed performance index. Zero moment point (ZMP) and friction conditions at the feet ensuring postural stability of the biped, as well as bounds on the joint angles and on the control torques, are treated as constraints. The resulting biped motions are dynamically stable and the overall motion behavior is remarkably close to that of humans [17].

However, some control algorithms were insufficient. In the study of Nicholls, various simple control techniques were tried. Proportional control and proportional plus integral control systems were implemented to modify the trunk motion in order to compensate lower limb movement. Simple control systems

allowed the robot to balance sufficiently while standing. However, these control systems were insufficient to stabilize the robot while walking [18].

In some other studies, not the full gait cycle but a period of it (e.g. the single support phase) or a special case is discussed. The study of Potkonjak and Vukobratovic is an example of these studies. They suggest a deductive approach that starts by considering a completely general problem. The general methodology is explained and the feasibility is supported by applying the general model to two illustrative examples: first, a well-known situation, the single-support phase of a biped motion and second, a completely different problem, gymnastic exercise on a horizontal bar [19].

Especially, in the last decade, by the financial support of industry, successful humanoid walkers were produced after the simulation studies. The first two legged robot of practical size was developed by Kato and et al. [20]. Since then, much research in this field has improved the performance of walking robots. ASIMO (Advanced Step in Innovative MObility) is one of the most sophisticated bipedal robots in the world [21]. It is the closest robot yet, to replicate the natural walking motion of humans. ASIMO can walk flexibly under real time conditions by Honda's "i-walk" (intelligent walk) technology. The company developed its first robot to walk on two legs in 1986.

Figure 1.5 ASIMO stepping down the stairs

Another humanoid walking robot, which is as talented as ASIMO, is HRP-2. Hirukawa and co-workers developed a software platform, called OpenHRP, for humanoid robotics which consists of a dynamic simulator and motion control library, for humanoid robots. Using OpenHRP and humanoid robots HRP-1S and HRP-2P, they showed the comparisons between the simulations and experiments at various aspects [22].

Figure 1.6 HRP-2 walking

In the MIT Leg Laboratory, a seven link planar bipedal robot, called Spring Flamingo was controlled to walk using a simple algorithm. In this study, a kneecap is used to prevent the leg from inverting and a compliant ankle is used to naturally transfer the center of pressure along the foot and help in toe off [23].

As an important feature of the present thesis, the addition of toe joints to the models extends the capabilities humanoid walkers. Hence, more realistic simulations are accomplished. Effectiveness of toe joints is discussed in [24]. Feet with toe joints are developed for humanoid H6. An experiment of the whole-body action in which knees are contacting to the ground is carried out to show the usefulness of toe joints for such actions. Then walking pattern generation system

is extended to use toe joints. Using this extended system, maximum speed of knee joints can be reduced at the same walking speed, and 80% faster walking speed is achieved on humanoid H6.

Both in the humanoid robot studies and in the other research areas related to bipedal locomotion, in order to identify the characteristics of the motion and to realize a stable walking, several methods are proposed in the last decades. Also, these methods serve as benchmarks for gait patterns. One of them is the ZMP (Zero Moment Point) method. This point is first named by Borelli in 1680 as the ground support point [25]. Vukobratovic and Juricic renamed Borelli's support point, the Zero Moment Point and discussed its applicability for legged machine control. They defined the ZMP as the "point of resulting reaction forces at the contact surface between the extremity and the ground" [26]. The ZMP may also be defined as the point on the ground at which the net moment due to inertial and gravitational forces has no component along the horizontal axes [21].

Another method is the application of the FRI (Foot Rotation Indicator). The FRI point was introduced by Goswami in 1999. It is a point on the foot-ground contact surface, within or outside the support base, where the net ground reaction force would have to act to achieve a zero moment condition about the foot with respect to the FRI point itself [27]. Certainly, these methods are helpful for the identification of biomechanical movement strategies. Therefore, the development of these methods is going to contribute to the control systems of the legged robots.

1.4 The Objective and Scope of the Thesis

The aim of the present study is to investigate the bipedal locomotion on a 3-dimensional mechanical model that imitates the lower limbs of a human being. For this reason, a computer simulation is developed which includes a control algorithm to achieve a desired sustainable gait. In the control algorithm, mainly, two methods are employed. These methods are the optimization and the prediction. The simulation covers both the single and the double support phases of a full gait cycle. These phases are also divided into two subphases for the left

and the right foot. In order to enhance the performance of the simulated humanoid walker, the foot is composed of two segments which are connected by a toe joint. The ease of modification of the simulation is determined as one of the objectives of the study. Therefore, a suitable software environment is selected to access each part of the simulation easily. By this way, the progress of the study in the future and upgrade of the simulation happen to be possible.

In chapter 2, four mechanical models, designed to simulate each phase of humanoid walking is presented. The dimensions and the inertial properties of the links are given. The general conventions used in the study are also declared in this chapter.

Chapter 3 covers all the kinematic and dynamic equations used in the simulations. A recursive formulation is used to obtain the position, velocity and acceleration expressions of each link. In addition to these expressions, the constraint equations correspond to the double support phase models are emphasized. The dynamic equations of the models are derived using the Newton – Euler formulation. The direct dynamic solution procedure of these equations is expressed. The computed torque control method is utilized to find the necessary actuating torques for the realization of desired joint accelerations. Because of the redundancy in the double support phase, a special optimization process accompanies the computed torque control algorithms of the double support phase simulation models. In this simulation study, an optimal predictive control algorithm is applied to humanoid gait. Application of this algorithm distinguishes the present study from the previous ones. The optimal predictive control algorithms for both the double and the single support phase models are also presented in chapter 3.

In chapter 4, the software environment which the simulation is built in and the simulation configuration parameters are introduced. Matlab®, which is a very useful technical computing software and Simulink® are used throughout the simulation study. In this chapter, the subsystems which constitute the simulation model and the operation principles of these subsystems are mentioned. Also, chapter 4 includes the generation of desired walking paths.

In chapter 5, the results of the simulations are presented. The torque values which provide the locomotion of the humanoid walker and the optimization weighting factors assigned in the optimal predictive control parts are discussed. The possible ways of improving the results are also stated in this chapter.

In chapter 6, the recommendations for future work and the summary of the study are given.

CHAPTER 2

PHYSICAL MODELING OF A HUMANOID WALKING SYSTEM

In this chapter, the physical characteristics of the simulation models are presented. Two different linkage systems are proposed demonstrating different phases of human gait. One of these systems is designed for the single support phase and the other one for the double support phase. Each system is used twice during a full gait cycle, once for the right leg and once for the left leg. The common features of the models are given below and details of them are explained in the consequent sections.

i. The models are three dimensional.

   Although, it were possible to investigate the motions in three separate orthogonal planes and considering these motions independent of each other, this method is not appropriated. In the study, the motions are examined regarding the true three dimensional space.

ii. All the joints used in the models are revolute joints and have actuating torques. For modeling the toe, one joint; for the ankle, two joints; for the knee, one joint and for the hip, two joints are used.

iii. At the joints, the frictional and damping effects are assumed to be negligible.

iv. The HAT (head + arms + trunk) is assumed to be rigidly connected to pelvis and they form a single link (body-1).

v. Each model consists of 6 rigid bodies:

   Left foot flat single support model: Body-6, 4, 1, 5, 7 and 11.
   Right foot flat single support model: Body-7, 5, 1, 4, 6 and 10.
   Left foot flat double support model: Body-6, 4, 1, 5, 7 and 11.
   Right foot flat double support model: Body-7, 5, 1, 4, 6 and 10.

The assignment of these bodies to the limbs is given in Table 2.1.

Table 2.1 The assignment of the model segments

Body-1:	HAT + pelvis		
Body-4:	Left thigh	Body-5:	Right thigh
Body-6:	Left shank	Body-7:	Right shank
Body-10:	Left foot	Body-11:	Right foot
Body-12:	Left toe	Body-13:	Right toe

vi. The joint angles are defined in such a way that they rotate about either x-direction or y-direction. Therefore, the popular Denavit – Hartenberg convention is not used in this study. Mass centers, body frames and general appearance of the model are illustrated in Figure 2.1. In this figure and in the other parts of the study,

$\vec{u}_1$ is the unit vector along x-axis,

$\vec{u}_2$ is the unit vector along y-axis,

$\vec{u}_3$ is the unit vector along z-axis.

vii. The body frames of the models are located at the joints at the proximal end of the links and their orientations are the same when the joint angles are zero. This assent is shown in Figure 2.2. The proximal means near to the mass center of body-1 and the distal means away from the mass center of body-1.

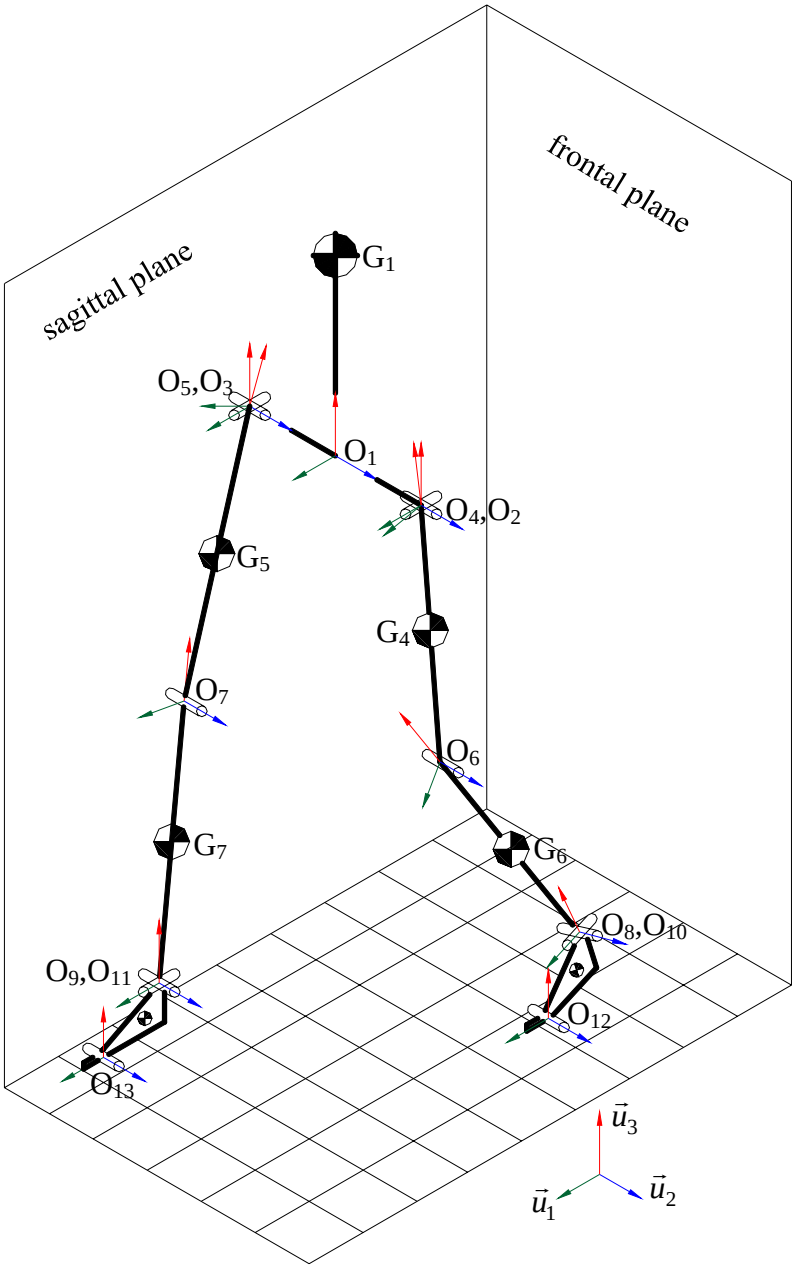

Figure 2.1 General schematic appearance of the humanoid walker

As it may have been noticed, the numbers 2, 3, 8 and 9 are not associated with body names. Because, the links 2, 3, 8 and 9 have no mass and they are virtual in fact. For example, the right hip joint is modeled as a Hooke's joint composed of two perpendicular revolute joints. Proximal one of them is along the x-direction

and distal one is along the y-direction. By assuming a virtual link of zero length (link-3) between these revolute joints, the kinematic and kinetic relations are expressed easily and simply in the analysis. This assumption is illustrated on Figure 2.2.

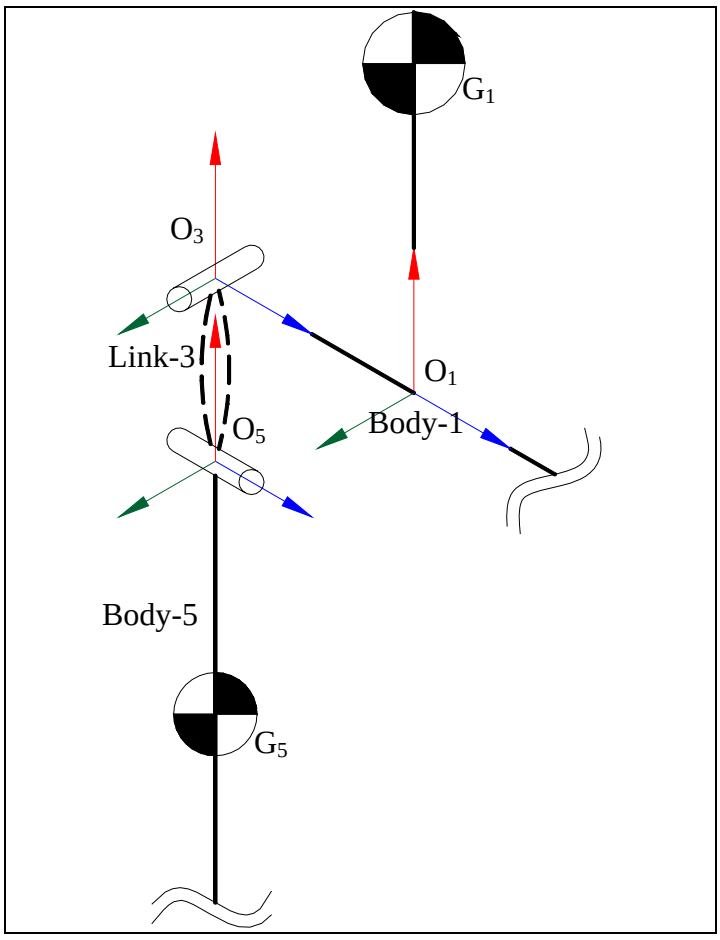

Figure 2.2 Right hip joint assembly

Also, throughout the study, odd numbers are employed for the right and even numbers are employed for the left leg segments, variables and parameters.

In order to define the joint variables, it is preferred to use the symbols and indices indicated in Table 2.2. Further, the positive sign conventions of these angles according to the right hand rule are explained in Table 2.3 and illustrated in Figure 2.3a and Figure 2.3b.

Table 2.2 The assignment of the joint variables

θ_2 : left hip roll angle	θ_3 : right hip roll angle
θ_4 : left hip pitch angle	θ_5 : right hip pitch angle
θ_6 : left knee angle	θ_7 : right knee angle
θ_8 : left ankle pitch angle	θ_9 : right ankle pitch angle
θ_{10} : left ankle roll angle	θ_{11} : right ankle roll angle
θ_{12} : left toe angle	θ_{13} : right toe angle

Table 2.3 The joint angle convention

θ_2	rotates	$\bar{u}_3^{(1)}$	into	$\bar{u}_3^{(2)}$	about	$\bar{u}_1^{(1)} = \bar{u}_1^{(2)}$
θ_3		$\bar{u}_3^{(1)}$		$\bar{u}_3^{(3)}$		$\bar{u}_1^{(1)} = \bar{u}_1^{(3)}$
θ_4		$\bar{u}_3^{(2)}$		$\bar{u}_3^{(4)}$		$\bar{u}_2^{(2)} = \bar{u}_2^{(4)}$
θ_5		$\bar{u}_3^{(3)}$		$\bar{u}_3^{(5)}$		$\bar{u}_2^{(3)} = \bar{u}_2^{(5)}$
θ_6		$\bar{u}_3^{(4)}$		$\bar{u}_3^{(6)}$		$\bar{u}_2^{(4)} = \bar{u}_2^{(6)}$
θ_7		$\bar{u}_3^{(5)}$		$\bar{u}_3^{(7)}$		$\bar{u}_2^{(5)} = \bar{u}_2^{(7)}$
θ_8		$\bar{u}_3^{(6)}$		$\bar{u}_3^{(8)}$		$\bar{u}_2^{(6)} = \bar{u}_2^{(8)}$
θ_9		$\bar{u}_3^{(7)}$		$\bar{u}_3^{(9)}$		$\bar{u}_2^{(7)} = \bar{u}_2^{(9)}$
θ_{10}		$\bar{u}_3^{(8)}$		$\bar{u}_3^{(10)}$		$\bar{u}_1^{(8)} = \bar{u}_1^{(10)}$
θ_{11}		$\bar{u}_3^{(9)}$		$\bar{u}_3^{(11)}$		$\bar{u}_1^{(9)} = \bar{u}_1^{(11)}$
θ_{12}		$\bar{u}_3^{(10)}$		$\bar{u}_3^{(12)}$		$\bar{u}_2^{(10)} = \bar{u}_2^{(12)}$
θ_{13}		$\bar{u}_3^{(11)}$		$\bar{u}_3^{(13)}$		$\bar{u}_2^{(11)} = \bar{u}_2^{(13)}$

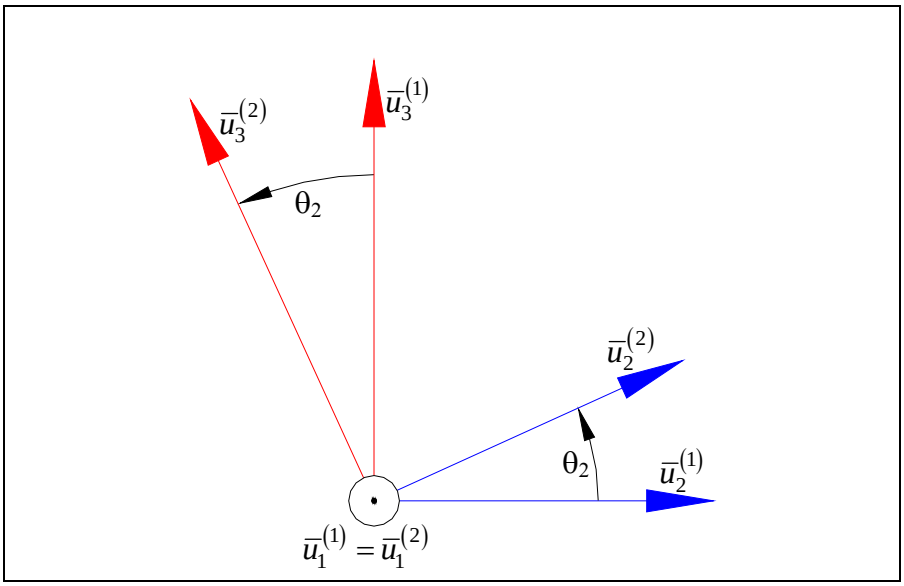

Figure 2.3a Positive sign convention for first axis rotations

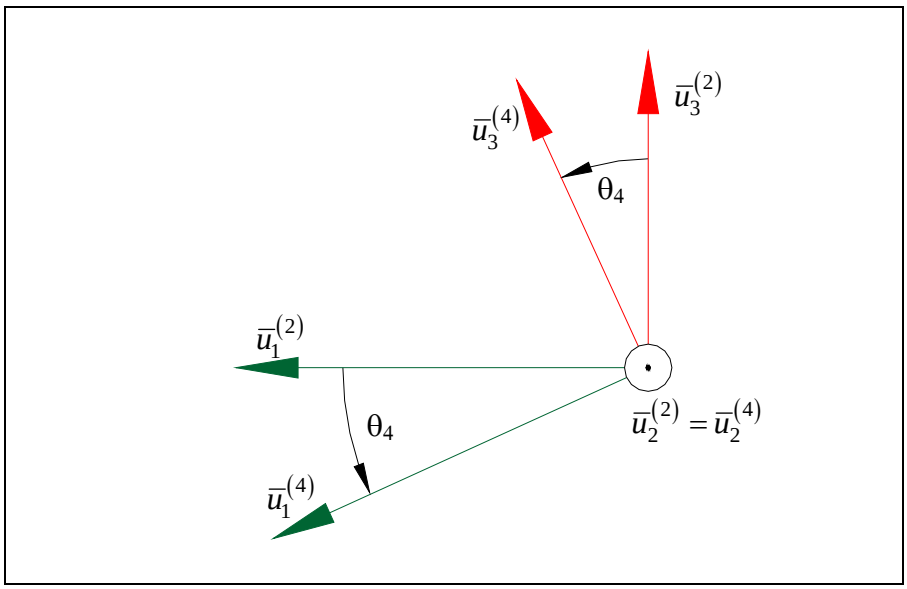

Figure 2.3b Positive sign convention for second axis rotations

At each joint between two links, there exist a total of three reaction forces, two reaction moments and one actuating torque. The actuating torque at a joint has the same index number with the joint variable of that joint. In Figure 2.4, the actuating torques, directed positively according to the right hand rule, are indicated on the proposed model, when the joint angles are zero.

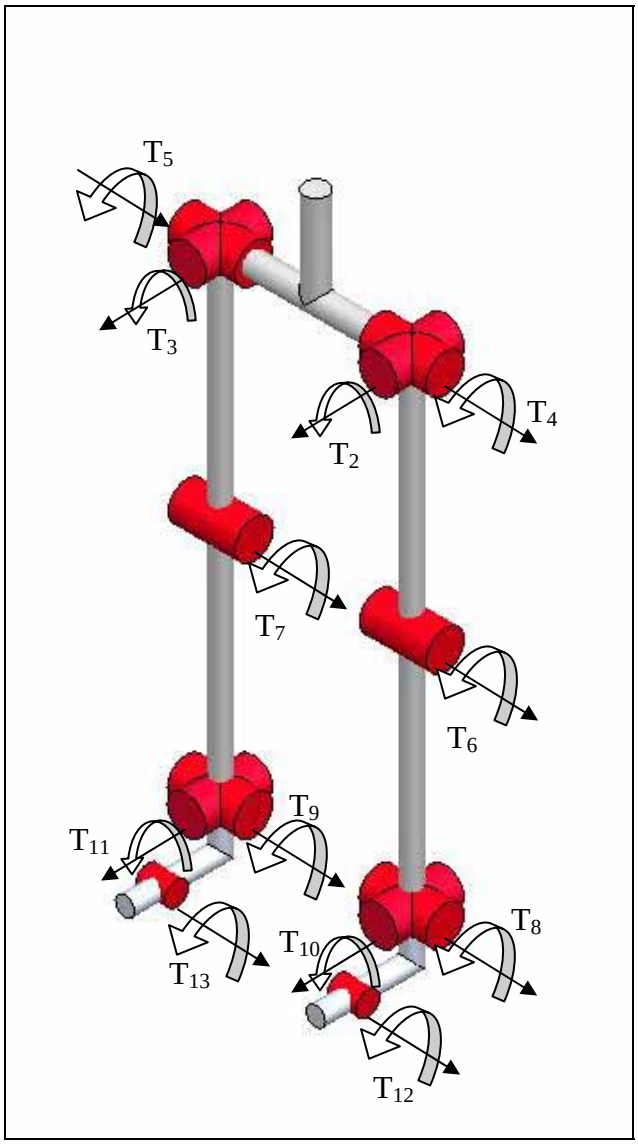

Figure 2.4 The actuating torques

2.1 Definitions of Model Parameters

For kinematic and kinetic analyses, some parameters like mass, inertia tensor components, link dimensions, etc. are required. These parameters determine the dynamic characteristics of a mechanical system. According to anthropometric data [29], these parameters are expressed as a fraction of body height and mass. In this study, to simulate a humanoid walking in a resemblance as close as possible to an actual human being, these fractions which define the aspects of the

models are used without any variation. This is provided by modeling the human legs in three dimensional space as actually it is.

The toes are assumed to be massless, because they never move individually. In the swing phase, the toe moves together with the foot and in the stance phase, it is assumed to be fixed on the ground. Moreover, the toes are too light compared to the other segments. So, their masses are incorporated to their feet.

In this study, the gait of a humanoid walker that has a mass of 56 kg and a height of 1.60 m is simulated. However, by initializing different values for total body mass and height at the beginning of simulations, the other parameters can be automatically changed. The parameters for the humanoid walker investigated in this study are presented in the tables 2.4, 2.5, 2.6 and shown in Figure 2.7.

Table 2.4 The mass of the bodies

$m = 56$ kg	
$m_1 = 0.678m = 37.968$ kg	
$m_4 = 0.1m = 5.6$ kg	$m_5 = 0.1m = 5.6$ kg
$m_6 = 0.0465m = 2.604$ kg	$m_7 = 0.0465m = 2.604$ kg
$m_{10} = 0.0145m = 0.812$ kg	$m_{11} = 0.0145m = 0.812$ kg

It is possible to consider that these values include the mass of the electric motors, batteries and other equipments which constitute a real humanoid walker.

The inertia tensor components of the bodies were calculated by using a commercial CAD software, Solidworks®. The solid models of each body were designed keeping their original mass and lengths constant. The solid model of body-1 looks like a rectangular box. The legs were modeled as cones and the foot has a triangular shape. All the inertia tensors were taken at the center of mass to use in Euler equations. In Table 2.5, the inertia tensor components are given.

Table 2.5 The inertia tensor components

Body-1	$I_{xx} = 1.5139$ $I_{yy} = 1.2851$ $I_{zz} = 0.3594$		
Body-4	$I_{xx} = 0.07679$ $I_{yy} = 0.07679$ $I_{zz} = 0.00977$	Body-5	$I_{xx} = 0.07679$ $I_{yy} = 0.07679$ $I_{zz} = 0.00977$
Body-6	$I_{xx} = 0.03465$ $I_{yy} = 0.03465$ $I_{zz} = 0.00208$	Body-7	$I_{xx} = 0.03465$ $I_{yy} = 0.03465$ $I_{zz} = 0.00208$
Body-10	$I_{xx} = 0.00049$ $I_{yy} = 0.00361$ $I_{zz} = 0.00384$	Body-11	$I_{xx} = 0.00049$ $I_{yy} = 0.00361$ $I_{zz} = 0.00384$
All values are in $kg.m^2$			

Table 2.6 The lengths of the bodies

$h = 1.60$ m	
$a_1 = 0.191h = 0.3056$ m	
$a_1^l = 0.5a_1 = 0.1528$ m	$a_1^r = 0.5a_1 = 0.1528$ m
$a_4 = 0.245h = 0.392$ m	$a_5 = 0.245h = 0.392$ m
$a_6 = 0.246h = 0.3936$ m	$a_7 = 0.246h = 0.3936$ m
$c_1 = 0.5a_1 = 0.1528$ m	
$c_4 = 0.5a_4 = 0.196$ m	$c_5 = 0.5a_5 = 0.196$ m
$c_6 = 0.5a_6 = 0.1968$ m	$c_7 = 0.5a_7 = 0.1968$ m

There are two different foot models used in the simulations. When the foot swings in the air during the single support phase, it's modeled as a single body.

On the other hand, during the double support phase, foot model is composed of two parts, connected to each other by a revolute joint. In Table 2.7, the dimensions related to the foot models are given.

Table 2.7 The lengths associated with the feet

$a_{10} = 0.039h = 0.0624$ m	$a_{11} = 0.039h = 0.0624$ m
$d_{10} = 0.152h = 0.2432$ m	$d_{11} = 0.152h = 0.2432$ m
$c_{10x} = 0.333d_{10} = 0.081$ m	$c_{11x} = 0.333d_{10} = 0.081$ m
$c_{10y} = 0$ m	$c_{11y} = 0$ m
$c_{10z} = 0.666a_{10} = 0.0415$ m	$c_{11z} = 0.666a_{10} = 0.0415$ m

2.2 Single Support Phase

The first phase of the gait cycle is the single support phase in which the body moves forward on one foot while the other foot swings in the air. For the right foot flat period, this phase starts with the left toe-off and ends with the left heel strike. During this phase, the left foot moves upward by a certain amount for ground clearance and it also moves a little sideway to avoid collision with the right leg segments. At the end of this phase, the left foot takes back its starting position in the y and z directions, but now it is in front of the body. In Figure 2.5, the model of this phase is shown when the right foot is on the ground and the left foot is moving forward just after the “right foot flat double support phase”.

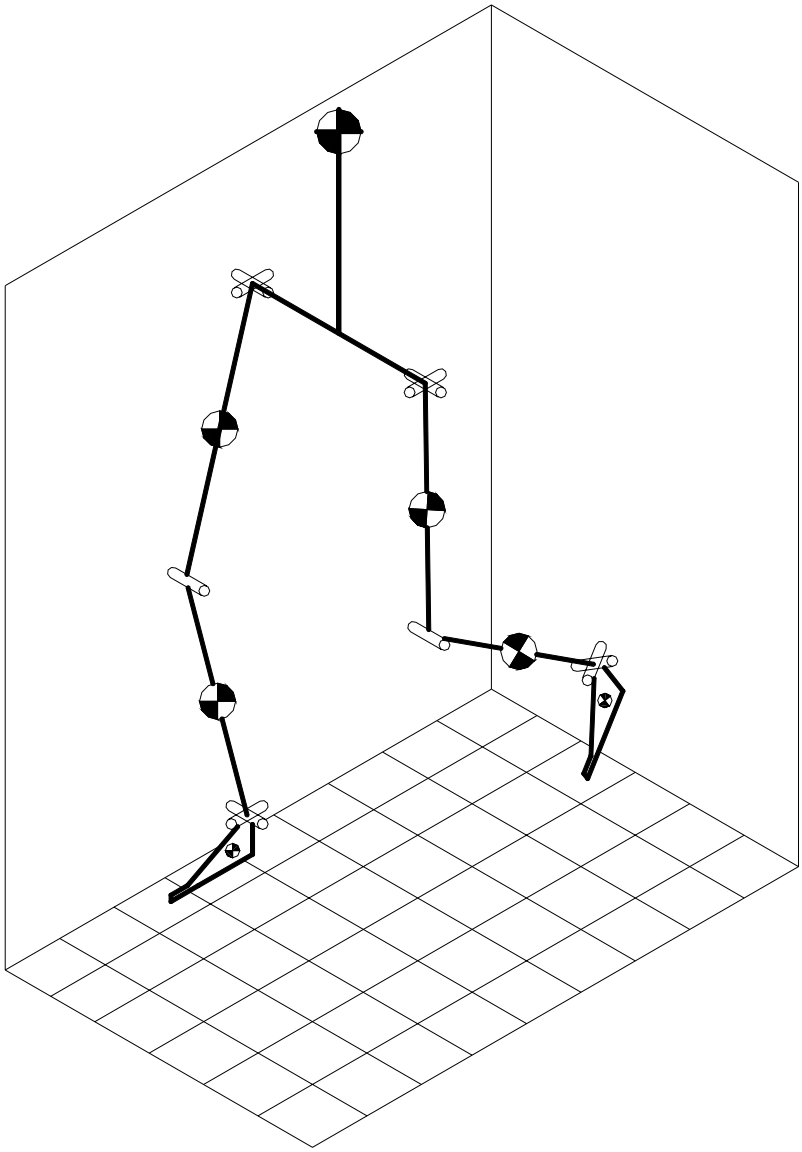

Figure 2.5 The right foot flat single support phase model

This model is composed of six bodies. These are the right shank, the right thigh, the HAT, the left thigh, the left shank and the left foot. The major factor which distinguishes this phase from the double support phase is the absence of the toe joints. The single support phase model forms an open kinematic chain, starting from the right ankle and ending at the heel point of the left foot.

In the model of this phase, the bodies are actuated by ten joint torques.

During the right foot flat single support phase, the right foot sole is flat on the ground and it is assumed to be fixed. For this reason, neither body-13 nor body-11 have any effect on this phase of gait. However, the left foot is important in the dynamics of walking. It is modeled as a single body attached to the left shank (body-6) by the ankle joint assembly and the toe is neglected. The left foot model in the right foot flat single support phase is shown in Figure 2.6.

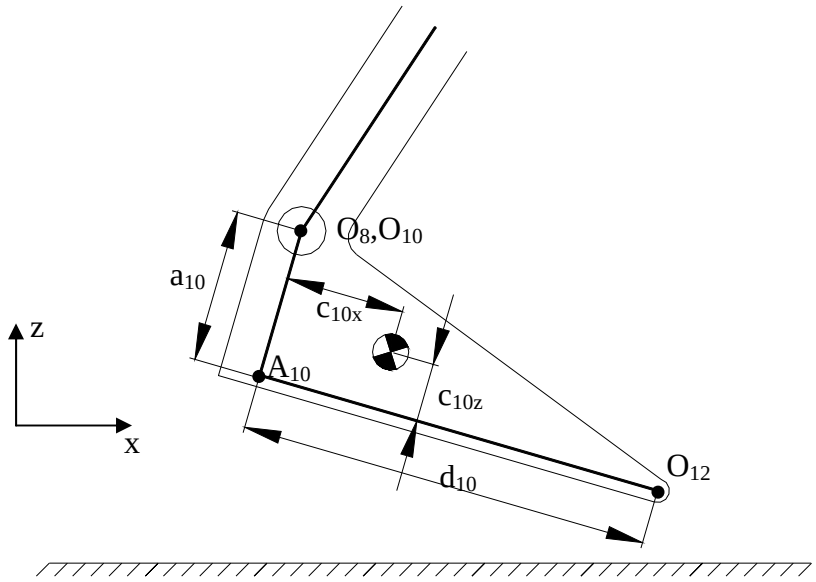

Figure 2.6 The left foot model in right foot flat single support phase

2.3 Double Support Phase

The second phase of the gait cycle is the double support phase. This phase starts at the instant when both feet get in contact with the ground flatly. After this initiation, while one foot rotates around its toe joint, the collateral one stays at rest. Actually, double support phase starts with the heel strike of swinging leg. Although, the foot rotates for a short while around the contact point on the heel, this period is not modeled. Because, after the heel strike, the foot becomes flat in an indeed negligibly short time and modeling the system in this short period requires a more complicated third kind of linkage representation, which is not worth the effort.

In a gait cycle, the double support phase occurs twice, once for the right leg and once for the left leg. The right and left legs only exchange their roles but they perform the same motions and can be simulated by the same model. In accordance with these explanations, the model of “the right foot flat double support phase” is illustrated in Figure 2.7.

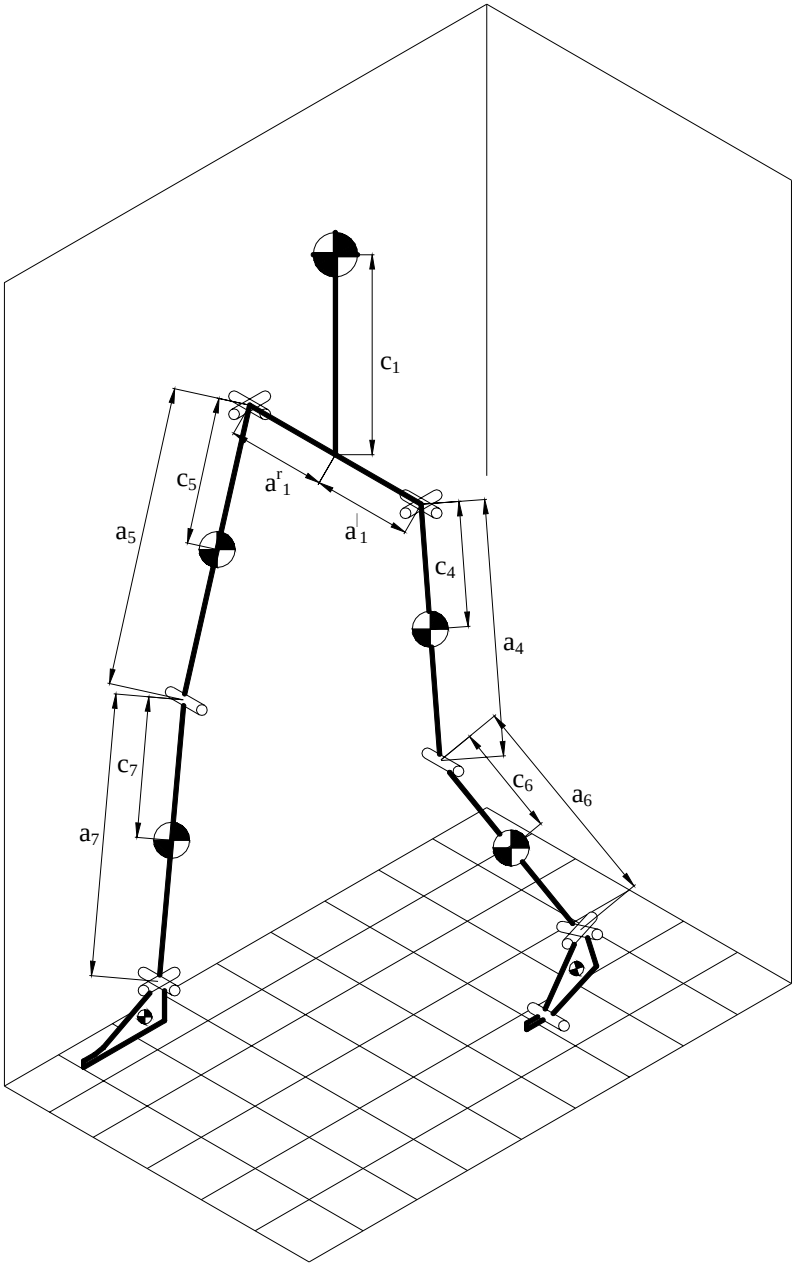

Figure 2.7 The right foot flat double support phase model

This model has 6 bodies: the right shank, the right thigh, HAT, the left thigh, the left shank, and the left foot. These bodies are driven by eleven torques at the joints.

Since this model is for the “right foot flat double support phase”, the right toe joint (with variable θ_{13}) is not used. It’s obvious that if it were the “left-foot flat double support phase”, then the left toe joint (with variable θ_{12}) would become unnecessary.

In this model, the left foot is connected to the ground by its toe joint and the right foot is fixed to the ground with its whole body. Therefore, the right leg moves on the right ankle, while, the left leg moves on the the left toe joint. Figure 2.8 illustrates the left foot model for the “right foot flat double support phase”.

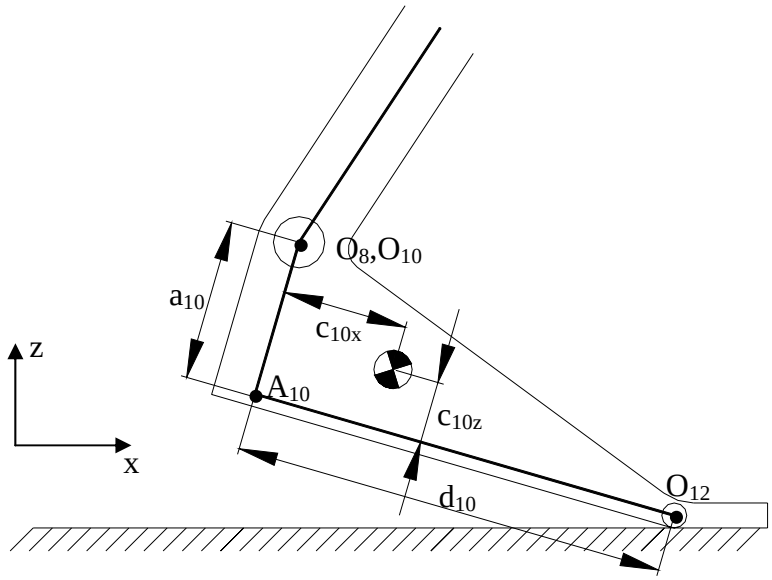

Figure 2.8 The left foot model in right foot flat double support phase

The system in the double support phase has eleven revolute joints but only five degrees of freedom in space. The reason of this deficiency in DOF is the closed kinematic chain formed due to both feet being grounded. In the following section, this fact is handled in detail.

2.3.1 Kinematic Constraints

During the double support phase, both feet are on the ground. This forms a closed linkage system. Since, the DOF of the three-dimensional space is six; there must be six scalar constraint equations which cause this loop closure. There are two ways to write the position of the origin O_1 of the body-1 frame with respect to a point on the ground. For instance, during the "right foot flat double support phase", the position of the origin O_1 can be first derived by starting from the right heel point (A_{11}) and second, from the left toe joint origin (O_{12}). These two points are stationary on the ground as it is mentioned before. Moreover, the orientation of body-1 with respect to the earth frame must be the same in whichever the way it is expressed. Thus, the six scalar constraint equations of the double support phase in the position level are obtained as described below.

In both of the double support phase models, considering the position of the origin O_1 , the three of the constraints in vector form are:

$$\overline{p}^{r}_{O_1} = \overline{p}^{l}_{O_1} \tag{2.1}$$

In the "right foot flat double suppport phase":

$$\overline{p}^{r}_{O_1} = \overline{p}_{A_{11}} + a_{11}\overline{u}_3 + a_7\hat{C}^{(11,7)}\overline{u}_3 + a_5\hat{C}^{(11,5)}\overline{u}_3 + a^r_1\hat{C}^{(11,1)}\overline{u}_2$$
$$\overline{p}^{l}_{O_1} = \overline{p}_{O_{12}} + a_{10}\hat{C}^{(12,10)}\overline{u}_3 + d_{10}\hat{C}^{(12,10)}\overline{u}_1 + a_6\hat{C}^{(12,6)}\overline{u}_3 + a_4\hat{C}^{(12,4)}\overline{u}_3 + a^l_1\hat{C}^{(12,1)}\overline{u}_2$$

and in the "left foot flat double support phase":

$$\overline{p}^{r}_{O_1} = \overline{p}_{O_{13}} + a_{11}\hat{C}^{(13,11)}\overline{u}_3 + d_{11}\hat{C}^{(13,11)}\overline{u}_1 + a_7\hat{C}^{(13,7)}\overline{u}_3 + a_5\hat{C}^{(13,5)}\overline{u}_3 + a^r_1\hat{C}^{(13,1)}\overline{u}_2$$
$$\overline{p}^{l}_{O_1} = \overline{p}_{A_{10}} + a_{10}\overline{u}_3 + a_6\hat{C}^{(10,6)}\overline{u}_3 + a_4\hat{C}^{(10,4)}\overline{u}_3 + a^l_1\hat{C}^{(10,1)}\overline{u}_2$$

Considering the orientation of body-1, the other three of the constraints can be expressed by means of orthonormal matrices* as in Equation (2.2) for the "right foot flat double suppport phase" and in Equation (2.3) for the "left foot flat double suppport phase":

* An orthonormal matrix (i.e. whose inverse is equal to its transpose) has 3 independent and 6 dependent parameters. So, Equation (2.2) leads to 3 scalar constraint equations.

$$\hat{C}^{(11,1)} = \hat{C}^{(12,1)} \tag{2.2}$$

$$\hat{C}^{(10,1)} = \hat{C}^{(13,1)} \tag{2.3}$$

These two orientation matrices associated with body-1 are obtained as shown in the equations (2.4) through (2.7) by the exponential rotation matrices [28].

$$\hat{C}^{(11,1)} = e^{-\tilde{u}_1\theta_{11}} e^{-\tilde{u}_2(\theta_9+\theta_7+\theta_5)} e^{-\tilde{u}_1\theta_3} \tag{2.4}$$

$$\hat{C}^{(12,1)} = e^{-\tilde{u}_2\theta_{12}} e^{-\tilde{u}_1\theta_{10}} e^{-\tilde{u}_2(\theta_8+\theta_6+\theta_4)} e^{-\tilde{u}_1\theta_2} \tag{2.5}$$

$$\hat{C}^{(10,1)} = e^{-\tilde{u}_1\theta_{10}} e^{-\tilde{u}_2(\theta_8+\theta_6+\theta_4)} e^{-\tilde{u}_1\theta_2} \tag{2.6}$$

$$\hat{C}^{(13,1)} = e^{-\tilde{u}_2\theta_{13}} e^{-\tilde{u}_1\theta_{11}} e^{-\tilde{u}_2(\theta_9+\theta_7+\theta_5)} e^{-\tilde{u}_1\theta_3} \tag{2.7}$$

CHAPTER 3

MATHEMATICAL MODELING AND CONTROL STRUCTURE

This chapter covers the kinematic and dynamic equations of four simulation models corresponding to four phases of gait, the control methodology, the computed torque control method, the use of optimization and prediction algorithms, the nominal paths of swinging feet and other mathematical explanations about the simulation study.

The equations which describe the mathematical modeling are presented for each of the four phases. The kinematic and dynamic equations of the right and left single support phases or double support phases resemble each other. Only, the indices of variables and physical parameters shift in a consistent manner. In this connection, presenting the equations of the right and left-foot flat phases one by one may be found excessive but it is useful to point out the distinctions clearly.

In the kinematics part, the position, velocity and acceleration expressions are derived recursively. Thus, compact equations are obtained instead of lengthy ones. This has also made the error checking operations easier. The positions of the body frame origins are calculated to demonstrate the silhouette of the walking model, while the mass center locations are computed to be incorporated in the dynamic equations.

The dynamic equations of the models are derived using the Newton - Euler formulation. There are several reasons of choosing this method. Firstly, these equations exhibit the dynamic relations of a body in an easily realizable way. Secondly, the reaction forces and moments at the joints are obtained as the by-products of this method. These reactions have a great importance both in the investigation of humanoid gait and in the design of a possible bipedal walking robot. Lastly, the derivation of the Newton-Euler equations of a system of bodies in the 3 dimensional space is rather simple, compared to Lagrange formulation.

In this chapter, after the kinematic and dynamic equations are presented, the application of the *computed torque method* is discussed and the necessary manipulations on the Newton-Euler equations are explained. At the end of the chapter, the *optimal predictive control* (OPC) algorithms for each phase are stated and the corresponding equations are attained.

3.1 Kinematic Equations

The following sections contain the expressions of the position, velocity and acceleration of the body frame origins and the mass centers. In addition, the recursive process to get the orientation matrices, angular velocities and angular accelerations of the bodies is stated. All of the matrix representations of these vectorial kinematic quantities are expressed in the earth fixed frame unless the contrary is indicated. Further, these expressions are derived one by one for the four separate models. Before that, the commonly used position vectors in all the four models ($\vec{\ell}_{i,j}$) are defined. These vectors are used as moment arms in the Euler equations. They are represented in the body fixed frames where they appear constant. They are directed from the mass center of the body to the joint origins. Two of these position vectors are illustrated in Figure 3.1.

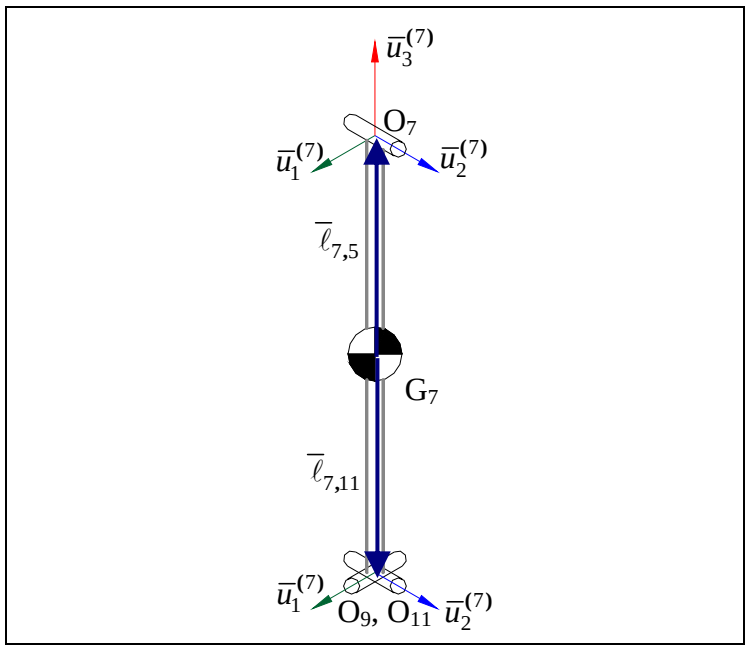

Figure 3.1 The position vectors $\bar{\ell}_{7,5}$ and $\bar{\ell}_{7,11}$

These position vectors are given below as a complete list:

$$
\begin{aligned}
&\bar{\ell}_{11,13} = \bar{\ell}^{(11)}_{11,13} = \frac{2}{3} d_{11}\bar{u}_1 - \frac{1}{3} a_{11}\bar{u}_3 \\
&\bar{\ell}_{11,7} = \bar{\ell}^{(11)}_{11,7} = -\frac{1}{3} d_{11}\bar{u}_1 + \frac{2}{3} a_{11}\bar{u}_3 \\
&\bar{\ell}_{7,11} = \bar{\ell}^{(7)}_{7,11} = -\left(a_7 - c_7\right)\bar{u}_3 \\
&\bar{\ell}_{7,5} = \bar{\ell}^{(7)}_{7,5} = c_7\bar{u}_3 \\
&\bar{\ell}_{5,7} = \bar{\ell}^{(5)}_{5,7} = -\left(a_5 - c_5\right)\bar{u}_3 \\
&\bar{\ell}_{5,1} = \bar{\ell}^{(5)}_{5,1} = c_5\bar{u}_3 \\
&\bar{\ell}_{1,4} = \bar{\ell}^{(1)}_{1,4} = a_1^l\bar{u}_2 - c_1\bar{u}_3 \\
&\bar{\ell}_{1,5} = \bar{\ell}^{(1)}_{1,5} = -a_1^r\bar{u}_2 - c_1\bar{u}_3 \\
&\bar{\ell}_{4,1} = \bar{\ell}^{(4)}_{4,1} = c_4\bar{u}_3 \\
&\bar{\ell}_{4,6} = \bar{\ell}^{(4)}_{4,6} = -\left(a_4 - c_4\right)\bar{u}_3 \\
&\bar{\ell}_{6,4} = \bar{\ell}^{(6)}_{6,4} = c_6\bar{u}_3 \\
&\bar{\ell}_{6,10} = \bar{\ell}^{(6)}_{6,10} = -\left(a_6 - c_6\right)\bar{u}_3 \\
&\bar{\ell}_{10,6} = \bar{\ell}^{(10)}_{10,6} = -\frac{1}{3} d_{10}\bar{u}_1 + \frac{2}{3} a_{10}\bar{u}_3 \\
&\bar{\ell}_{10,12} = \bar{\ell}^{(10)}_{10,12} = \frac{2}{3} d_{10}\bar{u}_1 - \frac{1}{3} a_{10}\bar{u}_3
\end{aligned}
\tag{3.1}
$$

3.1.1 Kinematic Equations of the Left Foot Flat Single Support Phase

In both of the single support phase models, while one foot swings forward, the other foot is assumed to be fixed on the ground. Thus, for the “left foot flat single support” phase, the left foot (body-10) is flat on the ground and the right foot (body-11) swings in the air. The models of the single support phases are linkages with open kinematic chains. For this reason, there is no constraint on the linkage. The recursion process for the derivation of kinematic expressions starts with the constant values of the left heel point (A_{10}) and ends at the right heel point (A_{11}). This results in quite long expressions especially for the kinematics of the links near the end point. The orientation matrices of the model segments with respect to the left foot (body-10) which is grounded flatly are as follows:

$$
\begin{aligned}
\hat{C}^{(10,8)} &= e^{-\tilde{u}_1\theta_{10}} \\
\hat{C}^{(10,6)} &= e^{-\tilde{u}_1\theta_{10}} e^{-\tilde{u}_2\theta_8} \\
\hat{C}^{(10,4)} &= e^{-\tilde{u}_1\theta_{10}} e^{-\tilde{u}_2(\theta_8+\theta_6)} \\
\hat{C}^{(10,2)} &= e^{-\tilde{u}_1\theta_{10}} e^{-\tilde{u}_2(\theta_8+\theta_6+\theta_4)} \\
\hat{C}^{(10,1)} &= e^{-\tilde{u}_1\theta_{10}} e^{-\tilde{u}_2(\theta_8+\theta_6+\theta_4)} e^{-\tilde{u}_1\theta_2} \\
\hat{C}^{(10,3)} &= e^{-\tilde{u}_1\theta_{10}} e^{-\tilde{u}_2(\theta_8+\theta_6+\theta_4)} e^{-\tilde{u}_1\theta_2} e^{\tilde{u}_1\theta_3} \\
\hat{C}^{(10,5)} &= e^{-\tilde{u}_1\theta_{10}} e^{-\tilde{u}_2(\theta_8+\theta_6+\theta_4)} e^{-\tilde{u}_1(\theta_2-\theta_3)} e^{\tilde{u}_2\theta_5} \\
\hat{C}^{(10,7)} &= e^{-\tilde{u}_1\theta_{10}} e^{-\tilde{u}_2(\theta_8+\theta_6+\theta_4)} e^{-\tilde{u}_1(\theta_2-\theta_3)} e^{\tilde{u}_2(\theta_5+\theta_7)} \\
\hat{C}^{(10,9)} &= e^{-\tilde{u}_1\theta_{10}} e^{-\tilde{u}_2(\theta_8+\theta_6+\theta_4)} e^{-\tilde{u}_1(\theta_2-\theta_3)} e^{\tilde{u}_2(\theta_5+\theta_7+\theta_9)} \\
\hat{C}^{(10,11)} &= e^{-\tilde{u}_1\theta_{10}} e^{-\tilde{u}_2(\theta_8+\theta_6+\theta_4)} e^{-\tilde{u}_1(\theta_2-\theta_3)} e^{\tilde{u}_2(\theta_5+\theta_7+\theta_9)} e^{\tilde{u}_1\theta_{11}}
\end{aligned}
\tag{3.2}
$$

In numerous equations, some combinations of these orientation matrices are needed. Some typical examples of such combinations are given below:

1) $\hat{C}^{(10,8)} = e^{-\tilde{u}_1\theta_{10}}$
$\hat{C}^{(8,6)} = e^{-\tilde{u}_2\theta_8}$
$\hat{C}^{(6,4)} = e^{-\tilde{u}_2\theta_6}$
$\hat{C}^{(4,2)} = e^{-\tilde{u}_2\theta_4}$
then, $\hat{C}^{(10,2)} = \hat{C}^{(10,8)}\hat{C}^{(8,6)}\hat{C}^{(6,4)}\hat{C}^{(4,2)}$

2) $\hat{C}^{(6,4)} = e^{-\tilde{u}_2\theta_6}$ then, $\hat{C}^{(4,6)} = e^{\tilde{u}_2\theta_6} = \hat{C}^{(6,4)^t} = \hat{C}^{(6,4)^{-1}}$

3) Since $\hat{C}^{(10,1)} = \hat{C}^{(13,1)}$ in the "left foot flat double support phase", then

$\hat{C}^{(13,1)}\hat{C}^{(1,10)} = \hat{C}^{(13,10)} = \hat{I}$

where; $\hat{I}$ is the 3x3 identity matrix

4) $e^{\tilde{u}_i\theta}\overline{u}_j = \overline{u}_j \cos\theta + \left(\tilde{u}_i\overline{u}_j\right)\sin\theta \;,\quad i \neq j$

5) $\overline{u}_j^t e^{\tilde{u}_i\theta} = \overline{u}_j^t \cos\theta + \left(\tilde{u}_j\overline{u}_i\right)^t \sin\theta \;,\quad i \neq j$

6) $e^{\tilde{n}\theta}\overline{n} = \overline{n}$

7) $e^{\tilde{n}\theta}\tilde{n} = \tilde{n}e^{\tilde{n}\theta} \neq \tilde{n}$

8) $\overline{m} = e^{\tilde{u}\beta}\overline{n} \;\Rightarrow\; \tilde{m} = e^{\tilde{u}\beta}\tilde{n}e^{-\tilde{u}\beta}$

For more details about the algebra of exponential rotation matrices, see [28].

Starting from the left fixed point O_{10} (the left ankle origin), the position vectors of the link origins of this model are given below:

$$
\begin{aligned}
\overline{p}_{O_{10}} &= \overline{p}_{A_{10}} + a_{10}\overline{u}_3 \\
\overline{p}_{O_8} &= \overline{p}_{O_{10}} \\
\overline{p}_{O_6} &= \overline{p}_{O_8} + a_6\hat{C}^{(10,6)}\overline{u}_3 \\
\overline{p}_{O_4} &= \overline{p}_{O_6} + a_4\hat{C}^{(10,4)}\overline{u}_3 \\
\overline{p}_{O_2} &= \overline{p}_{O_4} \\
\overline{p}_{O_1} &= \overline{p}_{O_2} + a_1^r\hat{C}^{(10,1)}\overline{u}_2 \\
\overline{p}_{O_3} &= \overline{p}_{O_1} + a_1^l\hat{C}^{(10,1)}\overline{u}_2 \\
\overline{p}_{O_5} &= \overline{p}_{O_3} \\
\overline{p}_{O_7} &= \overline{p}_{O_5} - a_5\hat{C}^{(10,5)}\overline{u}_3 \\
\overline{p}_{O_9} &= \overline{p}_{O_7} - a_7\hat{C}^{(10,7)}\overline{u}_3 \\
\overline{p}_{O_{11}} &= \overline{p}_{O_9} \\
\overline{p}_{A_{11}} &= \overline{p}_{O_{11}} - a_{11}\hat{C}^{(10,11)}\overline{u}_3
\end{aligned}
\tag{3.3}
$$

The positions of the mass centers are obtained by using the previously found positions of the link origins. These are presented with respect to the origin on the ground in the next group of equations.

$$
\begin{aligned}
\overline{p}_6 &= \overline{p}_{O_6} - c_6\hat{C}^{(10,6)}\overline{u}_3 \\
\overline{p}_4 &= \overline{p}_{O_4} - c_4\hat{C}^{(10,4)}\overline{u}_3 \\
\overline{p}_1 &= \overline{p}_{O_1} + c_1\hat{C}^{(10,1)}\overline{u}_3 \\
\overline{p}_5 &= \overline{p}_{O_5} - c_5\hat{C}^{(10,5)}\overline{u}_3 \\
\overline{p}_7 &= \overline{p}_{O_7} - c_7\hat{C}^{(10,7)}\overline{u}_3 \\
\overline{p}_{11} &= \overline{p}_{O_{11}} - \hat{C}^{(10,11)}\overline{\ell}_{11,7}
\end{aligned}
\tag{3.4}
$$

The angular velocities of the links are calculated recursively as other kinematic elements of the models:

$$
\begin{aligned}
\bar{\omega}_8 &= -\dot{\theta}_{10}\bar{u}_1 \\
\bar{\omega}_6 &= \bar{\omega}_8 - \dot{\theta}_8\hat{C}^{(10,8)}\bar{u}_2 \\
\bar{\omega}_4 &= \bar{\omega}_6 - \dot{\theta}_6\hat{C}^{(10,6)}\bar{u}_2 \\
\bar{\omega}_2 &= \bar{\omega}_4 - \dot{\theta}_4\hat{C}^{(10,4)}\bar{u}_2 \\
\bar{\omega}_1 &= \bar{\omega}_2 - \dot{\theta}_2\hat{C}^{(10,2)}\bar{u}_1 \\
\bar{\omega}_3 &= \bar{\omega}_1 + \dot{\theta}_3\hat{C}^{(10,1)}\bar{u}_1 \\
\bar{\omega}_5 &= \bar{\omega}_3 + \dot{\theta}_5\hat{C}^{(10,3)}\bar{u}_2 \\
\bar{\omega}_7 &= \bar{\omega}_5 + \dot{\theta}_7\hat{C}^{(10,5)}\bar{u}_2 \\
\bar{\omega}_9 &= \bar{\omega}_7 + \dot{\theta}_9\hat{C}^{(10,7)}\bar{u}_2 \\
\bar{\omega}_{11} &= \bar{\omega}_9 + \dot{\theta}_{11}\hat{C}^{(10,9)}\bar{u}_1
\end{aligned}
\tag{3.5}
$$

The velocities of the link origins are obtained by using the angular velocities:

$$
\begin{aligned}
\bar{v}_{O_{10}} &= \bar{0} \\
\bar{v}_{O_8} &= \bar{v}_{O_{10}} \\
\bar{v}_{O_6} &= \bar{v}_{O_8} + a_6\tilde{\omega}_6\hat{C}^{(10,6)}\bar{u}_3 \\
\bar{v}_{O_4} &= \bar{v}_{O_6} + a_4\tilde{\omega}_4\hat{C}^{(10,4)}\bar{u}_3 \\
\bar{v}_{O_2} &= \bar{v}_{O_4} \\
\bar{v}_{O_1} &= \bar{v}_{O_2} - a_1^l\tilde{\omega}_1\hat{C}^{(10,1)}\bar{u}_2 \\
\bar{v}_{O_3} &= \bar{v}_{O_1} - a_1^r\tilde{\omega}_1\hat{C}^{(10,1)}\bar{u}_2 \\
\bar{v}_{O_5} &= \bar{v}_{O_3} \\
\bar{v}_{O_7} &= \bar{v}_{O_5} - a_5\tilde{\omega}_5\hat{C}^{(10,5)}\bar{u}_3 \\
\bar{v}_{O_9} &= \bar{v}_{O_7} - a_7\tilde{\omega}_7\hat{C}^{(10,7)}\bar{u}_3 \\
\bar{v}_{O_{11}} &= \bar{v}_{O_9}
\end{aligned}
\tag{3.6}
$$

The angular accelerations of the links in the “left foot flat single support phase” are listed as shown below:

$$
\begin{aligned}
\bar{\alpha}_8 &= -\ddot{\theta}_{10}\bar{u}_1 \\
\bar{\alpha}_6 &= \bar{\alpha}_8 - \ddot{\theta}_8\hat{C}^{(10,8)}\bar{u}_2 - \dot{\theta}_8\tilde{\omega}_8\hat{C}^{(10,8)}\bar{u}_2 \\
\bar{\alpha}_4 &= \bar{\alpha}_6 - \ddot{\theta}_6\hat{C}^{(10,6)}\bar{u}_2 - \dot{\theta}_6\tilde{\omega}_6\hat{C}^{(10,6)}\bar{u}_2 \\
\bar{\alpha}_2 &= \bar{\alpha}_4 - \ddot{\theta}_4\hat{C}^{(10,4)}\bar{u}_2 - \dot{\theta}_4\tilde{\omega}_4\hat{C}^{(10,4)}\bar{u}_2 \\
\bar{\alpha}_1 &= \bar{\alpha}_2 - \ddot{\theta}_2\hat{C}^{(10,2)}\bar{u}_1 - \dot{\theta}_2\tilde{\omega}_2\hat{C}^{(10,2)}\bar{u}_1 \\
\bar{\alpha}_3 &= \bar{\alpha}_1 + \ddot{\theta}_3\hat{C}^{(10,1)}\bar{u}_1 + \dot{\theta}_3\tilde{\omega}_1\hat{C}^{(10,1)}\bar{u}_1 \\
\bar{\alpha}_5 &= \bar{\alpha}_3 + \ddot{\theta}_5\hat{C}^{(10,3)}\bar{u}_2 + \dot{\theta}_5\tilde{\omega}_3\hat{C}^{(10,3)}\bar{u}_2 \\
\bar{\alpha}_7 &= \bar{\alpha}_5 + \ddot{\theta}_7\hat{C}^{(10,5)}\bar{u}_2 + \dot{\theta}_7\tilde{\omega}_5\hat{C}^{(10,5)}\bar{u}_2 \\
\bar{\alpha}_9 &= \bar{\alpha}_7 + \ddot{\theta}_9\hat{C}^{(10,7)}\bar{u}_2 + \dot{\theta}_9\tilde{\omega}_7\hat{C}^{(10,7)}\bar{u}_2 \\
\bar{\alpha}_{11} &= \bar{\alpha}_9 + \ddot{\theta}_{11}\hat{C}^{(10,9)}\bar{u}_1 + \dot{\theta}_{11}\tilde{\omega}_9\hat{C}^{(10,9)}\bar{u}_1
\end{aligned}
\tag{3.7}
$$

The accelerations of the link origins are as follows:

$$
\begin{aligned}
\bar{a}_{O_8} &= \bar{0} \\
\bar{a}_{O_6} &= \bar{a}_{O_8} + a_6\left[\tilde{\alpha}_6 + \tilde{\omega}_6^2\right]\hat{C}^{(10,6)}\bar{u}_3 \\
\bar{a}_{O_4} &= \bar{a}_{O_5} + a_4\left[\tilde{\alpha}_4 + \tilde{\omega}_4^2\right]\hat{C}^{(10,4)}\bar{u}_3 \\
\bar{a}_{O_2} &= \bar{a}_{O_4} \\
\bar{a}_{O_1} &= \bar{a}_{O_2} - a_1^l\left[\tilde{\alpha}_1 + \tilde{\omega}_1^2\right]\hat{C}^{(10,1)}\bar{u}_2 \\
\bar{a}_{O_3} &= \bar{a}_{O_1} - a_1^r\left[\tilde{\alpha}_1 + \tilde{\omega}_1^2\right]\hat{C}^{(10,1)}\bar{u}_2 \\
\bar{a}_{O_5} &= \bar{a}_{O_3} \\
\bar{a}_{O_7} &= \bar{a}_{O_5} - a_5\left[\tilde{\alpha}_5 + \tilde{\omega}_5^2\right]\hat{C}^{(10,5)}\bar{u}_3 \\
\bar{a}_{O_9} &= \bar{a}_{O_7} - a_7\left[\tilde{\alpha}_7 + \tilde{\omega}_7^2\right]\hat{C}^{(10,7)}\bar{u}_3 \\
\bar{a}_{O_{11}} &= \bar{a}_{O_9}
\end{aligned}
\tag{3.8}
$$

In the equation group (3.9), the accelerations of the mass centers are given:

$$
\begin{aligned}
&\bar{a}_8 = \bar{0} \\
&\bar{a}_6 = \bar{a}_{O_6} - c_6\left[\tilde{\alpha}_6 + \tilde{\omega}_6^2\right]\hat{C}^{(10,6)}\bar{u}_3 \\
&\bar{a}_4 = \bar{a}_{O_4} - c_4\left[\tilde{\alpha}_4 + \tilde{\omega}_4^2\right]\hat{C}^{(10,4)}\bar{u}_3 \\
&\bar{a}_2 = \bar{a}_{O_2} \\
&\bar{a}_1 = \bar{a}_{O_1} + c_1\left[\tilde{\alpha}_1 + \tilde{\omega}_1^2\right]\hat{C}^{(10,1)}\bar{u}_3 \\
&\bar{a}_3 = \bar{a}_{O_3} \\
&\bar{a}_5 = \bar{a}_{O_5} - c_5\left[\tilde{\alpha}_5 + \tilde{\omega}_5^2\right]\hat{C}^{(10,5)}\bar{u}_3 \\
&\bar{a}_7 = \bar{a}_{O_7} - c_7\left[\tilde{\alpha}_7 + \tilde{\omega}_7^2\right]\hat{C}^{(10,7)}\bar{u}_3 \\
&\bar{a}_9 = \bar{a}_{O_9} \\
&\bar{a}_{11} = \bar{a}_{O_{11}} - \left[\tilde{\alpha}_{11} + \tilde{\omega}_{11}^2\right]\hat{C}^{(10,11)}\bar{\ell}_{11,7}
\end{aligned}
\tag{3.9}
$$

3.1.2 Kinematic Equations of the Right Foot Flat Single Support Phase

During this phase of gait, only the right foot (body-11) is stationary on the ground and the left foot (body-10) swings in the air. This model is just the mirror image of the previous single support model. The orientation matrices of both left and right leg segments with respect to right foot (body-11) are as follows:

$$
\begin{aligned}
&\hat{C}^{(11,9)} = e^{-\tilde{u}_1\theta_{11}} \\
&\hat{C}^{(11,7)} = e^{-\tilde{u}_1\theta_{11}}e^{-\tilde{u}_2\theta_9} \\
&\hat{C}^{(11,5)} = e^{-\tilde{u}_1\theta_{11}}e^{-\tilde{u}_2(\theta_9+\theta_7)} \\
&\hat{C}^{(11,3)} = e^{-\tilde{u}_1\theta_{11}}e^{-\tilde{u}_2(\theta_9+\theta_7+\theta_5)} \\
&\hat{C}^{(11,1)} = e^{-\tilde{u}_1\theta_{11}}e^{-\tilde{u}_2(\theta_9+\theta_7+\theta_5)}e^{-\tilde{u}_1\theta_3} \\
&\hat{C}^{(11,2)} = e^{-\tilde{u}_1\theta_{11}}e^{-\tilde{u}_2(\theta_9+\theta_7+\theta_5)}e^{-\tilde{u}_1\theta_3}e^{\tilde{u}_1\theta_2} \\
&\hat{C}^{(11,4)} = e^{-\tilde{u}_1\theta_{11}}e^{-\tilde{u}_2(\theta_9+\theta_7+\theta_5)}e^{-\tilde{u}_1(\theta_3-\theta_2)}e^{\tilde{u}_2\theta_4} \\
&\hat{C}^{(11,6)} = e^{-\tilde{u}_1\theta_{11}}e^{-\tilde{u}_2(\theta_9+\theta_7+\theta_5)}e^{-\tilde{u}_1(\theta_3-\theta_2)}e^{\tilde{u}_2(\theta_4+\theta_6)} \\
&\hat{C}^{(11,8)} = e^{-\tilde{u}_1\theta_{11}}e^{-\tilde{u}_2(\theta_9+\theta_7+\theta_5)}e^{-\tilde{u}_1(\theta_3-\theta_2)}e^{\tilde{u}_2(\theta_4+\theta_6+\theta_8)} \\
&\hat{C}^{(11,10)} = e^{-\tilde{u}_1\theta_{11}}e^{-\tilde{u}_2(\theta_9+\theta_7+\theta_5)}e^{-\tilde{u}_1(\theta_3-\theta_2)}e^{\tilde{u}_2(\theta_4+\theta_6+\theta_8)}e^{\tilde{u}_1\theta_{10}}
\end{aligned}
\tag{3.10}
$$

The position vectors of the link origins are derived in the equation group (3.11).

$$
\begin{aligned}
\overline{p}_{O_{11}} &= \overline{p}_{A_{11}} + a_{11}\overline{u}_3 \\
\overline{p}_{O_9} &= \overline{p}_{O_{11}} \\
\overline{p}_{O_7} &= \overline{p}_{O_9} + a_7\hat{C}^{(11,7)}\overline{u}_3 \\
\overline{p}_{O_5} &= \overline{p}_{O_7} + a_5\hat{C}^{(11,5)}\overline{u}_3 \\
\overline{p}_{O_3} &= \overline{p}_{O_5} \\
\overline{p}_{O_1} &= \overline{p}_{O_3} + a_1^r\hat{C}^{(11,1)}\overline{u}_2 \\
\overline{p}_{O_2} &= \overline{p}_{O_1} + a_1^l\hat{C}^{(11,1)}\overline{u}_2 \\
\overline{p}_{O_4} &= \overline{p}_{O_2} \\
\overline{p}_{O_6} &= \overline{p}_{O_4} - a_4\hat{C}^{(11,4)}\overline{u}_3 \\
\overline{p}_{O_8} &= \overline{p}_{O_6} - a_6\hat{C}^{(11,6)}\overline{u}_3 \\
\overline{p}_{O_{10}} &= \overline{p}_{O_8} \\
\overline{p}_{A_{10}} &= \overline{p}_{O_{10}} - a_{10}\hat{C}^{(11,10)}\overline{u}_3
\end{aligned}
\tag{3.11}
$$

The position vectors of the mass centers are attained in the following equations:

$$
\begin{aligned}
\overline{p}_7 &= \overline{p}_{O_7} - c_7\hat{C}^{(11,7)}\overline{u}_3 \\
\overline{p}_5 &= \overline{p}_{O_5} - c_5\hat{C}^{(11,5)}\overline{u}_3 \\
\overline{p}_1 &= \overline{p}_{O_1} + c_1\hat{C}^{(11,1)}\overline{u}_3 \\
\overline{p}_4 &= \overline{p}_{O_4} - c_4\hat{C}^{(11,4)}\overline{u}_3 \\
\overline{p}_6 &= \overline{p}_{O_6} - c_6\hat{C}^{(11,6)}\overline{u}_3 \\
\overline{p}_{10} &= \overline{p}_{O_{10}} - \hat{C}^{(11,10)}\overline{\ell}_{10,6}
\end{aligned}
\tag{3.12}
$$

The angular velocities of the links are acquired by the joint velocities.

$$
\begin{aligned}
\bar{\omega}_9 &= -\dot{\theta}_{11}\bar{u}_1 \\
\bar{\omega}_7 &= \bar{\omega}_9 - \dot{\theta}_9\hat{C}^{(11,9)}\bar{u}_2 \\
\bar{\omega}_5 &= \bar{\omega}_7 - \dot{\theta}_7\hat{C}^{(11,7)}\bar{u}_2 \\
\bar{\omega}_3 &= \bar{\omega}_5 - \dot{\theta}_5\hat{C}^{(11,5)}\bar{u}_2 \\
\bar{\omega}_1 &= \bar{\omega}_3 - \dot{\theta}_3\hat{C}^{(11,3)}\bar{u}_1 \\
\bar{\omega}_2 &= \bar{\omega}_1 + \dot{\theta}_2\hat{C}^{(11,1)}\bar{u}_1 \\
\bar{\omega}_4 &= \bar{\omega}_2 + \dot{\theta}_4\hat{C}^{(11,2)}\bar{u}_2 \\
\bar{\omega}_6 &= \bar{\omega}_4 + \dot{\theta}_6\hat{C}^{(11,4)}\bar{u}_2 \\
\bar{\omega}_8 &= \bar{\omega}_6 + \dot{\theta}_8\hat{C}^{(11,6)}\bar{u}_2 \\
\bar{\omega}_{10} &= \bar{\omega}_8 + \dot{\theta}_{10}\hat{C}^{(11,8)}\bar{u}_1
\end{aligned}
\tag{3.13}
$$

The velocities of the link origins are derived below:

$$
\begin{aligned}
\bar{v}_{O_{11}} &= \bar{0} \\
\bar{v}_{O_9} &= \bar{v}_{O_{11}} \\
\bar{v}_{O_7} &= \bar{v}_{O_9} + a_7\tilde{\omega}_7\hat{C}^{(11,7)}\bar{u}_3 \\
\bar{v}_{O_5} &= \bar{v}_{O_7} + a_5\tilde{\omega}_5\hat{C}^{(11,5)}\bar{u}_3 \\
\bar{v}_{O_3} &= \bar{v}_{O_5} \\
\bar{v}_{O_1} &= \bar{v}_{O_3} + a_1^r\tilde{\omega}_1\hat{C}^{(11,1)}\bar{u}_2 \\
\bar{v}_{O_2} &= \bar{v}_{O_1} + a_1^l\tilde{\omega}_1\hat{C}^{(11,1)}\bar{u}_2 \\
\bar{v}_{O_4} &= \bar{v}_{O_2} \\
\bar{v}_{O_6} &= \bar{v}_{O_4} - a_4\tilde{\omega}_4\hat{C}^{(11,4)}\bar{u}_3 \\
\bar{v}_{O_8} &= \bar{v}_{O_6} - a_6\tilde{\omega}_6\hat{C}^{(11,6)}\bar{u}_3 \\
\bar{v}_{O_{10}} &= \bar{v}_{O_8}
\end{aligned}
\tag{3.14}
$$

The equation group (3.15) denotes the angular accelerations of the links.

$$
\begin{aligned}
\bar{\alpha}_9 &= -\ddot{\theta}_{11}\bar{u}_1 \\
\bar{\alpha}_7 &= \bar{\alpha}_9 - \ddot{\theta}_9\hat{C}^{(11,9)}\bar{u}_2 - \dot{\theta}_9\tilde{\omega}_9\hat{C}^{(11,9)}\bar{u}_2 \\
\bar{\alpha}_5 &= \bar{\alpha}_7 - \ddot{\theta}_7\hat{C}^{(11,7)}\bar{u}_2 - \dot{\theta}_7\tilde{\omega}_7\hat{C}^{(11,7)}\bar{u}_2 \\
\bar{\alpha}_3 &= \bar{\alpha}_5 - \ddot{\theta}_5\hat{C}^{(11,5)}\bar{u}_2 - \dot{\theta}_5\tilde{\omega}_5\hat{C}^{(11,5)}\bar{u}_2 \\
\bar{\alpha}_1 &= \bar{\alpha}_3 - \ddot{\theta}_3\hat{C}^{(11,3)}\bar{u}_1 - \dot{\theta}_3\tilde{\omega}_3\hat{C}^{(11,3)}\bar{u}_1 \\
\bar{\alpha}_2 &= \bar{\alpha}_1 + \ddot{\theta}_2\hat{C}^{(11,1)}\bar{u}_1 + \dot{\theta}_2\tilde{\omega}_1\hat{C}^{(11,1)}\bar{u}_1 \\
\bar{\alpha}_4 &= \bar{\alpha}_2 + \ddot{\theta}_4\hat{C}^{(11,2)}\bar{u}_2 + \dot{\theta}_4\tilde{\omega}_2\hat{C}^{(11,2)}\bar{u}_2 \\
\bar{\alpha}_6 &= \bar{\alpha}_4 + \ddot{\theta}_6\hat{C}^{(11,4)}\bar{u}_2 + \dot{\theta}_6\tilde{\omega}_4\hat{C}^{(11,4)}\bar{u}_2 \\
\bar{\alpha}_8 &= \bar{\alpha}_6 + \ddot{\theta}_8\hat{C}^{(11,6)}\bar{u}_2 + \dot{\theta}_8\tilde{\omega}_6\hat{C}^{(11,6)}\bar{u}_2 \\
\bar{\alpha}_{10} &= \bar{\alpha}_8 + \ddot{\theta}_{10}\hat{C}^{(11,8)}\bar{u}_1 + \dot{\theta}_{10}\tilde{\omega}_8\hat{C}^{(11,8)}\bar{u}_1
\end{aligned}
\tag{3.15}
$$

Next, the accelerations of the link origins are introduced.

$$
\begin{aligned}
\bar{a}_{O_9} &= \bar{0} \\
\bar{a}_{O_7} &= \bar{a}_{O_9} + a_7\left[\tilde{\alpha}_7 + \tilde{\omega}_7^2\right]\hat{C}^{(11,7)}\bar{u}_3 \\
\bar{a}_{O_5} &= \bar{a}_{O_7} + a_5\left[\tilde{\alpha}_5 + \tilde{\omega}_5^2\right]\hat{C}^{(11,5)}\bar{u}_3 \\
\bar{a}_{O_3} &= \bar{a}_{O_5} \\
\bar{a}_{O_1} &= \bar{a}_{O_3} + a_1^r\left[\tilde{\alpha}_1 + \tilde{\omega}_1^2\right]\hat{C}^{(11,1)}\bar{u}_2 \\
\bar{a}_{O_2} &= \bar{a}_{O_1} + a_1^l\left[\tilde{\alpha}_1 + \tilde{\omega}_1^2\right]\hat{C}^{(11,1)}\bar{u}_2 \\
\bar{a}_{O_4} &= \bar{a}_{O_2} \\
\bar{a}_{O_6} &= \bar{a}_{O_4} - a_4\left[\tilde{\alpha}_4 + \tilde{\omega}_4^2\right]\hat{C}^{(11,4)}\bar{u}_3 \\
\bar{a}_{O_8} &= \bar{a}_{O_6} - a_6\left[\tilde{\alpha}_6 + \tilde{\omega}_6^2\right]\hat{C}^{(11,6)}\bar{u}_3 \\
\bar{a}_{O_{10}} &= \bar{a}_{O_8}
\end{aligned}
\tag{3.16}
$$

The accelerations of the mass centers are computed by the following expressions during the “right foot flat single support phase”:

$$
\begin{aligned}
\bar{a}_9 &= \bar{0} \\
\bar{a}_7 &= \bar{a}_{O_7} - c_7\left[\tilde{\alpha}_7 + \tilde{\omega}_7^2\right]\hat{C}^{(11,7)}\bar{u}_3 \\
\bar{a}_5 &= \bar{a}_{O_5} - c_5\left[\tilde{\alpha}_5 + \tilde{\omega}_5^2\right]\hat{C}^{(11,5)}\bar{u}_3 \\
\bar{a}_3 &= \bar{a}_{O_3} \\
\bar{a}_1 &= \bar{a}_{O_1} + c_1\left[\tilde{\alpha}_1 + \tilde{\omega}_1^2\right]\hat{C}^{(11,1)}\bar{u}_3 \\
\bar{a}_2 &= \bar{a}_{O_2} \\
\bar{a}_4 &= \bar{a}_{O_4} - c_4\left[\tilde{\alpha}_4 + \tilde{\omega}_4^2\right]\hat{C}^{(11,4)}\bar{u}_3 \\
\bar{a}_6 &= \bar{a}_{O_6} - c_6\left[\tilde{\alpha}_6 + \tilde{\omega}_6^2\right]\hat{C}^{(11,6)}\bar{u}_3 \\
\bar{a}_8 &= \bar{a}_{O_8} \\
\bar{a}_{10} &= \bar{a}_{O_{10}} - \left[\tilde{\alpha}_{10} + \tilde{\omega}_{10}^2\right]\hat{C}^{(11,10)}\bar{\ell}_{10,6}
\end{aligned}
\tag{3.17}
$$

3.1.3 Kinematic Equations of the Left Foot Flat Double Support Phase

During this phase, the left foot (body-10) and the right toe (body-13) are stationary on the ground. This causes a closed kinematic chain as described in Chapter 2. For this reason, the kinematic expressions corresponding to the right leg segments are derived starting from the right stationary point and the kinematic expressions correspond to the left leg segments are derived starting from the left stationary point. In the “left foot flat double support phase”, the origin O_{13} is the right stationary point and the origin O_{10} is the left stationary point. By writing in this way, the kinematic equations become more compact. Actually, it also makes the representation of the constraint equations easier. As the first kinematic expressions, the orientation matrices of the right leg segments with respect to the right toe (body-13) are presented below:

$$
\begin{aligned}
\hat{C}^{(13,11)} &= e^{-\tilde{u}_2\theta_{13}} \\
\hat{C}^{(13,9)} &= e^{-\tilde{u}_2\theta_{13}} e^{-\tilde{u}_1\theta_{11}} \\
\hat{C}^{(13,7)} &= e^{-\tilde{u}_2\theta_{13}} e^{-\tilde{u}_1\theta_{11}} e^{-\tilde{u}_2\theta_9} \\
\hat{C}^{(13,5)} &= e^{-\tilde{u}_2\theta_{13}} e^{-\tilde{u}_1\theta_{11}} e^{-\tilde{u}_2(\theta_9+\theta_7)} \\
\hat{C}^{(13,3)} &= e^{-\tilde{u}_2\theta_{13}} e^{-\tilde{u}_1\theta_{11}} e^{-\tilde{u}_2(\theta_9+\theta_7+\theta_5)} \\
\hat{C}^{(13,1)} &= e^{-\tilde{u}_2\theta_{13}} e^{-\tilde{u}_1\theta_{11}} e^{-\tilde{u}_2(\theta_9+\theta_7+\theta_5)} e^{-\tilde{u}_1\theta_3}
\end{aligned}
\tag{3.18}
$$

Since, the left toe angle (θ_{12}) is zero during the left foot flat double support phase, $\hat{C}^{(12,10)}$ is equal to the identity matrix and the orientations of the left leg segments can be written with respect to the left foot (body-10) instead of the left toe (body-12).

$$
\begin{aligned}
\hat{C}^{(10,8)} &= e^{-\tilde{u}_1\theta_{10}} \\
\hat{C}^{(10,6)} &= e^{-\tilde{u}_1\theta_{10}} e^{-\tilde{u}_2\theta_8} \\
\hat{C}^{(10,4)} &= e^{-\tilde{u}_1\theta_{10}} e^{-\tilde{u}_2(\theta_8+\theta_6)} \\
\hat{C}^{(10,2)} &= e^{-\tilde{u}_1\theta_{10}} e^{-\tilde{u}_2(\theta_4+\theta_6+\theta_8)} \\
\hat{C}^{(10,1)} &= e^{-\tilde{u}_1\theta_{10}} e^{-\tilde{u}_2(\theta_4+\theta_6+\theta_8)} e^{-\tilde{u}_1\theta_2}
\end{aligned}
\tag{3.19}
$$

At this point, it must be declared that;

$$
\hat{C}^{(13,1)} = \hat{C}^{(10,1)} \tag{3.20}
$$

It was noted in the previous chapter that Equation (3.20) results three scalar constraint equations of the “left foot flat double support phase”.

Starting from the right stationary point O_{13}, the positions of the link origins of this model are given below:

$$
\begin{aligned}
\bar{p}_{O_{11}} &= \bar{p}_{O_{13}} + \hat{C}^{(13,11)}\left(-d_{11}\bar{u}_1 + a_{11}\bar{u}_3\right) \\
\bar{p}_{A_{11}} &= \bar{p}_{O_{13}} - \hat{C}^{(13,11)} d_{11}\bar{u}_1 \\
\bar{p}_{O_7} &= \bar{p}_{O_{11}} + a_7\hat{C}^{(13,7)}\bar{u}_3 \\
\bar{p}_{O_5} &= \bar{p}_{O_7} + a_5\hat{C}^{(13,5)}\bar{u}_3 \\
\bar{p}_{O_1}\left(\text{right}\right) &= \bar{p}_{O_5} + a_1^r\hat{C}^{(13,1)}\bar{u}_2
\end{aligned}
\tag{3.21}
$$

Starting from the left stationary point O_{10}, the position of the origin of link-1 is also obtained same as the version expressed in terms of the right leg variables:

$$\begin{aligned}
\overline{p}_{O_6} &= \overline{p}_{O_{10}} + a_6\hat{C}^{(10,6)}\overline{u}_3 \\
\overline{p}_{O_4} &= \overline{p}_{O_6} + a_4\hat{C}^{(10,4)}\overline{u}_3 \\
\overline{p}_{O_1}(\text{left}) &= \overline{p}_{O_4} - a_1^l\hat{C}^{(10,1)}\overline{u}_2
\end{aligned} \tag{3.22}$$

The constraint equation ties up the two sides as

$$\overline{p}_{O_1}(\text{right}) = \overline{p}_{O_1}(\text{left}) = \overline{p}_{O_1} \tag{3.23}$$

The position vectors of the mass centers with respect to the origin on the ground are as follow:

$$\begin{aligned}
\overline{p}_{11} &= \overline{p}_{O_{11}} - \hat{C}^{(13,11)}\overline{\ell}_{11,7} \\
\overline{p}_7 &= \overline{p}_{O_7} - \hat{C}^{(13,7)}\overline{\ell}_{7,5} \\
\overline{p}_5 &= \overline{p}_{O_5} - \hat{C}^{(13,5)}\overline{\ell}_{5,1} \\
\overline{p}_1(\text{right}) &= \overline{p}_{O_1}(\text{right}) + c_1\hat{C}^{(13,1)}\overline{u}_3
\end{aligned} \tag{3.24}$$

$$\begin{aligned}
\overline{p}_6 &= \overline{p}_{O_6} - \hat{C}^{(10,6)}\overline{\ell}_{6,4} \\
\overline{p}_4 &= \overline{p}_{O_4} - \hat{C}^{(10,4)}\overline{\ell}_{4,1} \\
\overline{p}_1(\text{left}) &= \overline{p}_{O_1}(\text{left}) + c_1\hat{C}^{(10,1)}\overline{u}_3
\end{aligned} \tag{3.25}$$

The angular velocities of the links during the “left foot flat double support phase” are arranged in the following order:

$$\begin{aligned}
\overline{\omega}_{11} &= -\dot{\theta}_{13}\overline{u}_2 \\
\overline{\omega}_9 &= \overline{\omega}_{11} - \dot{\theta}_{11}\hat{C}^{(13,11)}\overline{u}_1 \\
\overline{\omega}_7 &= \overline{\omega}_9 - \dot{\theta}_9\hat{C}^{(13,9)}\overline{u}_2 \\
\overline{\omega}_5 &= \overline{\omega}_7 - \dot{\theta}_7\hat{C}^{(13,7)}\overline{u}_2 \\
\overline{\omega}_3 &= \overline{\omega}_5 - \dot{\theta}_5\hat{C}^{(13,5)}\overline{u}_2 \\
\overline{\omega}_1(\text{right}) &= \overline{\omega}_3 - \dot{\theta}_3\hat{C}^{(13,3)}\overline{u}_1
\end{aligned} \tag{3.26}$$

$$
\begin{aligned}
\bar{\omega}_8 &= -\dot{\theta}_{10}\bar{u}_1 \\
\bar{\omega}_6 &= \bar{\omega}_8 - \dot{\theta}_8\hat{C}^{(10,8)}\bar{u}_2 \\
\bar{\omega}_4 &= \bar{\omega}_6 - \dot{\theta}_6\hat{C}^{(10,6)}\bar{u}_2 \\
\bar{\omega}_2 &= \bar{\omega}_4 - \dot{\theta}_4\hat{C}^{(10,4)}\bar{u}_2 \\
\bar{\omega}_1\left(\text{left}\right) &= \bar{\omega}_2 - \dot{\theta}_2\hat{C}^{(10,2)}\bar{u}_1
\end{aligned}
\tag{3.27}
$$

At this point, the first part of the velocity level kinematic constraints of the double support models arises. Of course, the body-1 can have only one angular velocity whether the recursion starts from left or right. This implies the following angular velocity constraint equation, which embeds three scalar equations:

$$
\bar{\omega}_1\left(\text{right}\right) = \bar{\omega}_1\left(\text{left}\right) = \bar{\omega}_1 \tag{3.28}
$$

Below are the velocities of the link origins:

$$
\begin{aligned}
\bar{v}_{O_{13}} &= \bar{0} \\
\bar{v}_{O_{11}} &= \bar{v}_{O_{13}} + \tilde{\omega}_{11}\hat{C}^{(13,11)}\left(-d_{11}\bar{u}_1 + a_{11}\bar{u}_3\right) \\
\bar{v}_{O_9} &= \bar{v}_{O_{11}} \\
\bar{v}_{O_7} &= \bar{v}_{O_9} + a_7\tilde{\omega}_7\hat{C}^{(13,7)}\bar{u}_3 \\
\bar{v}_{O_5} &= \bar{v}_{O_7} + a_5\tilde{\omega}_5\hat{C}^{(13,5)}\bar{u}_3 \\
\bar{v}_{O_3} &= \bar{v}_{O_5} \\
\bar{v}_{O_1}\left(\text{right}\right) &= \bar{v}_{O_3} + a_1^r\tilde{\omega}_1\hat{C}^{(13,1)}\bar{u}_2
\end{aligned}
\tag{3.29}
$$

$$
\begin{aligned}
\bar{v}_{O_{10}} &= \bar{v}_{O_8} = \bar{0} \\
\bar{v}_{O_6} &= \bar{v}_{O_8} + a_6\tilde{\omega}_6\hat{C}^{(10,6)}\bar{u}_3 \\
\bar{v}_{O_4} &= \bar{v}_{O_6} + a_4\tilde{\omega}_4\hat{C}^{(10,4)}\bar{u}_3 \\
\bar{v}_{O_2} &= \bar{v}_{O_4} \\
\bar{v}_{O_1}\left(\text{left}\right) &= \bar{v}_{O_2} - a_1^l\tilde{\omega}_1\hat{C}^{(10,1)}\bar{u}_2
\end{aligned}
\tag{3.30}
$$

Hence, the last three scalar constraint equations at the velocity level of this phase arise as

$$
\bar{v}_{O_1}\left(\text{right}\right) = \bar{v}_{O_1}\left(\text{left}\right) = \bar{v}_{O_1} \tag{3.31}
$$

The angular accelerations of the links in the “left foot flat double support phase” are listed as follows:

$$
\begin{aligned}
\bar{\alpha}_{11} &= -\ddot{\theta}_{13}\bar{u}_2 \\
\bar{\alpha}_{9} &= \bar{\alpha}_{11} - \ddot{\theta}_{11}\hat{C}^{(13,11)}\bar{u}_1 - \dot{\theta}_{11}\tilde{\omega}_{11}\hat{C}^{(13,11)}\bar{u}_1 \\
\bar{\alpha}_{7} &= \bar{\alpha}_{9} - \ddot{\theta}_{9}\hat{C}^{(13,9)}\bar{u}_2 - \dot{\theta}_{9}\tilde{\omega}_{9}\hat{C}^{(13,9)}\bar{u}_2 \\
\bar{\alpha}_{5} &= \bar{\alpha}_{7} - \ddot{\theta}_{7}\hat{C}^{(13,7)}\bar{u}_2 - \dot{\theta}_{7}\tilde{\omega}_{7}\hat{C}^{(13,7)}\bar{u}_2 \\
\bar{\alpha}_{3} &= \bar{\alpha}_{5} - \ddot{\theta}_{5}\hat{C}^{(13,5)}\bar{u}_2 - \dot{\theta}_{5}\tilde{\omega}_{5}\hat{C}^{(13,5)}\bar{u}_2 \\
\bar{\alpha}_{1}(\text{right}) &= \bar{\alpha}_{3} - \ddot{\theta}_{3}\hat{C}^{(13,3)}\bar{u}_1 - \dot{\theta}_{3}\tilde{\omega}_{3}\hat{C}^{(13,3)}\bar{u}_1
\end{aligned}
\tag{3.32}
$$

$$
\begin{aligned}
\bar{\alpha}_{8} &= -\ddot{\theta}_{10}\bar{u}_1 \\
\bar{\alpha}_{6} &= \bar{\alpha}_{8} - \ddot{\theta}_{8}\hat{C}^{(10,8)}\bar{u}_2 - \dot{\theta}_{8}\tilde{\omega}_{8}\hat{C}^{(10,8)}\bar{u}_2 \\
\bar{\alpha}_{4} &= \bar{\alpha}_{6} - \ddot{\theta}_{6}\hat{C}^{(10,6)}\bar{u}_2 - \dot{\theta}_{6}\tilde{\omega}_{6}\hat{C}^{(10,6)}\bar{u}_2 \\
\bar{\alpha}_{2} &= \bar{\alpha}_{4} - \ddot{\theta}_{4}\hat{C}^{(10,4)}\bar{u}_2 - \dot{\theta}_{4}\tilde{\omega}_{4}\hat{C}^{(10,4)}\bar{u}_2 \\
\bar{\alpha}_{1}(\text{left}) &= \bar{\alpha}_{2} - \ddot{\theta}_{2}\hat{C}^{(10,2)}\bar{u}_1 - \dot{\theta}_{2}\tilde{\omega}_{2}\hat{C}^{(10,2)}\bar{u}_1
\end{aligned}
\tag{3.33}
$$

At this point, the first part of the acceleration level kinematic constraints of the double support models arises. The following angular acceleration constraint equation embeds three scalar equations:

$$
\bar{\alpha}_{1}(\text{right}) = \bar{\alpha}_{1}(\text{left}) = \bar{\alpha}_{1} \tag{3.34}
$$

After this, the accelerations of the link origins are derived:

$$
\begin{aligned}
\bar{a}_{O_{13}} &= \bar{0} \\
\bar{a}_{O_{11}} &= \bar{a}_{O_{13}} + \left[\tilde{\alpha}_{11} + \tilde{\omega}_{11}^2\right]\hat{C}^{(13,11)}\left(-d_{11}\bar{u}_1 + a_{11}\bar{u}_3\right) \\
\bar{a}_{O_{9}} &= \bar{a}_{O_{11}} \\
\bar{a}_{O_{7}} &= \bar{a}_{O_{9}} + a_7\left[\tilde{\alpha}_{7} + \tilde{\omega}_{7}^2\right]\hat{C}^{(13,7)}\bar{u}_3 \\
\bar{a}_{O_{5}} &= \bar{a}_{O_{7}} + a_5\left[\tilde{\alpha}_{5} + \tilde{\omega}_{5}^2\right]\hat{C}^{(13,5)}\bar{u}_3 \\
\bar{a}_{O_{3}} &= \bar{a}_{O_{5}} \\
\bar{a}_{O_{1}}(\text{right}) &= \bar{a}_{O_{3}} + a_1^r\left[\tilde{\alpha}_{1} + \tilde{\omega}_{1}^2\right]\hat{C}^{(13,1)}\bar{u}_2
\end{aligned}
\tag{3.35}
$$

$$
\begin{aligned}
&\bar{a}_{O_{10}} = \bar{a}_{O_8} = \bar{0} \\
&\bar{a}_{O_6} = \bar{a}_{O_8} + a_6\left[\tilde{\alpha}_6 + \tilde{\omega}_6^2\right]\hat{C}^{(10,6)}\bar{u}_3 \\
&\bar{a}_{O_4} = \bar{a}_{O_6} + a_4\left[\tilde{\alpha}_4 + \tilde{\omega}_4^2\right]\hat{C}^{(10,4)}\bar{u}_3 \\
&\bar{a}_{O_2} = \bar{a}_{O_4} \\
&\bar{a}_{O_1}\left(\text{left}\right) = \bar{a}_{O_2} - a_1^l\left[\tilde{\alpha}_1 + \tilde{\omega}_1^2\right]\hat{C}^{(10,1)}\bar{u}_2
\end{aligned}
\tag{3.36}
$$

Finally, the accelerations of the mass centers are presented:

$$
\begin{aligned}
&\bar{a}_{13} = \bar{0} \\
&\bar{a}_{11} = \bar{a}_{O_{13}} - \left[\tilde{\alpha}_{11} + \tilde{\omega}_{11}^2\right]\hat{C}^{(13,11)}\bar{\ell}_{11,13} \\
&\bar{a}_9 = \bar{a}_{O_9} \\
&\bar{a}_7 = \bar{a}_{O_9} - \left[\tilde{\alpha}_7 + \tilde{\omega}_7^2\right]\hat{C}^{(13,7)}\bar{\ell}_{7,11} \\
&\bar{a}_5 = \bar{a}_{O_7} - \left[\tilde{\alpha}_5 + \tilde{\omega}_5^2\right]\hat{C}^{(13,5)}\bar{\ell}_{5,7} \\
&\bar{a}_1\left(\text{right}\right) = \bar{a}_{O_3} - \left[\tilde{\alpha}_1 + \tilde{\omega}_1^2\right]\hat{C}^{(13,1)}\bar{\ell}_{1,5}
\end{aligned}
\tag{3.37}
$$

$$
\begin{aligned}
&\bar{a}_{10} = \bar{a}_8 = \bar{0} \\
&\bar{a}_6 = \bar{a}_{O_8} - \left[\tilde{\alpha}_6 + \tilde{\omega}_6^2\right]\hat{C}^{(10,6)}\bar{\ell}_{6,10} \\
&\bar{a}_4 = \bar{a}_{O_6} - \left[\tilde{\alpha}_4 + \tilde{\omega}_4^2\right]\hat{C}^{(10,4)}\bar{\ell}_{4,6} \\
&\bar{a}_1\left(\text{left}\right) = \bar{a}_{O_2} - \left[\tilde{\alpha}_1 + \tilde{\omega}_1^2\right]\hat{C}^{(10,1)}\bar{\ell}_{1,4}
\end{aligned}
\tag{3.38}
$$

The last three acceleration level constraint equations can be derived either by $\bar{a}_{O_1}$ or by $\bar{a}_1$. In the simulations, the acceleration of the origin of body-1 was utilized. That is,

$$
\bar{a}_{O_1}\left(\text{right}\right) = \bar{a}_{O_1}\left(\text{left}\right) = \bar{a}_{O_1} \tag{3.39}
$$

3.1.4 Kinematic Equations of the Right Foot Flat Double Support Phase

Through this phase of gait, the right foot (body-11) and the left toe (body-12) are attached to the ground rigidly. Hence, a closed kinematic chain similar to the "left-foot flat double support phase" occurs and brings six scalar constraint equations at each of the position, velocity and acceleration levels. Once more, the

double support model is examined kinematically beneath but this time the left foot sole is fixed. As happened in the single support phase, the “right foot flat double support phase” model is the mirror image of the “left foot flat double support phase” model. The derivation of the kinematic equations starts with the orientation matrices of the left leg segments with respect to the left toe (body-12). These orientation matrices are,

$$\begin{aligned}
\hat{C}^{(12,10)} &= e^{-\tilde{u}_2\theta_{12}} \\
\hat{C}^{(12,8)} &= e^{-\tilde{u}_2\theta_{12}} e^{-\tilde{u}_1\theta_{10}} \\
\hat{C}^{(12,6)} &= e^{-\tilde{u}_2\theta_{12}} e^{-\tilde{u}_1\theta_{10}} e^{-\tilde{u}_2\theta_8} \\
\hat{C}^{(12,4)} &= e^{-\tilde{u}_2\theta_{12}} e^{-\tilde{u}_1\theta_{10}} e^{-\tilde{u}_2(\theta_8+\theta_6)} \\
\hat{C}^{(12,2)} &= e^{-\tilde{u}_2\theta_{12}} e^{-\tilde{u}_1\theta_{10}} e^{-\tilde{u}_2(\theta_8+\theta_6+\theta_4)} \\
\hat{C}^{(12,1)} &= e^{-\tilde{u}_2\theta_{12}} e^{-\tilde{u}_1\theta_{10}} e^{-\tilde{u}_2(\theta_8+\theta_6+\theta_4)} e^{-\tilde{u}_1\theta_2}
\end{aligned} \tag{3.40}$$

Since, the right toe angle (θ_{13}) is zero during the “right foot flat double support phase”, $\hat{C}^{(13,11)}$ is equal to the identity matrix and the orientations of the right leg segments can be written with respect to the right foot (body-11) instead of the right toe (body-13).

$$\begin{aligned}
\hat{C}^{(11,9)} &= e^{-\tilde{u}_1\theta_{11}} \\
\hat{C}^{(11,7)} &= e^{-\tilde{u}_1\theta_{11}} e^{-\tilde{u}_2\theta_9} \\
\hat{C}^{(11,5)} &= e^{-\tilde{u}_1\theta_{11}} e^{-\tilde{u}_2(\theta_9+\theta_7)} \\
\hat{C}^{(11,3)} &= e^{-\tilde{u}_1\theta_{11}} e^{-\tilde{u}_2(\theta_5+\theta_7+\theta_9)} \\
\hat{C}^{(11,1)} &= e^{-\tilde{u}_1\theta_{11}} e^{-\tilde{u}_2(\theta_5+\theta_7+\theta_9)} e^{-\tilde{u}_1\theta_3}
\end{aligned} \tag{3.41}$$

At this point, it must be declared that;

$$\hat{C}^{(12,1)} = \hat{C}^{(11,1)} \tag{3.42}$$

It was noted in the previous chapter that Equation (3.40) results three scalar constraint equations of the “right foot flat double support phase”.

Starting from the left motionless point O_{12}, the position vectors of the link origins of this model are given below:

$$
\begin{aligned}
\overline{p}_{O_{10}} &= \overline{p}_{O_{12}} + \hat{C}^{(12,10)}\left(-d_{10}\overline{u}_1 + a_{10}\overline{u}_3\right) \\
\overline{p}_{A_{10}} &= \overline{p}_{O_{12}} - \hat{C}^{(12,10)} d_{10}\overline{u}_1 \\
\overline{p}_{O_6} &= \overline{p}_{O_{10}} + a_6\hat{C}^{(12,6)}\overline{u}_3 \\
\overline{p}_{O_4} &= \overline{p}_{O_6} + a_4\hat{C}^{(12,4)}\overline{u}_3 \\
\overline{p}_{O_1}\left(\text{left}\right) &= \overline{p}_{O_4} - a_1^l\hat{C}^{(12,1)}\overline{u}_2
\end{aligned}
\tag{3.43}
$$

Starting from the right stationary point O_{11}, the position vector of the origin of link-1 is also obtained same as the preceding one:

$$
\begin{aligned}
\overline{p}_{O_7} &= \overline{p}_{O_{11}} + a_7\hat{C}^{(11,7)}\overline{u}_3 \\
\overline{p}_{O_5} &= \overline{p}_{O_7} + a_5\hat{C}^{(11,5)}\overline{u}_3 \\
\overline{p}_{O_1}(\text{right}) &= \overline{p}_{O_5} + a_1^r\hat{C}^{(11,1)}\overline{u}_2
\end{aligned}
\tag{3.44}
$$

The three constraint equations are represented in column matrix form as

$$
\overline{p}_{O_1}(\text{right}) = \overline{p}_{O_1}(\text{left}) = \overline{p}_{O_1} \tag{3.45}
$$

The position vectors of the mass centers in the “right foot flat double support phase”, with respect to the origin on the ground are as follow:

$$
\begin{aligned}
\overline{p}_{10} &= \overline{p}_{O_{10}} - \hat{C}^{(12,10)}\overline{\ell}_{10,6} \\
\overline{p}_6 &= \overline{p}_{O_6} - \hat{C}^{(12,6)}\overline{\ell}_{6,4} \\
\overline{p}_4 &= \overline{p}_{O_4} - \hat{C}^{(12,4)}\overline{\ell}_{4,1} \\
\overline{p}_1\left(\text{left}\right) &= \overline{p}_{O_1}\left(\text{left}\right) + c_1\hat{C}^{(12,1)}\overline{u}_3
\end{aligned}
\tag{3.46}
$$

$$
\begin{aligned}
\overline{p}_7 &= \overline{p}_{O_7} - \hat{C}^{(11,7)}\overline{\ell}_{7,5} \\
\overline{p}_5 &= \overline{p}_{O_5} - \hat{C}^{(11,5)}\overline{\ell}_{5,1} \\
\overline{p}_1\left(\text{right}\right) &= \overline{p}_{O_1}\left(\text{right}\right) + c_1\hat{C}^{(11,1)}\overline{u}_3
\end{aligned}
\tag{3.47}
$$

The angular velocities of the links during this phase are listed by the following equations:

$$
\begin{aligned}
&\bar{\omega}_{10} = -\dot{\theta}_{12}\bar{u}_2 \\
&\bar{\omega}_8 = \bar{\omega}_{10} - \dot{\theta}_{10}\hat{C}^{(12,10)}\bar{u}_1 \\
&\bar{\omega}_6 = \bar{\omega}_8 - \dot{\theta}_8\hat{C}^{(12,8)}\bar{u}_2 \\
&\bar{\omega}_4 = \bar{\omega}_6 - \dot{\theta}_6\hat{C}^{(12,6)}\bar{u}_2 \\
&\bar{\omega}_2 = \bar{\omega}_4 - \dot{\theta}_4\hat{C}^{(12,4)}\bar{u}_2 \\
&\bar{\omega}_1(\text{left}) = \bar{\omega}_2 - \dot{\theta}_2\hat{C}^{(12,2)}\bar{u}_1
\end{aligned}
\tag{3.48}
$$

$$
\begin{aligned}
&\bar{\omega}_9 = -\dot{\theta}_{11}\bar{u}_1 \\
&\bar{\omega}_7 = \bar{\omega}_9 - \dot{\theta}_9\hat{C}^{(11,9)}\bar{u}_2 \\
&\bar{\omega}_5 = \bar{\omega}_7 - \dot{\theta}_7\hat{C}^{(11,7)}\bar{u}_2 \\
&\bar{\omega}_3 = \bar{\omega}_5 - \dot{\theta}_5\hat{C}^{(11,5)}\bar{u}_2 \\
&\bar{\omega}_1(\text{right}) = \bar{\omega}_3 - \dot{\theta}_3\hat{C}^{(11,3)}\bar{u}_1
\end{aligned}
\tag{3.49}
$$

These angular velocity calculations end up with three scalar velocity constraint equations shown below:

$$
\bar{\omega}_1(\text{right}) = \bar{\omega}_1(\text{left}) = \bar{\omega}_1 \tag{3.50}
$$

The velocities of the link origins are presented as follows:

$$
\begin{aligned}
&\bar{v}_{O_{12}} = \bar{0} \\
&\bar{v}_{O_{10}} = \bar{v}_{O_{12}} + \tilde{\omega}_{10}\hat{C}^{(12,10)}\left(-d_{10}\bar{u}_1 + a_{10}\bar{u}_3\right) \\
&\bar{v}_{O_8} = \bar{v}_{O_{10}} \\
&\bar{v}_{O_6} = \bar{v}_{O_8} + a_6\tilde{\omega}_6\hat{C}^{(12,6)}\bar{u}_3 \\
&\bar{v}_{O_4} = \bar{v}_{O_6} + a_4\tilde{\omega}_4\hat{C}^{(12,4)}\bar{u}_3 \\
&\bar{v}_{O_2} = \bar{v}_{O_4} \\
&\bar{v}_{O_1}(\text{left}) = \bar{v}_{O_2} - a_1^l\tilde{\omega}_1\hat{C}^{(12,1)}\bar{u}_2
\end{aligned}
\tag{3.51}
$$

$$
\begin{aligned}
&\bar{v}_{O_{11}} = \bar{v}_{O_9} = \bar{0} \\
&\bar{v}_{O_7} = \bar{v}_{O_9} + a_7 \tilde{\omega}_7 \hat{C}^{(11,7)} \bar{u}_3 \\
&\bar{v}_{O_5} = \bar{v}_{O_7} + a_5 \tilde{\omega}_5 \hat{C}^{(11,5)} \bar{u}_3 \\
&\bar{v}_{O_3} = \bar{v}_{O_5} \\
&\bar{v}_{O_1}\left(\text{right}\right) = \bar{v}_{O_3} + a_1^r \tilde{\omega}_1 \hat{C}^{(11,1)} \bar{u}_2
\end{aligned}
\tag{3.52}
$$

The last three scalar constraint equations at the velocity level come arise as

$$
\bar{v}_{O_1}\left(\text{right}\right) = \bar{v}_{O_1}\left(\text{left}\right) = \bar{v}_{O_1} \tag{3.53}
$$

The angular accelerations of the links in the “right foot flat double support phase” can be obtained in the consequent manner:

$$
\begin{aligned}
&\bar{\alpha}_{10} = -\ddot{\theta}_{12} \bar{u}_2 \\
&\bar{\alpha}_8 = \bar{\alpha}_{10} - \ddot{\theta}_{10} \hat{C}^{(12,10)} \bar{u}_1 - \dot{\theta}_{10} \tilde{\omega}_{10} \hat{C}^{(12,10)} \bar{u}_1 \\
&\bar{\alpha}_6 = \bar{\alpha}_8 - \ddot{\theta}_8 \hat{C}^{(12,8)} \bar{u}_2 - \dot{\theta}_8 \tilde{\omega}_8 \hat{C}^{(12,8)} \bar{u}_2 \\
&\bar{\alpha}_4 = \bar{\alpha}_6 - \ddot{\theta}_6 \hat{C}^{(12,6)} \bar{u}_2 - \dot{\theta}_6 \tilde{\omega}_6 \hat{C}^{(12,6)} \bar{u}_2 \\
&\bar{\alpha}_2 = \bar{\alpha}_4 - \ddot{\theta}_4 \hat{C}^{(12,4)} \bar{u}_2 - \dot{\theta}_4 \tilde{\omega}_4 \hat{C}^{(12,4)} \bar{u}_2 \\
&\bar{\alpha}_1\left(\text{left}\right) = \bar{\alpha}_2 - \ddot{\theta}_2 \hat{C}^{(12,2)} \bar{u}_1 - \dot{\theta}_2 \tilde{\omega}_2 \hat{C}^{(12,2)} \bar{u}_1
\end{aligned}
\tag{3.54}
$$

$$
\begin{aligned}
&\bar{\alpha}_9 = -\ddot{\theta}_{11} \bar{u}_1 \\
&\bar{\alpha}_7 = \bar{\alpha}_9 - \ddot{\theta}_9 \hat{C}^{(11,9)} \bar{u}_2 - \dot{\theta}_9 \tilde{\omega}_9 \hat{C}^{(11,9)} \bar{u}_2 \\
&\bar{\alpha}_5 = \bar{\alpha}_7 - \ddot{\theta}_7 \hat{C}^{(11,7)} \bar{u}_2 - \dot{\theta}_7 \tilde{\omega}_7 \hat{C}^{(11,7)} \bar{u}_2 \\
&\bar{\alpha}_3 = \bar{\alpha}_5 - \ddot{\theta}_5 \hat{C}^{(11,5)} \bar{u}_2 - \dot{\theta}_5 \tilde{\omega}_5 \hat{C}^{(11,5)} \bar{u}_2 \\
&\bar{\alpha}_1\left(\text{right}\right) = \bar{\alpha}_3 - \ddot{\theta}_3 \hat{C}^{(11,3)} \bar{u}_1 - \dot{\theta}_3 \tilde{\omega}_3 \hat{C}^{(11,3)} \bar{u}_1
\end{aligned}
\tag{3.55}
$$

The next expression carries out three of six scalar constraint equations corresponding to acceleration level.

$$
\bar{\alpha}_1\left(\text{right}\right) = \bar{\alpha}_1\left(\text{left}\right) = \bar{\alpha}_1 \tag{3.56}
$$

The, the accelerations of the link origins are obtained.

$$
\begin{aligned}
&\bar{a}_{O_{12}} = \bar{0} \\
&\bar{a}_{O_{10}} = \bar{a}_{O_{12}} + \left[\tilde{\alpha}_{10} + \tilde{\omega}_{10}^2\right]\hat{C}^{(12,10)}\left(-d_{10}\bar{u}_1 + a_{10}\bar{u}_3\right) \\
&\bar{a}_{O_8} = \bar{a}_{O_{10}} \\
&\bar{a}_{O_6} = \bar{a}_{O_8} + a_6\left[\tilde{\alpha}_6 + \tilde{\omega}_6^2\right]\hat{C}^{(12,6)}\bar{u}_3 \\
&\bar{a}_{O_4} = \bar{a}_{O_6} + a_4\left[\tilde{\alpha}_4 + \tilde{\omega}_4^2\right]\hat{C}^{(12,4)}\bar{u}_3 \\
&\bar{a}_{O_2} = \bar{a}_{O_4} \\
&\bar{a}_{O_1}\left(\text{left}\right) = \bar{a}_{O_2} - a_1^l\left[\tilde{\alpha}_1 + \tilde{\omega}_1^2\right]\hat{C}^{(12,1)}\bar{u}_2
\end{aligned}
\tag{3.57}
$$

$$
\begin{aligned}
&\bar{a}_{O_{11}} = \bar{a}_{O_9} = \bar{0} \\
&\bar{a}_{O_7} = \bar{a}_{O_9} + a_7\left[\tilde{\alpha}_7 + \tilde{\omega}_7^2\right]\hat{C}^{(11,7)}\bar{u}_3 \\
&\bar{a}_{O_5} = \bar{a}_{O_7} + a_5\left[\tilde{\alpha}_5 + \tilde{\omega}_5^2\right]\hat{C}^{(11,5)}\bar{u}_3 \\
&\bar{a}_{O_3} = \bar{a}_{O_5} \\
&\bar{a}_{O_1}\left(\text{right}\right) = \bar{a}_{O_3} + a_1^r\left[\tilde{\alpha}_1 + \tilde{\omega}_1^2\right]\hat{C}^{(11,1)}\bar{u}_2
\end{aligned}
\tag{3.58}
$$

As the final kinematic expressions, the accelerations of the mass centers are presented.

$$
\begin{aligned}
&\bar{a}_{12} = \bar{0} \\
&\bar{a}_{10} = \bar{a}_{O_{12}} - \left[\tilde{\alpha}_{10} + \tilde{\omega}_{10}^2\right]\hat{C}^{(12,10)}\bar{\ell}_{10,12} \\
&\bar{a}_8 = \bar{a}_{O_8} \\
&\bar{a}_6 = \bar{a}_{O_8} - \left[\tilde{\alpha}_6 + \tilde{\omega}_6^2\right]\hat{C}^{(12,6)}\bar{\ell}_{6,10} \\
&\bar{a}_4 = \bar{a}_{O_6} - \left[\tilde{\alpha}_4 + \tilde{\omega}_4^2\right]\hat{C}^{(12,4)}\bar{\ell}_{4,6} \\
&\bar{a}_1\left(\text{left}\right) = \bar{a}_{O_2} - \left[\tilde{\alpha}_1 + \tilde{\omega}_1^2\right]\hat{C}^{(12,1)}\bar{\ell}_{1,4}
\end{aligned}
\tag{3.59}
$$

$$
\begin{aligned}
&\bar{a}_{11} = \bar{a}_9 = \bar{0} \\
&\bar{a}_7 = \bar{a}_{O_9} - \left[\tilde{\alpha}_7 + \tilde{\omega}_7^2\right]\hat{C}^{(11,7)}\bar{\ell}_{7,11} \\
&\bar{a}_5 = \bar{a}_{O_7} - \left[\tilde{\alpha}_5 + \tilde{\omega}_5^2\right]\hat{C}^{(11,5)}\bar{\ell}_{5,7} \\
&\bar{a}_1\left(\text{right}\right) = \bar{a}_{O_3} - \left[\tilde{\alpha}_1 + \tilde{\omega}_1^2\right]\hat{C}^{(11,1)}\bar{\ell}_{1,5}
\end{aligned}
\tag{3.60}
$$

The last three scalar acceleration level constraint equations can be derived using the above equation groups. The following expression includes these last three scalar constraint equations of the “right foot flat double support phase”.

$$\bar{a}_{O_1}\left(\text{right}\right) = \bar{a}_{O_1}\left(\text{left}\right) = \bar{a}_{O_1} \tag{3.61}$$

During this simulation study, all the above kinematic equations are converted into Matlab® codes and written in m-files. For each of the models, the kinematic expressions are collected into one separate m-file. So, a total of four m-files are developed for the kinematic expressions.

3.2 Dynamic Equations

The dynamic equations are essential mainly in two parts of the simulation. The first one of these parts is the plant which demonstrates the state of the model at any instant producing the joint accelerations, the reaction forces and the reaction moments. This can also be called as the direct dynamics solution. The second part comprises the computed torque algorithm which produces the required joint torques for the desired motion.

In this study, the Newton – Euler formulation was used to generate the dynamic equations. Therefore, 3 scalar Newton equations correspond to translation and 3 scalar Euler equations correspond to rotation were derived for each body. The body fixed frames were chosen as the resolution frames for every body in these equations. For this reason, the velocities and the accelerations found in the previous sections must be multiplied by the appropriate transformation matrices to alter their resolution frames.

The reaction forces and moments between the bodies are also obtained by the help of Newton – Euler equations. According to the “Newton’s Third Law of Motion”, the following relations are used in the dynamic equations:

$$\vec{\bar{F}}_{i,j} = -\vec{\bar{F}}_{j,i}$$

and

$$\vec{\bar{M}}_{i,j} = -\vec{\bar{M}}_{j,i}$$

The reaction forces and the reaction moments are different at each one of the four models. These reactions are considered in the dynamic equations of that model and computed by the direct dynamic solution. In Figure 3.2, some sample reactions are illustrated. The convention used in the indices can be realized better by the reactions between body-5/body-7 and body-7/body-10.

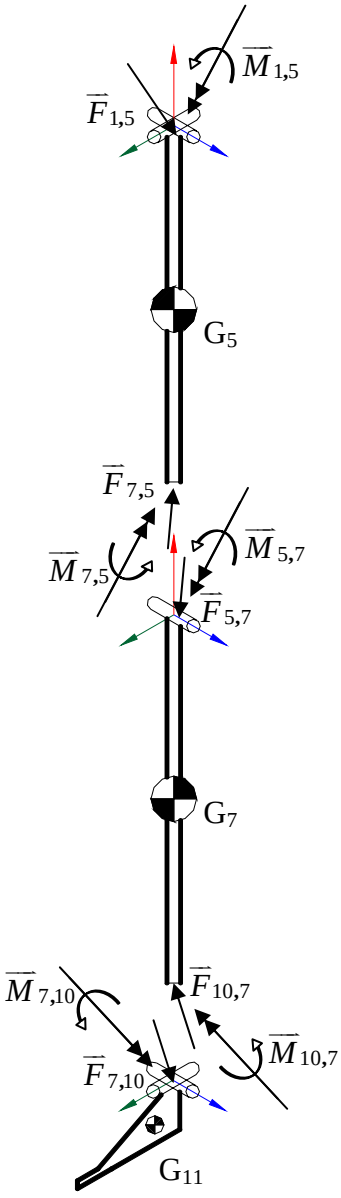

Figure 3.2 Representation of some reaction forces and moments

Another key subject about the dynamic equations is the gravitational acceleration vector. As any other term of the equations, they are also resolved in the body fixed frames. The details of these vectors are given below.

$$\begin{aligned}
\bar{g}_1^{(1)} &= -g\hat{C}^{(1,0)}\bar{u}_3 \\
\bar{g}_4^{(4)} &= -g\hat{C}^{(4,0)}\bar{u}_3 \\
\bar{g}_5^{(5)} &= -g\hat{C}^{(5,0)}\bar{u}_3 \\
\bar{g}_6^{(6)} &= -g\hat{C}^{(6,0)}\bar{u}_3 \\
\bar{g}_7^{(7)} &= -g\hat{C}^{(7,0)}\bar{u}_3 \\
\bar{g}_{10}^{(10)} &= -g\hat{C}^{(10,0)}\bar{u}_3 \\
g_{11}^{(11)} &= -g\hat{C}^{(11,0)}\bar{u}_3
\end{aligned} \tag{3.62}$$

In these expressions, “0” stands for the earth fixed frame and “g” (gravity) is taken as 9.81 m/s^2.

Moreover, the Euler equations and the inertia tensors are expressed about the mass centers. Hence, there appear no moment terms in the Euler equations due to the weights of the bodies.

In the following sections, the Newton – Euler equations belonging to each phase were presented for the aim of plant’s explanation. The solution of these equations is discussed for four different simulation models. In advance, the computed torque algorithm is clarified by the related modifications of these Newton – Euler equations.

3.2.1 Newton-Euler Equations of the Left Foot Flat Single Support Phase

In this phase, the model is composed of 6 bodies, which are connected to each other by 10 joints. 36 scalar Newton – Euler equations belong to these bodies are given in matrix form starting from the left shank (body-6):

Body-6:

$$m_6\bar{a}_6^{(6)} = \bar{F}_{10,6}^{(6)} + \bar{F}_{4,6}^{(6)} + m_6\bar{g}^{(6)} \tag{3.63}$$

$$\hat{J}_6^{(6)}\bar{\alpha}_6^{(6)} + \tilde{\omega}_6^{(6)}\hat{J}_6^{(6)}\bar{\omega}_6^{(6)} = \bar{M}_{10,6}^{(6)} + \bar{M}_{4,6}^{(6)} + \tilde{\ell}_{6,4}\bar{F}_{4,6}^{(6)} + \tilde{\ell}_{6,10}\bar{F}_{10,6}^{(6)} \tag{3.64}$$

Body-4:

$$m_4\bar{a}_4^{(4)} = -\hat{C}^{(4,6)}\bar{F}_{4,6}^{(6)} + \bar{F}_{1,4}^{(4)} + m_4\bar{g}^{(4)} \tag{3.65}$$

$$\hat{J}_4^{(4)}\bar{\alpha}_4^{(4)} + \tilde{\omega}_4^{(4)}\hat{J}_4^{(4)}\bar{\omega}_4^{(4)} = -\hat{C}^{(4,6)}\bar{M}_{4,6}^{(6)} + \bar{M}_{1,4}^{(4)} - \tilde{\ell}_{4/6}\hat{C}^{(4,6)}\bar{F}_{4,6}^{(6)} + \tilde{\ell}_{4,1}\bar{F}_{1,4}^{(4)} \tag{3.66}$$

Body-1:

$$m_1\bar{a}_1^{(1)} = -\bar{F}_{1,5}^{(1)} - \hat{C}^{(1,4)}\bar{F}_{1,4}^{(4)} + m_1\bar{g}^{(1)} \tag{3.67}$$

$$\hat{J}_1^{(1)}\bar{\alpha}_1^{(1)} + \tilde{\omega}_1^{(1)}\hat{J}_1^{(1)}\bar{\omega}_1^{(1)} = -\bar{M}_{1,5}^{(1)} - \hat{C}^{(1,4)}\bar{M}_{1,4}^{(4)} - \tilde{\ell}_{1,5}\bar{F}_{1,5}^{(1)} - \tilde{\ell}_{1,4}\hat{C}^{(1,4)}\bar{F}_{1,4}^{(4)} \tag{3.68}$$

Body-5:

$$m_5\bar{a}_5^{(5)} = \hat{C}^{(5,1)}\bar{F}_{1,5}^{(1)} - \bar{F}_{5,7}^{(5)} + m_5\bar{g}^{(5)} \tag{3.69}$$

$$\hat{J}_5^{(5)}\bar{\alpha}_5^{(5)} + \tilde{\omega}_5^{(5)}\hat{J}_5^{(5)}\bar{\omega}_5^{(5)} = \hat{C}^{(5,1)}\bar{M}_{1,5}^{(1)} - \bar{M}_{5,7}^{(5)} + \tilde{\ell}_{5,1}\hat{C}^{(5,1)}\bar{F}_{1,5}^{(1)} - \tilde{\ell}_{5,7}\bar{F}_{5,7}^{(5)} \tag{3.70}$$

Body-7:

$$m_7\bar{a}_7^{(7)} = \hat{C}^{(7,5)}\bar{F}_{5,7}^{(5)} - \bar{F}_{7,11}^{(7)} + m_7\bar{g}^{(7)} \tag{3.71}$$

$$\hat{J}_7^{(7)}\bar{\alpha}_7^{(7)} + \tilde{\omega}_7^{(7)}\hat{J}_7^{(7)}\bar{\omega}_7^{(7)} = \hat{C}^{(7,5)}\bar{M}_{5,7}^{(5)} - \bar{M}_{7,11}^{(7)} + \tilde{\ell}_{7,5}\hat{C}^{(7,5)}\bar{F}_{5,7}^{(5)} - \tilde{\ell}_{7,11}\bar{F}_{7,11}^{(7)} \tag{3.72}$$

Body-11:

$$m_{11}\bar{a}_{11}^{(11)} = \hat{C}^{(11,7)}\bar{F}_{7,11}^{(7)} + m_{11}\bar{g}^{(11)} \tag{3.73}$$

$$\hat{J}_{11}^{(11)}\bar{\alpha}_{11}^{(11)} + \tilde{\omega}_{11}^{(11)}\hat{J}_{11}^{(11)}\bar{\omega}_{11}^{(11)} = \hat{C}^{(11,7)}\bar{M}_{7,11}^{(7)} + \tilde{\ell}_{11,7}\hat{C}^{(11,7)}\bar{F}_{7,11}^{(7)} \tag{3.74}$$

There are totally 36 unknowns in these equations for direct dynamics purposes. In Table 3.1, these unknowns are shown.

Table 3.1 The unknowns in the left foot flat single support phase

Types of unknowns	Names of unknowns	Number of unknowns
Joint Accelerations	$\ddot{\theta}_{10}, \ddot{\theta}_8, \ddot{\theta}_6, \ddot{\theta}_4, \ddot{\theta}_2, \ddot{\theta}_3, \ddot{\theta}_5, \ddot{\theta}_7, \ddot{\theta}_9, \ddot{\theta}_{11}$	10
Reaction Forces	$\bar{F}_{10,6}^{(6)}, \bar{F}_{4,6}^{(6)}, \bar{F}_{1,4}^{(4)}, \bar{F}_{1,5}^{(1)}, \bar{F}_{5,7}^{(5)}, \bar{F}_{7,11}^{(7)}$	18
Reaction Moments	$M_{10,6}^{(6)z}, M_{4,6}^{(6)x}, M_{4,6}^{(6)z}, M_{1,4}^{(4)z}, M_{1,5}^{(1)z}, M_{5,7}^{(5)x}, M_{5,7}^{(5)z}, M_{7,11}^{(7)z}$	8

In the “left foot flat single support phase”, the number of dynamic equations is equal to the number of unknowns. Hence, the solution is available using the Newton – Euler equations.

The matrix inversion method is used to find these unknowns. For both of the single support phase models, a 36 by 36 coefficient matrix ($\hat{\Gamma}$) is build. For this purpose, the coefficients are detached from the unknowns in each of the 36 scalar dynamic equations and they are sorted properly in the matrix, $\hat{\Gamma}$. It is a hard process to examine 10 unknown joint accelerations in every acceleration term of the dynamic equations and the coefficients of 26 unknown reaction components. For a better demonstration, this coefficient matrix is illustrated by a table in the Appendices. In the m-files corresponding to the “left foot flat single support phase” dynamic equations, these coefficients are written in detail.

The remaining part of the dynamic equations is the position and velocity relevant known terms. For the solution, they are collected into a column matrix. This column matrix also includes 10 actuating torque values which come from the computed torque control block.

As a result, 36 Newton – Euler equations of the "left foot flat single support phase" model are represented in the following form.

$$\hat{\Gamma}_{(36x36)} \begin{bmatrix} \ddot{\bar{q}} \\ \bar{F} \\ \bar{M} \end{bmatrix}_{(36x1)} = \bar{K}_{(36x1)} \tag{3.75}$$

where

$\hat{\Gamma}$ is the coefficient matrix

$\begin{bmatrix} \ddot{\bar{q}} \\ \bar{F} \\ \bar{M} \end{bmatrix}$ is the vector of unknowns

$\bar{K}$ is the vector of knowns

Thus, the direct dynamics solution is accomplished via the following equation unless the coefficient matrix is singular.

$$\begin{bmatrix} \ddot{\bar{q}} \\ \bar{F} \\ \bar{M} \end{bmatrix} = \hat{\Gamma}^{-1} \bar{K} \tag{3.76}$$

At every step of simulation, the elements of $\hat{\Gamma}$ and $\bar{K}$ matrices are calculated again with the new joint variables and actuating torques. Then, the coefficient matrix is inverted and 36 unknown parameters are obtained. This process iterates until the next simulation phase.

3.2.2 Newton-Euler Equations of the Right Foot Flat Single Support Phase

The left foot (body-10) swings in the air through this phase, while the right foot (body-11) is stationary on the ground. The dynamic equations are derived using the Newton – Euler formulation. Since this model has six bodies, again, 36 scalar equations of motion are written to find the unknown joint accelerations and reactions. The dynamic equations of the "right foot flat single support phase" are given below in matrix form starting from the right shank (body-7):

Body-7:

$$m_7\bar{a}_7^{(7)} = \bar{F}_{11,7}^{(7)} + \bar{F}_{5,7}^{(7)} + m_7\bar{g}^{(7)} \tag{3.77}$$

$$\hat{J}_7^{(7)}\bar{\alpha}_7^{(7)} + \tilde{\omega}_7^{(7)}\hat{J}_7^{(7)}\bar{\omega}_7^{(7)} = \bar{M}_{11,7}^{(7)} + \bar{M}_{5,7}^{(7)} + \tilde{\ell}_{7,5}\bar{F}_{5,7}^{(7)} + \tilde{\ell}_{7,11}\bar{F}_{11,7}^{(7)} \tag{3.78}$$

Body-5:

$$m_5\bar{a}_5^{(5)} = -\hat{C}^{(5,7)}\bar{F}_{5,7}^{(7)} + \bar{F}_{1,5}^{(5)} + m_5\bar{g}^{(5)} \tag{3.79}$$

$$\begin{aligned}\hat{J}_5^{(5)}\bar{\alpha}_5^{(5)} + \tilde{\omega}_5^{(5)}\hat{J}_5^{(5)}\bar{\omega}_5^{(5)} = &-\hat{C}^{(5,7)}\bar{M}_{5,7}^{(7)} + \bar{M}_{1,5}^{(5)} - \tilde{\ell}_{5,7}\hat{C}^{(5,7)}\bar{F}_{5,7}^{(7)} \\ &+ \tilde{\ell}_{5,1}\bar{F}_{1,5}^{(5)}\end{aligned} \tag{3.80}$$

Body-1:

$$m_1\bar{a}_1^{(1)} = -\bar{F}_{1,4}^{(1)} - \hat{C}^{(1,5)}\bar{F}_{1,5}^{(5)} + m_1\bar{g}^{(1)} \tag{3.81}$$

$$\begin{aligned}\hat{J}_1^{(1)}\bar{\alpha}_1^{(1)} + \tilde{\omega}_1^{(1)}\hat{J}_1^{(1)}\bar{\omega}_1^{(1)} = &-\bar{M}_{1,4}^{(1)} - \hat{C}^{(1,5)}\bar{M}_{1,5}^{(5)} - \tilde{\ell}_{1,4}\bar{F}_{1,4}^{(1)} \\ &- \tilde{\ell}_{1,5}\hat{C}^{(1,5)}\bar{F}_{1,5}^{(5)}\end{aligned} \tag{3.82}$$

Body-4:

$$m_4\bar{a}_4^{(4)} = \hat{C}^{(4,1)}\bar{F}_{1,4}^{(1)} - \bar{F}_{4,6}^{(4)} + m_4\bar{g}^{(4)} \tag{3.83}$$

$$\begin{aligned}\hat{J}_4^{(4)}\bar{\alpha}_4^{(4)} + \tilde{\omega}_4^{(4)}\hat{J}_4^{(4)}\bar{\omega}_4^{(4)} = &\hat{C}^{(4,1)}\bar{M}_{1,4}^{(1)} - \bar{M}_{4,6}^{(4)} + \tilde{\ell}_{4,1}\hat{C}^{(4,1)}\bar{F}_{1,4}^{(1)} \\ &- \tilde{\ell}_{4,6}\bar{F}_{4,6}^{(4)}\end{aligned} \tag{3.84}$$

Body-6:

$$m_6\bar{a}_6^{(6)} = \hat{C}^{(6,4)}\bar{F}_{4,6}^{(4)} - \bar{F}_{6,10}^{(6)} + m_6\bar{g}^{(6)} \tag{3.85}$$

$$\begin{aligned}\hat{J}_6^{(6)}\bar{\alpha}_6^{(6)} + \tilde{\omega}_6^{(6)}\hat{J}_6^{(6)}\bar{\omega}_6^{(6)} = &\hat{C}^{(6,4)}\bar{M}_{4,6}^{(4)} - \bar{M}_{6,10}^{(6)} \\ &+ \tilde{\ell}_{6,4}\hat{C}^{(6,4)}\bar{F}_{4,6}^{(4)} - \tilde{\ell}_{6,10}\bar{F}_{6,10}^{(6)}\end{aligned} \tag{3.86}$$

Body-10:

$$m_{10}\bar{a}_{10}^{(10)} = \hat{C}^{(10,6)}\bar{F}_{6,10}^{(6)} + m_{10}\bar{g}^{(10)} \tag{3.87}$$

$$\hat{J}_{10}^{(10)}\bar{\alpha}_{10}^{(10)} + \tilde{\omega}_{10}^{(10)}\hat{J}_{10}^{(10)}\bar{\omega}_{10}^{(10)} = \hat{C}^{(10,6)}\bar{M}_{6,10}^{(6)} + \tilde{\ell}_{10,6}\hat{C}^{(10,6)}\bar{F}_{6,10}^{(6)} \tag{3.88}$$

There are 36 unknowns in these equations. These are presented in Table 3.2.

Table 3.2 The unknowns in the right foot flat single support phase

Types of unknowns	Names of unknowns	Number of unknowns
Joint Accelerations	$\ddot{\theta}_{11}, \ddot{\theta}_{9}, \ddot{\theta}_{7}, \ddot{\theta}_{5}, \ddot{\theta}_{3}, \ddot{\theta}_{2}, \ddot{\theta}_{4}, \ddot{\theta}_{6}, \ddot{\theta}_{8}, \ddot{\theta}_{10}$	10
Reaction Forces	$\bar{F}_{11,7}^{(7)}, \bar{F}_{5,7}^{(7)}, \bar{F}_{1,5}^{(5)}, \bar{F}_{1,4}^{(1)}, \bar{F}_{4,6}^{(4)}, \bar{F}_{6,10}^{(6)}$	18
Reaction Moments	$M_{11,7}^{(7)z}, M_{5,7}^{(7)x}, M_{5,7}^{(7)z}, M_{1,5}^{(5)z},$ $M_{1,4}^{(1)z}, M_{4,6}^{(4)x}, M_{4,6}^{(4)z}, M_{6,10}^{(6)z}$	8

The operations are performed in the same way as the previous single support phase. After that, in the next part of the simulations, the resulting joint accelerations are integrated once to get the joint velocities and once again to get the joint angular displacements.

3.2.3 Newton-Euler Equations of the Left Foot Flat Double Support Phase

As mentioned in Chapter 2, the "left foot flat double support phase" model includes 6 bodies which are connected to each other by 11 joints. Below, 36 scalar Newton – Euler equations of these bodies in matrix form starting from the right foot (body-11) are given:

Body-11:

$$m_{11}\bar{a}_{11}^{(11)} = -\hat{C}^{(11,13)}\bar{F}_{11,13}^{(13)} + \bar{F}_{7,11}^{(11)} + m_{11}\bar{g}^{(11)} \tag{3.89}$$

$$\begin{aligned}\hat{J}_{11}^{(11)}\bar{\alpha}_{11}^{(11)} + \tilde{\omega}_{11}^{(11)}\hat{J}_{11}^{(11)}\bar{\omega}_{11}^{(11)} = &-\hat{C}^{(11,13)}\bar{M}_{11,13}^{(13)} + \bar{M}_{7,11}^{(11)} \\ &- \tilde{\ell}_{11,13}\hat{C}^{(11,13)}\bar{F}_{11,13}^{(13)} + \tilde{\ell}_{11,7}\bar{F}_{7,11}^{(11)}\end{aligned} \tag{3.90}$$

Body-7:

$$m_7\bar{a}_7^{(7)} = -\hat{C}^{(7,11)}\bar{F}_{7,11}^{(11)} + \bar{F}_{5,7}^{(7)} + m_7\bar{g}^{(7)} \tag{3.91}$$

$$\begin{aligned}\hat{J}_7^{(7)}\bar{\alpha}_7^{(7)} + \tilde{\omega}_7^{(7)}\hat{J}_7^{(7)}\bar{\omega}_7^{(7)} = &-\hat{C}^{(7,11)}\bar{M}_{7,11}^{(11)} + \bar{M}_{5,7}^{(7)} \\ &- \tilde{\ell}_{7,11}\hat{C}^{(7,11)}\bar{F}_{7,11}^{(11)} + \tilde{\ell}_{7,5}\bar{F}_{5,7}^{(7)}\end{aligned} \tag{3.92}$$

Body-5:

$$m_5\bar{a}_5^{(5)} = -\hat{C}^{(5,7)}\bar{F}_{5,7}^{(7)} + \bar{F}_{1,5}^{(5)} + m_5\bar{g}^{(5)} \tag{3.93}$$

$$\begin{aligned}\hat{J}_5^{(5)}\bar{\alpha}_5^{(5)} + \tilde{\omega}_5^{(5)}\hat{J}_5^{(5)}\bar{\omega}_5^{(5)} = &-\hat{C}^{(5,7)}\bar{M}_{5,7}^{(7)} + \bar{M}_{1,5}^{(5)} \\ &- \tilde{\ell}_{5,7}\hat{C}^{(5,7)}\bar{F}_{5,7}^{(7)} + \tilde{\ell}_{5,1}\bar{F}_{1,5}^{(5)}\end{aligned} \tag{3.94}$$

Body-1:

$$m_1\bar{a}_1^{(1)} = \bar{F}_{4,1}^{(1)} - \hat{C}^{(1,5)}\bar{F}_{1,5}^{(5)} + m_1\bar{g}^{(1)} \tag{3.95}$$

$$\begin{aligned}\hat{J}_1^{(1)}\bar{\alpha}_1^{(1)} + \tilde{\omega}_1^{(1)}\hat{J}_1^{(1)}\bar{\omega}_1^{(1)} = &-\hat{C}^{(1,5)}\bar{M}_{1,5}^{(5)} - \hat{C}^{(1,4)}\bar{M}_{1,4}^{(4)} \\ &- \tilde{\ell}_{1,5}\hat{C}^{(1,5)}\bar{F}_{1,5}^{(5)} + \tilde{\ell}_{1,4}\bar{F}_{4,1}^{(1)}\end{aligned} \tag{3.96}$$

Body-4:

$$m_4\bar{a}_4^{(4)} = -\hat{C}^{(4,1)}\bar{F}_{4,1}^{(1)} + \bar{F}_{6,4}^{(4)} + m_4\bar{g}^{(4)} \tag{3.97}$$

$$\begin{aligned}\hat{J}_4^{(4)}\bar{\alpha}_4^{(4)} + \tilde{\omega}_4^{(4)}\hat{J}_4^{(4)}\bar{\omega}_4^{(4)} = &\bar{M}_{1,4}^{(4)} - \hat{C}^{(4,6)}\bar{M}_{4,6}^{(6)} \\ &- \tilde{\ell}_{4,1}\hat{C}^{(4,1)}\bar{F}_{4,1}^{(1)} + \tilde{\ell}_{4,6}\bar{F}_{6,4}^{(4)}\end{aligned} \tag{3.98}$$

Body-6:

$$m_6\bar{a}_6^{(6)} = -\hat{C}^{(6,4)}\bar{F}_{6,4}^{(4)} + \bar{F}_{10,6}^{(6)} + m_6\bar{g}^{(6)} \tag{3.99}$$

$$\begin{aligned}\hat{J}_6^{(6)}\bar{\alpha}_6^{(6)} + \tilde{\omega}_6^{(6)}\hat{J}_6^{(6)}\bar{\omega}_6^{(6)} = &\bar{M}_{4,6}^{(6)} - \hat{C}^{(6,10)}\bar{M}_{6,10}^{(10)} \\ &- \tilde{\ell}_{6,4}\hat{C}^{(6,4)}\bar{F}_{6,4}^{(4)} + \tilde{\ell}_{6,10}\bar{F}_{10,6}^{(6)}\end{aligned} \tag{3.100}$$

When the joint angles, the joint velocities and the actuating torques are known, totally 42 unknowns remain in these equations. In Table 3.3, these unknown variables are shown with their numbers:

Table 3.3 The unknowns in the left foot flat double support phase

Types of unknowns	Names of unknowns	Number of unknowns
Joint Accelerations	$\ddot{\theta}_{13},\ddot{\theta}_{11},\ddot{\theta}_{9},\ddot{\theta}_{7},\ddot{\theta}_{5},\ddot{\theta}_{3},\ddot{\theta}_{2},\ddot{\theta}_{4},\ddot{\theta}_{6},\ddot{\theta}_{8},\ddot{\theta}_{10}$	11
Reaction Forces	$\bar{F}_{11,13}^{(13)},\bar{F}_{7,11}^{(11)},\bar{F}_{5,7}^{(7)},\bar{F}_{1,5}^{(5)},\bar{F}_{4,1}^{(1)},\bar{F}_{6,4}^{(4)},\bar{F}_{10,6}^{(6)},$	21
Reaction Moments	$M_{11,13}^{(13)x},M_{11,13}^{(13)z},M_{7,11}^{(11)z},M_{5,7}^{(7)x},M_{5,7}^{(7)z},$ $M_{1,5}^{(5)z},M_{4,1}^{(1)z},M_{6,4}^{(4)x},M_{6,4}^{(4)z},M_{10,6}^{(6)z}$	10

As it may have been noticed, the number of equations is not sufficient to solve for 42 unknowns. However, there are several constraint equations for double support phases obtained at the kinematics part. The acceleration level constraint equations of the "left foot flat double support phase" model can be used in the solution. So, adding these 6 scalar constraint equations, a total of 42 equations exist in order to find 42 unknowns. These equations are recalled below:

$$\bar{\alpha}_1\left(\text{right}\right)=\bar{\alpha}_1\left(\text{left}\right)=\bar{\alpha}_1 \tag{3.101}$$

$$\bar{a}_{O_1}\left(\text{right}\right)=\bar{a}_{O_1}\left(\text{left}\right)=\bar{a}_{O_1} \tag{3.102}$$

As in the single support phases, the matrix inversion method is used to find the unknowns in the double support phases. Differently, for the double support phases, a 42 by 42 matrix is constructed. The elements of this large matrix are the coefficients of the unknown variables of this phase. The coefficients of unknown accelerations are rather difficult to sort, because there exist so many $\ddot{\theta}$ terms in six different $\bar{a}_i$ and $\bar{\alpha}_i$ expressions. This coefficient matrix is illustrated by a table in the appendices and every coefficient are expressed in the m-files correspond to the "left foot flat double support phase" dynamic equations.

On the other hand, all the known terms of each equation, which includes θ's and $\dot{\theta}$'s were gathered and put into column matrix form. This column matrix has also the actuating torque values in its rows. The introduced form of dynamic equations is shown below:

$$\hat{\Gamma}_{(42\,x42)} \begin{bmatrix} \ddot{\bar{q}} \\ \bar{F} \\ \bar{M} \end{bmatrix}_{(42\,x1)} = \bar{K}_{(42\,x1)} \tag{3.103}$$

By this way, a linear system of equations, each row representing an independent equation, happens to be reached. The solution is obtained via the following equation unless $\hat{\Gamma}$ is singular.

$$\begin{bmatrix} \ddot{\bar{q}} \\ \bar{F} \\ \bar{M} \end{bmatrix} = \hat{\Gamma}^{-1}\bar{K} \tag{3.104}$$

At every step of simulation, these resultant accelerations are integrated numerically and are turned back to the plant as the computed joint angles and the joint velocities.

3.2.4 Newton-Euler Equations of Right Foot Flat Double Support Phase

During the "right foot flat double support phase", the right foot (body-11) and the left toe (body-12) are assumed to be fixed to the ground. The derivation of the dynamic equations and the solution method in this phase are similar to the previous double support phase. The difference occurs in the indices. There are 36 scalar Newton – Euler equations, coming from 6 bodies, and 6 scalar constraint equations from the kinematics. Totally, 42 scalar equations of motion are obtained to be employed both in the plant block and in the computed torque control block of the simulations. Below, the Newton – Euler equations in matrix form are sorted from body-10 to body-7:

Body-10:

$$m_{10}\bar{a}_{10}^{(10)} = -\hat{C}^{(10,12)}\bar{F}_{10,12}^{(12)} + \bar{F}_{6,10}^{(10)} + m_{10}\bar{g}^{(10)} \tag{3.105}$$

$$\hat{J}_{10}^{(10)}\bar{\alpha}_{10}^{(10)}+\tilde{\omega}_{10}^{(10)}\hat{J}_{10}^{(10)}\bar{\omega}_{10}^{(10)}=-\hat{C}^{(10,12)}\bar{M}_{10,12}^{(12)}+\bar{M}_{6,10}^{(10)}-\tilde{\ell}_{10,12}\hat{C}^{(10,12)}\bar{F}_{10,12}^{(12)}+\tilde{\ell}_{10,6}\bar{F}_{6,10}^{(10)} \tag{3.106}$$

Body-6:

$$m_6\bar{a}_6^{(6)}=-\hat{C}^{(6,10)}\bar{F}_{6,10}^{(10)}+\bar{F}_{4,6}^{(6)}+m_6\bar{g}^{(6)} \tag{3.107}$$

$$\hat{J}_6^{(6)}\bar{\alpha}_6^{(6)}+\tilde{\omega}_6^{(6)}\hat{J}_6^{(6)}\bar{\omega}_6^{(6)}=-\hat{C}^{(6,10)}\bar{M}_{6,10}^{(10)}+\bar{M}_{4,6}^{(6)}-\tilde{\ell}_{6,10}\hat{C}^{(6,10)}\bar{F}_{6,10}^{(10)}+\tilde{\ell}_{6,4}\bar{F}_{4,6}^{(6)} \tag{3.108}$$

Body-4:

$$m_4\bar{a}_4^{(4)}=-\hat{C}^{(4,6)}\bar{F}_{4,6}^{(6)}+\bar{F}_{1,4}^{(4)}+m_4\bar{g}^{(4)} \tag{3.109}$$

$$\hat{J}_4^{(4)}\bar{\alpha}_4^{(4)}+\tilde{\omega}_4^{(4)}\hat{J}_4^{(4)}\bar{\omega}_4^{(4)}=-\hat{C}^{(4,6)}\bar{M}_{4,6}^{(6)}+\bar{M}_{1,4}^{(4)}-\tilde{\ell}_{4,6}\hat{C}^{(4,6)}\bar{F}_{4,6}^{(6)}+\tilde{\ell}_{4,1}\bar{F}_{1,4}^{(4)} \tag{3.110}$$

Body-1:

$$m_1\bar{a}_1^{(1)}=\bar{F}_{5,1}^{(1)}-\hat{C}^{(1,4)}\bar{F}_{1,4}^{(4)}+m_1\bar{g}^{(1)} \tag{3.111}$$

$$\hat{J}_1^{(1)}\bar{\alpha}_1^{(1)}+\tilde{\omega}_1^{(1)}\hat{J}_1^{(1)}\bar{\omega}_1^{(1)}=-\hat{C}^{(1,4)}\bar{M}_{1,4}^{(4)}-\hat{C}^{(1,5)}\bar{M}_{1,5}^{(5)}-\tilde{\ell}_{1,4}\hat{C}^{(1,4)}\bar{F}_{1,4}^{(4)}+\tilde{\ell}_{1,5}\bar{F}_{5,1}^{(1)} \tag{3.112}$$

Body-5:

$$m_5\bar{a}_5^{(5)}=-\hat{C}^{(5,1)}\bar{F}_{5,1}^{(1)}+\bar{F}_{7,5}^{(5)}+m_5\bar{g}^{(5)} \tag{3.113}$$

$$\hat{J}_5^{(5)}\bar{\alpha}_5^{(5)}+\tilde{\omega}_5^{(5)}\hat{J}_5^{(5)}\bar{\omega}_5^{(5)}=\bar{M}_{1,5}^{(5)}-\hat{C}^{(5,7)}\bar{M}_{5,7}^{(7)}-\tilde{\ell}_{5,1}\hat{C}^{(5,1)}\bar{F}_{5,1}^{(1)}+\tilde{\ell}_{5,7}\bar{F}_{7,5}^{(5)} \tag{3.114}$$

Body-7:

$$m_7\bar{a}_7^{(7)}=-\hat{C}^{(7,5)}\bar{F}_{7,5}^{(5)}+\bar{F}_{11,7}^{(7)}+m_7\bar{g}^{(7)} \tag{3.115}$$

$$\hat{J}_7^{(7)}\bar{\alpha}_7^{(7)}+\tilde{\omega}_7^{(7)}\hat{J}_7^{(7)}\bar{\omega}_7^{(7)}=\bar{M}_{5,7}^{(7)}-\hat{C}^{(7,11)}\bar{M}_{7,11}^{(11)}-\tilde{\ell}_{7,5}\hat{C}^{(7,5)}\bar{F}_{7,5}^{(5)}+\tilde{\ell}_{7,11}\bar{F}_{11,7}^{(7)} \tag{3.116}$$

The number of unknown variables in this phase is 42. These unknowns are tabulated in Table 3.4.

Table 3.4 The unknowns in the right foot flat double support phase

Types of unknowns	Names of unknowns	Number of unknowns
Joint Accelerations	$\ddot{\theta}_{12}, \ddot{\theta}_{10}, \ddot{\theta}_{8}, \ddot{\theta}_{6}, \ddot{\theta}_{4}, \ddot{\theta}_{2}, \ddot{\theta}_{3}, \ddot{\theta}_{5}, \ddot{\theta}_{7}, \ddot{\theta}_{9}, \ddot{\theta}_{11}$	11
Reaction Forces	$\bar{F}_{10,12}^{(12)}, \bar{F}_{6,10}^{(10)}, \bar{F}_{4,6}^{(6)}, \bar{F}_{1,4}^{(4)}, \bar{F}_{5,1}^{(1)}, \bar{F}_{7,5}^{(5)}, \bar{F}_{11,7}^{(7)},$	21
Reaction Moments	$M_{10,12}^{(12)x}, M_{10,12}^{(12)z}, M_{6,10}^{(10)z}, M_{4,6}^{(6)x}, M_{4,6}^{(6)z},$ $M_{1,4}^{(4)z}, M_{5,1}^{(1)z}, M_{7,5}^{(5)x}, M_{7,5}^{(5)z}, M_{11,7}^{(7)z}$	10

Utilizing these 42 scalar equations, the coefficient matrix is created. The coefficient matrix table can be examined in the Appendices. In order to find the unknown variables, the 42 by 42 coefficient matrix is inverted and multiplied from left by the vector of knowns. Consequently, the joint accelerations, the reaction forces and the reaction moments are acquired at the same time by a single operation as it happens in each of the four direct dynamics solutions.

Up to here, the kinematic expressions of the simulation models and the equations of motion were developed and shown. The unknown variables of each phase were emphasized and the solution method was mentioned. As a part of this study, these expressions, equations and matrix representations were converted into Matlab® code in m-files. Then, these m-files were embedded in the simulation blocks.

In the next section, the generation of the required torque values and the control algorithm used to achieve bipedal walking are explained for both the double and the single support phases.

3.3 Computed Torque Control Method

As a matter of fact, a well-developed control algorithm is required to keep the human model in the desired posture (usually upright position), to satisfy some gait parameters like stride length, cycle time or speed and also to perform all these things in an energy-efficient way. Naturally, as it is observed in human beings' gait, this algorithm must contain feedback of joint states to form an operational closed loop.

The first part of this control algorithm is the computation of the torque values which appear in the vector of knowns in direct dynamics solutions. The computed torque control method is utilized for this purpose. It is commonly used in robotics applications. The primary process of this method is to get the dynamic equations in the form shown below.

$$\hat{M}\left(\overline{q}\right)\ddot{\overline{q}} + \overline{B}\left(\overline{q},\dot{\overline{q}}\right) = \hat{A}\left(\overline{q}\right)\overline{T} \tag{3.117}$$

In this equation, $\hat{M}$ is the mass matrix, $\overline{B}$ is the bias vector and $\hat{A}$ is the coefficient matrix of the actuating torques. Hence, one can solve this equations system for $\overline{T}$, taking $\ddot{\overline{q}}$ as the vector of command accelerations ($\ddot{\overline{q}} = \overline{u}$). If $\mathbf{det(}\hat{A}\mathbf{)} \neq 0$, the solution is obtained as

$$\overline{T} = \hat{A}^{-1}\left(\hat{M}\,\overline{u} + \overline{B}\right) \tag{3.118}$$

As it happens at the initial state of simulation, if $\mathbf{det(}\hat{A}\mathbf{)} = 0$, then the pelvis origin may be moved a negligibly small distance in the y-direction to avoid singularity. Although, it is advantageous by some means to use the Newton – Euler formulation for deriving equations of motion, some additional operations are required to put them into the form expressed in Equation (3.114). In order to get this form, the reaction forces and the reaction moments in the dynamic equations must be allocated and they must be kept apart. For this purpose, a partitioning procedure has been developed. This procedure and the application of the computed torque control method to humanoid gait simulation are explained in two separate parts for the single and the double support phases.

3.3.1 Computed Torque Control Method for the Single Support Phase

The single support phase models are open linkage systems. In these models, while one foot is stuck on the ground, the other foot moves freely. There are ten joints and obviously ten actuating torques in these models. As the result of this method, the actuating torques are generated by using the command accelerations coming from the controller block. The resultant torques are sent to the plant block as an input vector. The application of the computed torque control method necessitates the elimination of the reaction forces and the reaction moments in the dynamic equations. The following process explains the computed torque control method for the single support phases.

Formerly, the matrix representation of the dynamic equations was in the structure seen in Equation (3.116).

$$\hat{\Gamma}_{(36\,x\,36)} \begin{bmatrix} \ddot{\bar{q}} \\ \bar{F} \\ \bar{M} \end{bmatrix}_{(36\,x\,1)} = \bar{K}_{(36\,x\,1)} \tag{3.119}$$

The matrices in this structure are divided into suitable partitions shown below to remove the reaction forces and the reaction moments.

$$\left[\begin{array}{c|c} \hat{D}_{11} & \hat{D}_{12} \\ \hline \hat{D}_{21} & \hat{D}_{22} \end{array}\right] \left[\begin{array}{c} \ddot{\bar{q}} \\ \hline \bar{P} \end{array}\right] + \left[\begin{array}{c} \bar{b}_1 \\ \hline \bar{b}_2 \end{array}\right] = \left[\begin{array}{c} \hat{A}_1 \\ \hline \hat{A}_2 \end{array}\right] \bar{T}$$

where

$$\bar{P} = \begin{bmatrix} \bar{F} \\ \bar{M} \end{bmatrix}$$

The coefficient matrix ($\hat{\Gamma}$) is divided into sub-matrices: $\hat{D}_{11}, \hat{D}_{12}, \hat{D}_{21}, \hat{D}_{22}$. $\hat{D}_{11}$ is a 10x10, $\hat{D}_{12}$ is a 10x26, $\hat{D}_{21}$ is a 26x10 and $\hat{D}_{22}$ is a 26x26 sub-matrix. The next two equations can be derived easily from the structure shown above.

$$\hat{D}_{11}\ddot{\bar{q}} + \hat{D}_{12}\bar{P} + \bar{b}_1 = \hat{A}_1\bar{T} \tag{3.120}$$

$$\hat{D}_{21}\ddot{\bar{q}} + \hat{D}_{22}\bar{P} + \bar{b}_2 = \hat{A}_2\bar{T} \tag{3.121}$$

The vector of the reactions in the second equation can be extracted as

$$\bar{P} = \hat{D}_{22}^{-1}\left(\hat{A}_2\bar{T} - \hat{D}_{21}\ddot{\bar{q}} - \bar{b}_2\right) \tag{3.122}$$

The following equations are obtained, substituting Equation (3.122) into (3.120).

$$\hat{D}_{11}\ddot{\bar{q}} + \hat{D}_{12}\hat{D}_{22}^{-1}\left(\hat{A}_2\bar{T} - \hat{D}_{21}\ddot{\bar{q}} - \bar{b}_2\right) + \bar{b}_1 = \hat{A}_1\bar{T}$$

$$\left(\hat{D}_{11} - \hat{D}_{12}\hat{D}_{22}^{-1}\hat{D}_{21}\right)\ddot{\bar{q}} + \left(\bar{b}_1 - \hat{D}_{12}\hat{D}_{22}^{-1}\bar{b}_2\right) = \left(\hat{A}_1 - \hat{D}_{12}\hat{D}_{22}^{-1}\hat{A}_2\right)\bar{T}$$

Here, the coefficients can be re-named as

$$\hat{M} = \left(\hat{D}_{11} - \hat{D}_{12}\hat{D}_{22}^{-1}\hat{D}_{21}\right)$$
$$\bar{B} = \left(\bar{b}_1 - \hat{D}_{12}\hat{D}_{22}^{-1}\bar{b}_2\right)$$
$$\hat{A} = \left(\hat{A}_1 - \hat{D}_{12}\hat{D}_{22}^{-1}\hat{A}_2\right)$$

Hence, the reaction forces and the reaction moments in the dynamic equations have been removed. Besides, the Newton – Euler equations have been re-organized to suit the computed torque control method. There is a critical point in the derivation of these expressions. If the 26x26 sub-matrix "$\hat{D}_{22}$" happens to be singular, this method is useless. Incidentally, it has been experienced that if the partitioning is not made properly, $\hat{D}_{22}$ turns out to be singular. Therefore, in order to have a non-singular "$\hat{D}_{22}$" matrix, some rows of the primary coefficient matrix $\hat{\Gamma}$ are interchanged together with consistent changes in $\bar{K}$. For this aim, a short program was written in Matlab®. This program tries several alternative row

interchanges randomly and selects one of the non-singular arrangements.

3.3.2 Computed Torque Control Method for the Double Support Phase

For the double support phase models, this method covers the optimization of actuating torques in addition to the re-arrangement of the Newton – Euler equations. This is because the double support phase models are closed linkage systems. Only, five of the eleven joint variables are independent. There are obviously eleven actuating torques in the double support phase models and they are redundant. For this reason, the actuating torques of the double support phase models are to be determined according to an optimization criterion. This optimization procedure and the computation of these eleven actuating torque values are summarized below. The optimization problem can be defined as follows.

Minimize

$$J = \frac{1}{2}\bar{T}^t \hat{W} \bar{T} \tag{3.123}$$

subject to

$$\hat{A}\bar{T} = \hat{M}\,\bar{u} + \bar{B} = \bar{C} \tag{3.124}$$

The solution to this problem can be obtained by augmenting J as

$$J = \frac{1}{2}\bar{T}^t \hat{W} \bar{T} + \bar{\lambda}^t \left(\bar{C} - \hat{A}\bar{T}\right) \tag{3.125}$$

where

$\bar{\lambda}$ is the vector of the Lagrange multipliers,

$\hat{W} = \text{diag}\left[w_k\right]$ is the weighting matrix,

w_k is the weighting factor of the k^{th} actuating torque.

Moreover, inserting the angular velocities into the weighting matrix makes it not only a torque optimization but also a power optimization. The coefficient matrices ($\hat{\Gamma}$) of the double support phase models had been previously found in

dynamic equations section. Hence, they are available to generate the mass matrices of this method. However, their size was 36 by 42 without the 6 scalar constraint equations. In a similar manner described for the single support phase, these coefficient matrices must be divided into suitable partitions to eliminate the vector of reactions and to obtain the desired structure. As recalled, the dynamic equations excluding the constraint equations were in the form shown below.

$$\hat{\Gamma}_{(36\text{x}42)} \begin{bmatrix} \ddot{\bar{q}} \\ \bar{F} \\ \bar{M} \end{bmatrix}_{(42\text{x}1)} = \bar{K}_{(36\text{x}1)}$$

At this stage, it is converted into the form given by Equation (3.114). One can use the following procedure for this aim.

$$\left[\begin{array}{c|c} \hat{D}_{11} & \hat{D}_{12} \\ \hline \hat{D}_{21} & \hat{D}_{22} \end{array}\right] \left[\begin{array}{c} \ddot{\bar{q}} \\ \hline \bar{P} \end{array}\right] + \left[\begin{array}{c} \bar{b}_1 \\ \hline \bar{b}_2 \end{array}\right] = \left[\begin{array}{c} \hat{A}_1 \\ \hline \hat{A}_2 \end{array}\right] \bar{T}$$

where

$$\bar{P} = \begin{bmatrix} \bar{F} \\ \bar{M} \end{bmatrix}$$

$\hat{D}_{11}$ is a 5x11, $\hat{D}_{12}$ is a 5x31, $\hat{D}_{21}$ is a 31x11 and $\hat{D}_{22}$ is a 31x31 sub-matrix. The expression above can be divided into the next two equations.

$$\hat{D}_{11}\ddot{\bar{q}} + \hat{D}_{12}\bar{P} + \bar{b}_1 = \hat{A}_1\bar{T} \tag{3.126}$$

$$\hat{D}_{21}\ddot{\bar{q}} + \hat{D}_{22}\bar{P} + \bar{b}_2 = \hat{A}_2\bar{T} \tag{3.127}$$

Re-arranging Equation (3.127), the vector of reactions is expressed as

$$\bar{P} = \hat{D}_{22}^{-1}\left(\hat{A}_2\bar{T} - \hat{D}_{21}\ddot{\bar{q}} - \bar{b}_2\right) \tag{3.128}$$

Then, substituting Equation (3.128) into Equation (3.126), the following

equations are obtained:

$$\hat{D}_{11}\ddot{\bar{q}} + \hat{D}_{12}\hat{D}_{22}^{-1}\left(\hat{A}_2\bar{T} - \hat{D}_{21}\ddot{\bar{q}} - \bar{b}_2\right) + \bar{b}_1 = \hat{A}_1\bar{T} \tag{3.129}$$

$$\left(\hat{D}_{11} - \hat{D}_{12}\hat{D}_{22}^{-1}\hat{D}_{21}\right)\ddot{\bar{q}} + \left(\bar{b}_1 - \hat{D}_{12}\hat{D}_{22}^{-1}\bar{b}_2\right) = \left(\hat{A}_1 - \hat{D}_{12}\hat{D}_{22}^{-1}\hat{A}_2\right)\bar{T} \tag{3.130}$$

Here, the coefficients can be re-named as

$$\hat{M} = \left(\hat{D}_{11} - \hat{D}_{12}\hat{D}_{22}^{-1}\hat{D}_{21}\right)$$
$$\bar{B} = \left(\bar{b}_1 - \hat{D}_{12}\hat{D}_{22}^{-1}\bar{b}_2\right)$$
$$\hat{A} = \left(\hat{A}_1 - \hat{D}_{12}\hat{D}_{22}^{-1}\hat{A}_2\right)$$

As a result, the reaction forces and moments in the dynamic equations are thus eliminated. Besides, the Newton – Euler equations are transformed into a new arrangement that is suitable for computed torque control method. Nevertheless, there is a critical point in the derivation of these expressions, similar to the single support phase. They are valid while the 31x31 sub-matrix "$\hat{D}_{22}$" is not singular. In order to satisfy this condition, some rows of the primary coefficient matrices ($\hat{\Gamma}$) are interchanged with consistent changes in $\bar{K}$. For this aim, a short program, similar to the previous one, was written in Matlab®.

After this, the optimization procedure continues in the way shown below.

$$\frac{\partial J}{\partial \bar{T}} = \bar{0} \tag{3.131}$$

$$\hat{W}\bar{T} = \hat{A}^t\bar{\lambda} \quad \Rightarrow \quad \bar{T} = \hat{W}^{-1}\hat{A}^t\bar{\lambda} \tag{3.132}$$

$$\hat{A}\left(\hat{W}^{-1}\hat{A}^t\bar{\lambda}\right) = \bar{C} \tag{3.133}$$

$$\bar{\lambda} = \left(\hat{A}\hat{W}^{-1}\hat{A}^t\right)^{-1}\bar{C} \tag{3.134}$$

$$\bar{T} = \hat{W}^{-1}\hat{A}^t\left(\hat{A}\hat{W}^{-1}\hat{A}^t\right)^{-1}\bar{C} \tag{3.135}$$

Finally, according to the given command accelerations, the eleven actuating

torques required in the double support phases are ready to be calculated at every step of the simulations.

Throughout the simulation, an optimal predictive control algorithm generates the vector of command accelerations ($\ddot{\bar{u}}$) for the use of computed torque control block. This algorithm is explained in the next section.

3.4 Optimal Predictive Control (OPC) Algorithm

In this thesis, an optimal predictive control algorithm is proposed to manage the desired motion of the humanoid model with minimum control effort as well as minimum deviation from the desired motion. The optimization process provides the ability to adjust the control stiffness of the system. In other words, the user can obtain a simulation which meets his priorities by altering the weighting factors in the optimization. For instance, preferring greater weighting factors for the angular accelerations results in an increase in the tracking error but rather low torque values.

As the second feature of the control algorithm, the future values of the actual state variables are predicted. This prediction is achieved by using the Taylor series expansion. Since, the joint accelerations are used as the output of the controller, Taylor expansion is made to the second order.

In the optimal predictive control algorithm, the controlled variables are the errors between the *desired* and the *predicted* future values of the position and velocity of O_1, A_{10}, A_{11} and G_1 in the x, y and z-directions. So, the general performance measure is constructed as follows with the addition of joint accelerations to avoid extreme control effort.

$$\begin{aligned} J = & \frac{1}{2}\left[\bar{p}\left(t+\Delta t\right)-\bar{p}^{*}\left(t+\Delta t\right)\right]^{t}\hat{H}\left[\bar{p}\left(t+\Delta t\right)-\bar{p}^{*}\left(t+\Delta t\right)\right] \\ & +\frac{1}{2}\left[\bar{v}\left(t+\Delta t\right)-\bar{v}^{*}\left(t+\Delta t\right)\right]^{t}\hat{R}\left[\bar{v}\left(t+\Delta t\right)-\bar{v}^{*}\left(t+\Delta t\right)\right]+\frac{1}{2}\ddot{\bar{q}}^{t}\hat{S}\ddot{\bar{q}} \end{aligned} \tag{3.136}$$

In the expression of *J*,

$\bar{p}\left(t+\Delta t\right)$ is the predicted position vector at time $t+\Delta t$,

$\bar{v}(t+\Delta t)$ is the predicted velocity vector at time $t+\Delta t$,

$\bar{p}^{*}(t+\Delta t)$ is the desired position vector at time $t+\Delta t$,

$\bar{v}^{*}(t+\Delta t)$ is the desired velocity vector at time $t+\Delta t$,

and

$\hat{H}, \hat{R}, \hat{S}$ are the position, velocity and acceleration related weighting factor matrices, respectively.

Δt is the prediction time range that indicates how far the algorithm predicts. As Δt gets longer, the error between the predictions and the real values gets larger because of the truncated expansion. On the other hand, smaller Δt values cause larger control effort. This means that Δt must be determined carefully to accomplish the desired simulation goals in a satisfactory manner.

The predicted position vector is obtained as shown below:

$$\bar{p}(t+\Delta t) = \bar{p}(t) + \frac{1}{2}\left(\bar{v}(t) + \bar{v}(t+\Delta t)\right)\Delta t \tag{3.137}$$

where

$$\bar{v}(t) = \hat{J}\left(\bar{q}(t)\right)\dot{\bar{q}}(t) \tag{3.138}$$

and

$$\bar{v}(t+\Delta t) = \hat{J}\left(\bar{q}(t+\Delta t)\right)\left[\dot{\bar{q}}(t) + \ddot{\bar{q}}(t)\Delta t\right] \tag{3.139}$$

Equation (3.139) expresses also the predicted velocity vector. The two different Jacobian matrices in the equations (3.138) and (3.139) are defined as

$$\hat{J}\left(\bar{q}(t)\right) = \left[\frac{\partial \bar{p}}{\partial \bar{q}}\right]_{\bar{q}=\bar{q}(t)} = \hat{J} \tag{3.140}$$

$$\hat{J}\left(\bar{q}(t+\Delta t)\right) = \hat{J}\left(\bar{q} + \dot{\bar{q}}\Delta t\right) = \left[\frac{\partial \bar{p}}{\partial \bar{q}}\right]_{\bar{q}=\bar{q}(t)+\dot{\bar{q}}\Delta t} = \hat{J}_{p} \tag{3.141}$$

The second Jacobian matrix is designated as $\hat{J}_p$, because it is calculated by the predicted joint angles not by the present joint angles. Then, substituting the equations (3.138) and (3.139) into equation (3.137), the predicted position vector is obtained as

$$\bar{p}\left(t+\Delta t\right)=\bar{p}\left(t\right)+\frac{1}{2}\left(\hat{J}\left(\bar{q}\right)\dot{\bar{q}}+\hat{J}\left(\bar{q}+\dot{\bar{q}}\Delta t\right)\left(\dot{\bar{q}}+\ddot{\bar{q}}\Delta t\right)\right)\Delta t \tag{3.142}$$

The aim in the optimal predictive control algorithm is to find the joint accelerations which minimize the performance measure given by Equation (3.136). The process starts with the equation below:

$$\frac{\partial J}{\partial \ddot{\bar{q}}}=\bar{0} \tag{3.143}$$

The solution is straight forward if one organizes Equation (3.143) in the following form:

$$\hat{G}\ddot{\bar{q}}+\bar{K}=\bar{0} \tag{3.144}$$

where

$$\hat{G}=\frac{1}{4}\Delta t^4\hat{J}_p^t\hat{H}\hat{J}_p+\Delta t^2\hat{J}_p^t\hat{R}\hat{J}_p+\hat{S} \tag{3.145}$$

and

$$\bar{K}=\frac{1}{2}\Delta t^2\hat{J}_p^t\hat{H}\bar{L}_1+\Delta t\hat{J}_p^t\hat{R}\bar{L}_2 \tag{3.146}$$

where

$$\bar{L}_1=\bar{p}\left(t\right)+\frac{1}{2}\left(\hat{J}+\hat{J}_p\right)\dot{\bar{q}}\left(t\right)\Delta t-\bar{p}^*\left(t+\Delta t\right) \tag{3.147}$$

$$\bar{L}_2=\hat{J}_p\left(t\right)\dot{\bar{q}}\left(t\right)-\bar{v}^*\left(t+\Delta t\right) \tag{3.148}$$

Finally,

$$\ddot{\bar{q}}=-\hat{G}^{-1}\bar{K} \tag{3.149}$$

Hence, the joint accelerations which minimize the performance measure are

obtained and they are sent to the computed torque block as the command accelerations.

Two different types of the aforesaid algorithm are presented in the ongoing sections. First type is derived for the double support phase and the second one is for the single support phase. Like some other parts of the simulation, in the optimal predictive control part, the difference between the left and right foot flat models is only the shifting of indices. Therefore, the procedure was not repeated for the left and right foot flat models of the same phase.

3.4.1 Single Support Phase OPC Algorithm

During the single support phase, the goal is to move the body forward on one foot while the other swings in the air. In this phase, the desired position and velocity of the origin O_1 and the mass center G_1 of body-1 and the heel point of the swinging foot are taken as the reference values. By controlling both the points O_1 and G_1, not only the desired location but also the desired orientation of HAT is achieved. Since, the "right foot flat single support phase" model is preferred to demonstrate, the positions of O_1, G1 and A_{10} are derived as follows:

$$\begin{aligned}\overline{p}_{O_1} = \overline{p}_{A_{11}} + a_{11}\overline{u}_3 + a_7 e^{-\tilde{u}_1\theta_{11}} e^{-\tilde{u}_2\theta_9}\overline{u}_3 + a_5 e^{-\tilde{u}_1\theta_{11}} e^{-\tilde{u}_2(\theta_9+\theta_7)}\overline{u}_3 \\ + a_1^r e^{-\tilde{u}_1\theta_{11}} e^{-\tilde{u}_2(\theta_9+\theta_7+\theta_5)} e^{-\tilde{u}_1\theta_3}\overline{u}_2\end{aligned} \tag{3.150}$$

$$\begin{aligned}\overline{p}_{G_1} = \overline{p}_{A_{11}} + a_{11}\overline{u}_3 + a_7 e^{-\tilde{u}_1\theta_{11}} e^{-\tilde{u}_2\theta_9}\overline{u}_3 + a_5 e^{-\tilde{u}_1\theta_{11}} e^{-\tilde{u}_2(\theta_9+\theta_7)}\overline{u}_3 \\ + e^{-\tilde{u}_1\theta_{11}} e^{-\tilde{u}_2(\theta_9+\theta_7+\theta_5)} e^{-\tilde{u}_1\theta_3}\left(a_1^r\overline{u}_2 + c_1\overline{u}_3\right)\end{aligned} \tag{3.151}$$

$$\begin{aligned}\overline{p}_{A_{10}} = \overline{p}_{A_{11}} + a_{11}\overline{u}_3 + a_7 e^{-\tilde{u}_1\theta_{11}} e^{-\tilde{u}_2\theta_9}\overline{u}_3 + a_5 e^{-\tilde{u}_1\theta_{11}} e^{-\tilde{u}_2(\theta_9+\theta_7)}\overline{u}_3 \\ + a_1 e^{-\tilde{u}_1\theta_{11}} e^{-\tilde{u}_2(\theta_9+\theta_7+\theta_5)}\overline{u}_2 - a_4 e^{-\tilde{u}_1\theta_{11}} e^{-\tilde{u}_2(\theta_9+\theta_7+\theta_5)} e^{-\tilde{u}_1(\theta_3-\theta_2)} e^{\tilde{u}_2\theta_4}\overline{u}_3 \\ - a_6 e^{-\tilde{u}_1\theta_{11}} e^{-\tilde{u}_2(\theta_9+\theta_7+\theta_5)} e^{-\tilde{u}_1(\theta_3-\theta_2)} e^{\tilde{u}_2(\theta_4+\theta_6)}\overline{u}_3 \\ - a_{10} e^{-\tilde{u}_1\theta_{11}} e^{-\tilde{u}_2(\theta_9+\theta_7+\theta_5)} e^{-\tilde{u}_1(\theta_3-\theta_2)} e^{\tilde{u}_2(\theta_4+\theta_6+\theta_8)} e^{\tilde{u}_1\theta_{10}}\overline{u}_3\end{aligned} \tag{3.152}$$

The functions that would be optimized at the position level of the single support phase are:

$$\overline{p} = \begin{bmatrix} p_1 \\ p_2 \\ p_3 \\ p_4 \\ p_5 \\ p_6 \\ p_7 \\ p_8 \\ p_9 \end{bmatrix} = \begin{bmatrix} \overline{u}_1^t \overline{p}_{O_1} \\ \overline{u}_2^t \overline{p}_{O_1} \\ \overline{u}_3^t \overline{p}_{O_1} \\ \overline{u}_1^t \overline{p}_{A_{10}} \\ \overline{u}_2^t \overline{p}_{A_{10}} \\ \overline{u}_3^t \overline{p}_{A_{10}} \\ \overline{u}_1^t \overline{p}_{G_1} \\ \overline{u}_2^t \overline{p}_{G_1} \\ \overline{u}_3^t \overline{p}_{G_1} \end{bmatrix} \tag{3.153}$$

The Jacobian matrix $\hat{J}$ is represented as

$$\hat{J} = \begin{bmatrix} \frac{\partial \overline{p}_{O_1}}{\partial \theta_{11}} & \frac{\partial \overline{p}_{O_1}}{\partial \theta_9} & \frac{\partial \overline{p}_{O_1}}{\partial \theta_7} & \frac{\partial \overline{p}_{O_1}}{\partial \theta_5} & \frac{\partial \overline{p}_{O_1}}{\partial \theta_3} & \frac{\partial \overline{p}_{O_1}}{\partial \theta_2} & \frac{\partial \overline{p}_{O_1}}{\partial \theta_4} & \frac{\partial \overline{p}_{O_1}}{\partial \theta_6} & \frac{\partial \overline{p}_{O_1}}{\partial \theta_8} & \frac{\partial \overline{p}_{O_1}}{\partial \theta_{10}} \\ \frac{\partial \overline{p}_{A_{10}}}{\partial \theta_{11}} & \frac{\partial \overline{p}_{A_{10}}}{\partial \theta_9} & \frac{\partial \overline{p}_{A_{10}}}{\partial \theta_7} & \frac{\partial \overline{p}_{A_{10}}}{\partial \theta_5} & \frac{\partial \overline{p}_{A_{10}}}{\partial \theta_3} & \frac{\partial \overline{p}_{A_{10}}}{\partial \theta_2} & \frac{\partial \overline{p}_{A_{10}}}{\partial \theta_4} & \frac{\partial \overline{p}_{A_{10}}}{\partial \theta_6} & \frac{\partial \overline{p}_{A_{10}}}{\partial \theta_8} & \frac{\partial \overline{p}_{A_{10}}}{\partial \theta_{10}} \\ \frac{\partial \overline{p}_{G_1}}{\partial \theta_{11}} & \frac{\partial \overline{p}_{G_1}}{\partial \theta_9} & \frac{\partial \overline{p}_{G_1}}{\partial \theta_7} & \frac{\partial \overline{p}_{G_1}}{\partial \theta_5} & \frac{\partial \overline{p}_{G_1}}{\partial \theta_3} & \frac{\partial \overline{p}_{G_1}}{\partial \theta_2} & \frac{\partial \overline{p}_{G_1}}{\partial \theta_4} & \frac{\partial \overline{p}_{G_1}}{\partial \theta_6} & \frac{\partial \overline{p}_{G_1}}{\partial \theta_8} & \frac{\partial \overline{p}_{G_1}}{\partial \theta_{10}} \end{bmatrix}$$

where

$$\frac{\partial \overline{p}_{O_1}}{\partial \theta_{11}} = -a_7 e^{-\tilde{u}_1 \theta_{11}} \tilde{u}_1 e^{-\tilde{u}_2 \theta_9} \overline{u}_3 - a_5 e^{-\tilde{u}_1 \theta_{11}} \tilde{u}_1 e^{-\tilde{u}_2 (\theta_9 + \theta_7)} \overline{u}_3 - a_1^r e^{-\tilde{u}_1 \theta_{11}} \tilde{u}_1 e^{-\tilde{u}_2 (\theta_9 + \theta_7 + \theta_5)} e^{-\tilde{u}_1 \theta_3} \overline{u}_2$$

$$\frac{\partial \overline{p}_{O_1}}{\partial \theta_9} = -a_7 e^{-\tilde{u}_1 \theta_{11}} e^{-\tilde{u}_2 \theta_9} \tilde{u}_2 \overline{u}_3 - a_5 e^{-\tilde{u}_1 \theta_{11}} e^{-\tilde{u}_2 (\theta_9 + \theta_7)} \tilde{u}_2 \overline{u}_3 - a_1^r e^{-\tilde{u}_1 \theta_{11}} e^{-\tilde{u}_2 (\theta_9 + \theta_7 + \theta_5)} \tilde{u}_2 e^{-\tilde{u}_1 \theta_3} \overline{u}_2$$

$$\frac{\partial \overline{p}_{O_1}}{\partial \theta_7} = -a_5 e^{-\tilde{u}_1 \theta_{11}} e^{-\tilde{u}_2 (\theta_9 + \theta_7)} \tilde{u}_2 \overline{u}_3 - a_1^r e^{-\tilde{u}_1 \theta_{11}} e^{-\tilde{u}_2 (\theta_9 + \theta_7 + \theta_5)} \tilde{u}_2 e^{-\tilde{u}_1 \theta_3} \overline{u}_2$$

$$\frac{\partial \overline{p}_{O_1}}{\partial \theta_5} = -a_1^r e^{-\tilde{u}_1 \theta_{11}} e^{-\tilde{u}_2 (\theta_9 + \theta_7 + \theta_5)} \tilde{u}_2 e^{-\tilde{u}_1 \theta_3} \overline{u}_2$$

$$\frac{\partial \overline{p}_{O_1}}{\partial \theta_3} = -a_1^r e^{-\tilde{u}_1 \theta_{11}} e^{-\tilde{u}_2 (\theta_9 + \theta_7 + \theta_5)} e^{-\tilde{u}_1 \theta_3} \tilde{u}_1 \overline{u}_2$$

$$\frac{\partial \overline{p}_{O_1}}{\partial \theta_2} = \frac{\partial \overline{p}_{O_1}}{\partial \theta_4} = \frac{\partial \overline{p}_{O_1}}{\partial \theta_6} = \frac{\partial \overline{p}_{O_1}}{\partial \theta_8} = \frac{\partial \overline{p}_{O_1}}{\partial \theta_{10}} = 0$$

and

$$\frac{\partial \overline{p}_{A_{10}}}{\partial \theta_{11}} = -a_7 e^{-\tilde{u}_1\theta_{11}} \tilde{u}_1 e^{-\tilde{u}_2\theta_9} \overline{u}_3 - a_5 e^{-\tilde{u}_1\theta_{11}} \tilde{u}_1 e^{-\tilde{u}_2(\theta_9+\theta_7)} \overline{u}_3 - a_1 e^{-\tilde{u}_1\theta_{11}} \tilde{u}_1 e^{-\tilde{u}_2(\theta_9+\theta_7+\theta_5)} e^{-\tilde{u}_1\theta_3} \overline{u}_2$$
$$+ a_4 e^{-\tilde{u}_1\theta_{11}} \tilde{u}_1 e^{-\tilde{u}_2(\theta_9+\theta_7+\theta_5)} e^{-\tilde{u}_1(\theta_3-\theta_2)} e^{\tilde{u}_2\theta_4} \overline{u}_3 + a_6 e^{-\tilde{u}_1\theta_{11}} \tilde{u}_1 e^{-\tilde{u}_2(\theta_9+\theta_7+\theta_5)} e^{-\tilde{u}_1(\theta_3-\theta_2)} e^{\tilde{u}_2(\theta_4+\theta_6)} \overline{u}_3$$
$$+ a_{10} e^{-\tilde{u}_1\theta_{11}} \tilde{u}_1 e^{-\tilde{u}_2(\theta_9+\theta_7+\theta_5)} e^{-\tilde{u}_1(\theta_3-\theta_2)} e^{\tilde{u}_2(\theta_4+\theta_6+\theta_8)} e^{\tilde{u}_1\theta_{10}} \overline{u}_3$$

$$\frac{\partial \overline{p}_{A_{10}}}{\partial \theta_9} = -a_7 e^{-\tilde{u}_1\theta_{11}} e^{-\tilde{u}_2\theta_9} \tilde{u}_2 \overline{u}_3 - a_5 e^{-\tilde{u}_1\theta_{11}} e^{-\tilde{u}_2(\theta_9+\theta_7)} \tilde{u}_2 \overline{u}_3 - a_1 e^{-\tilde{u}_1\theta_{11}} e^{-\tilde{u}_2(\theta_9+\theta_7+\theta_5)} \tilde{u}_2 e^{-\tilde{u}_1\theta_3} \overline{u}_2$$
$$+ a_4 e^{-\tilde{u}_1\theta_{11}} e^{-\tilde{u}_2(\theta_9+\theta_7+\theta_5)} \tilde{u}_2 e^{-\tilde{u}_1(\theta_3-\theta_2)} e^{\tilde{u}_2\theta_4} \overline{u}_3 + a_6 e^{-\tilde{u}_1\theta_{11}} e^{-\tilde{u}_2(\theta_9+\theta_7+\theta_5)} \tilde{u}_2 e^{-\tilde{u}_1(\theta_3-\theta_2)} e^{\tilde{u}_2(\theta_4+\theta_6)} \overline{u}_3$$
$$+ a_{10} e^{-\tilde{u}_1\theta_{11}} e^{-\tilde{u}_2(\theta_9+\theta_7+\theta_5)} \tilde{u}_2 e^{-\tilde{u}_1(\theta_3-\theta_2)} e^{\tilde{u}_2(\theta_4+\theta_6+\theta_8)} e^{\tilde{u}_1\theta_{10}} \overline{u}_3$$

$$\frac{\partial \overline{p}_{A_{10}}}{\partial \theta_7} = -a_5 e^{-\tilde{u}_1\theta_{11}} e^{-\tilde{u}_2(\theta_9+\theta_7)} \tilde{u}_2 \overline{u}_3 - a_1 e^{-\tilde{u}_1\theta_{11}} e^{-\tilde{u}_2(\theta_9+\theta_7+\theta_5)} \tilde{u}_2 e^{-\tilde{u}_1\theta_3} \overline{u}_2$$
$$+ a_4 e^{-\tilde{u}_1\theta_{11}} e^{-\tilde{u}_2(\theta_9+\theta_7+\theta_5)} \tilde{u}_2 e^{-\tilde{u}_1(\theta_3-\theta_2)} e^{\tilde{u}_2\theta_4} \overline{u}_3 + a_6 e^{-\tilde{u}_1\theta_{11}} e^{-\tilde{u}_2(\theta_9+\theta_7+\theta_5)} \tilde{u}_2 e^{-\tilde{u}_1(\theta_3-\theta_2)} e^{\tilde{u}_2(\theta_4+\theta_6)} \overline{u}_3$$
$$+ a_{10} e^{-\tilde{u}_1\theta_{11}} e^{-\tilde{u}_2(\theta_9+\theta_7+\theta_5)} \tilde{u}_2 e^{-\tilde{u}_1(\theta_3-\theta_2)} e^{\tilde{u}_2(\theta_4+\theta_6+\theta_8)} e^{\tilde{u}_1\theta_{10}} \overline{u}_3$$

$$\frac{\partial \overline{p}_{A_{10}}}{\partial \theta_5} = -a_1^r e^{-\tilde{u}_1\theta_{11}} e^{-\tilde{u}_2(\theta_9+\theta_7+\theta_5)} \tilde{u}_2 e^{-\tilde{u}_1\theta_3} \overline{u}_2$$
$$+ a_4 e^{-\tilde{u}_1\theta_{11}} e^{-\tilde{u}_2(\theta_9+\theta_7+\theta_5)} \tilde{u}_2 e^{-\tilde{u}_1(\theta_3-\theta_2)} e^{\tilde{u}_2\theta_4} \overline{u}_3 + a_6 e^{-\tilde{u}_1\theta_{11}} e^{-\tilde{u}_2(\theta_9+\theta_7+\theta_5)} \tilde{u}_2 e^{-\tilde{u}_1(\theta_3-\theta_2)} e^{\tilde{u}_2(\theta_4+\theta_6)} \overline{u}_3$$
$$+ a_{10} e^{-\tilde{u}_1\theta_{11}} e^{-\tilde{u}_2(\theta_9+\theta_7+\theta_5)} \tilde{u}_2 e^{-\tilde{u}_1(\theta_3-\theta_2)} e^{\tilde{u}_2(\theta_4+\theta_6+\theta_8)} e^{\tilde{u}_1\theta_{10}} \overline{u}_3$$

and

$$\frac{\partial \overline{p}_{A_{10}}}{\partial \theta_3} = -a_1 e^{-\tilde{u}_1\theta_{11}} e^{-\tilde{u}_2(\theta_9+\theta_7+\theta_5)} e^{-\tilde{u}_1\theta_3} \tilde{u}_1 \overline{u}_2 + a_4 e^{-\tilde{u}_1\theta_{11}} e^{-\tilde{u}_2(\theta_9+\theta_7+\theta_5)} e^{-\tilde{u}_1(\theta_3-\theta_2)} \tilde{u}_1 e^{\tilde{u}_2\theta_4} \overline{u}_3$$
$$+ a_6 e^{-\tilde{u}_1\theta_{11}} e^{-\tilde{u}_2(\theta_9+\theta_7+\theta_5)} e^{-\tilde{u}_1(\theta_3-\theta_2)} \tilde{u}_1 e^{\tilde{u}_2(\theta_4+\theta_6)} \overline{u}_3$$
$$+ a_{10} e^{-\tilde{u}_1\theta_{11}} e^{-\tilde{u}_2(\theta_9+\theta_7+\theta_5)} e^{-\tilde{u}_1(\theta_3-\theta_2)} \tilde{u}_1 e^{\tilde{u}_2(\theta_4+\theta_6+\theta_8)} e^{\tilde{u}_1\theta_{10}} \overline{u}_3$$

$$\frac{\partial \overline{p}_{A_{10}}}{\partial \theta_2} = -a_4 e^{-\tilde{u}_1\theta_{11}} e^{-\tilde{u}_2(\theta_9+\theta_7+\theta_5)} e^{-\tilde{u}_1(\theta_3-\theta_2)} \tilde{u}_1 e^{\tilde{u}_2\theta_4} \overline{u}_3$$
$$- a_6 e^{-\tilde{u}_1\theta_{11}} e^{-\tilde{u}_2(\theta_9+\theta_7+\theta_5)} e^{-\tilde{u}_1(\theta_3-\theta_2)} \tilde{u}_1 e^{\tilde{u}_2(\theta_4+\theta_6)} \overline{u}_3$$
$$- a_{10} e^{-\tilde{u}_1\theta_{11}} e^{-\tilde{u}_2(\theta_9+\theta_7+\theta_5)} e^{-\tilde{u}_1(\theta_3-\theta_2)} \tilde{u}_1 e^{\tilde{u}_2(\theta_4+\theta_6+\theta_8)} e^{\tilde{u}_1\theta_{10}} \overline{u}_3$$

$$\frac{\partial \overline{p}_{A_{10}}}{\partial \theta_4} = -a_4 e^{-\tilde{u}_1\theta_{11}} e^{-\tilde{u}_2(\theta_9+\theta_7+\theta_5)} e^{-\tilde{u}_1(\theta_3-\theta_2)} e^{\tilde{u}_2\theta_4} \tilde{u}_2 \overline{u}_3$$
$$- a_6 e^{-\tilde{u}_1\theta_{11}} e^{-\tilde{u}_2(\theta_9+\theta_7+\theta_5)} e^{-\tilde{u}_1(\theta_3-\theta_2)} e^{\tilde{u}_2(\theta_4+\theta_6)} \tilde{u}_2 \overline{u}_3$$
$$- a_{10} e^{-\tilde{u}_1\theta_{11}} e^{-\tilde{u}_2(\theta_9+\theta_7+\theta_5)} e^{-\tilde{u}_1(\theta_3-\theta_2)} e^{\tilde{u}_2(\theta_4+\theta_6+\theta_8)} \tilde{u}_2 e^{\tilde{u}_1\theta_{10}} \overline{u}_3$$

$$\frac{\partial \overline{p}_{A_{10}}}{\partial \theta_6} = -a_6 e^{-\tilde{u}_1\theta_{11}} e^{-\tilde{u}_2(\theta_9+\theta_7+\theta_5)} e^{-\tilde{u}_1(\theta_3-\theta_2)} e^{\tilde{u}_2(\theta_4+\theta_6)} \tilde{u}_2 \overline{u}_3$$

$$- a_{10} e^{-\tilde{u}_1\theta_{11}} e^{-\tilde{u}_2(\theta_9+\theta_7+\theta_5)} e^{-\tilde{u}_1(\theta_3-\theta_2)} e^{\tilde{u}_2(\theta_4+\theta_6+\theta_8)} \tilde{u}_2 e^{\tilde{u}_1\theta_{10}} \overline{u}_3$$

$$\frac{\partial \overline{p}_{A_{10}}}{\partial \theta_8} = -a_{10} e^{-\tilde{u}_1\theta_{11}} e^{-\tilde{u}_2(\theta_9+\theta_7+\theta_5)} e^{-\tilde{u}_1(\theta_3-\theta_2)} e^{\tilde{u}_2(\theta_4+\theta_6+\theta_8)} \tilde{u}_2 e^{\tilde{u}_1\theta_{10}} \overline{u}_3$$

$$\frac{\partial \overline{p}_{A_{10}}}{\partial \theta_{10}} = -a_{10} e^{-\tilde{u}_1\theta_{11}} e^{-\tilde{u}_2(\theta_9+\theta_7+\theta_5)} e^{-\tilde{u}_1(\theta_3-\theta_2)} e^{\tilde{u}_2(\theta_4+\theta_6+\theta_8)} e^{\tilde{u}_1\theta_{10}} \tilde{u}_1 \overline{u}_3$$

and

$$\frac{\partial \overline{p}_{G_1}}{\partial \theta_{11}} = -a_7 e^{-\tilde{u}_1\theta_{11}} \tilde{u}_1 e^{-\tilde{u}_2\theta_9} \overline{u}_3 - a_5 e^{-\tilde{u}_1\theta_{11}} \tilde{u}_1 e^{-\tilde{u}_2(\theta_9+\theta_7)} \overline{u}_3 - e^{-\tilde{u}_1\theta_{11}} \tilde{u}_1 e^{-\tilde{u}_2(\theta_9+\theta_7+\theta_5)} e^{-\tilde{u}_1\theta_3} \left(a_1^r \overline{u}_2 + c_1 \overline{u}_3 \right)$$

$$\frac{\partial \overline{p}_{G_1}}{\partial \theta_9} = -a_7 e^{-\tilde{u}_1\theta_{11}} e^{-\tilde{u}_2\theta_9} \tilde{u}_2 \overline{u}_3 - a_5 e^{-\tilde{u}_1\theta_{11}} e^{-\tilde{u}_2(\theta_9+\theta_7)} \tilde{u}_2 \overline{u}_3$$

$$- e^{-\tilde{u}_1\theta_{11}} e^{-\tilde{u}_2(\theta_9+\theta_7+\theta_5)} \tilde{u}_2 e^{-\tilde{u}_1\theta_3} \overline{u}_2 \left(a_1^r \overline{u}_2 + c_1 \overline{u}_3 \right)$$

$$\frac{\partial \overline{p}_{G_1}}{\partial \theta_7} = -a_5 e^{-\tilde{u}_1\theta_{11}} e^{-\tilde{u}_2(\theta_9+\theta_7)} \tilde{u}_2 \overline{u}_3 - e^{-\tilde{u}_1\theta_{11}} e^{-\tilde{u}_2(\theta_9+\theta_7+\theta_5)} \tilde{u}_2 e^{-\tilde{u}_1\theta_3} \overline{u}_2 \left(a_1^r \overline{u}_2 + c_1 \overline{u}_3 \right)$$

$$\frac{\partial \overline{p}_{G_1}}{\partial \theta_5} = -e^{-\tilde{u}_1\theta_{11}} e^{-\tilde{u}_2(\theta_9+\theta_7+\theta_5)} \tilde{u}_2 e^{-\tilde{u}_1\theta_3} \overline{u}_2 \left(a_1^r \overline{u}_2 + c_1 \overline{u}_3 \right)$$

$$\frac{\partial \overline{p}_{G_1}}{\partial \theta_3} = -e^{-\tilde{u}_1\theta_{11}} e^{-\tilde{u}_2(\theta_9+\theta_7+\theta_5)} e^{-\tilde{u}_1\theta_3} \tilde{u}_1 \overline{u}_2 \left(a_1^r \overline{u}_2 + c_1 \overline{u}_3 \right)$$

$$\frac{\partial \overline{p}_{G_1}}{\partial \theta_2} = \frac{\partial \overline{p}_{G_1}}{\partial \theta_4} = \frac{\partial \overline{p}_{G_1}}{\partial \theta_6} = \frac{\partial \overline{p}_{G_1}}{\partial \theta_8} = \frac{\partial \overline{p}_{G_1}}{\partial \theta_{10}} = 0$$

In the single support phase models, the following weighting matrices are used:

$$\hat{H} = diag\left[h_1, h_2, h_3, h_4, h_5, h_6, h_7, h_8, h_9 \right]$$

$$\hat{R} = \Delta t^2 diag\left[r_1, r_2, r_3, r_4, r_5, r_6, r_7, r_8, r_9 \right]$$

$$\hat{S} = 4\Delta t^4 diag\left[s_1, s_2, s_3, s_4, s_5, s_6, s_7, s_8, s_9, s_{10} \right]$$

As the result of the proposed algorithm, ten command accelerations are computed in an optimal way. These are $\ddot{\theta}_{11}, \ddot{\theta}_9, \ddot{\theta}_7, \ddot{\theta}_5, \ddot{\theta}_3, \ddot{\theta}_2, \ddot{\theta}_4, \ddot{\theta}_6, \ddot{\theta}_8, \ddot{\theta}_{10}$ for both the right and the left foot flat single support phases. After this, they are sent to the computed torque block.

3.4.2 Double Support Phase OPC Algorithm

As mentioned before, during the double support phase, the goal is to move the body forward while both feet are attached to the ground. In this phase, the desired position and velocity of body-1's origin O_1 and the mass center, G1, of the same body are taken as the reference values. Thus, the location and the orientation of HAT are controlled. Since the "right foot flat double support phase" model is preferred, the position vectors with respect to the earth fixed frame are derived as:

$$\begin{aligned}\overline{p}_{O_1} = \overline{p}_{A_{11}} + a_{11}\overline{u}_3 + a_7 e^{-\tilde{u}_1\theta_{11}} e^{-\tilde{u}_2\theta_9}\overline{u}_3 + a_5 e^{-\tilde{u}_1\theta_{11}} e^{-\tilde{u}_2(\theta_9+\theta_7)}\overline{u}_3 \\ + a_1^r e^{-\tilde{u}_1\theta_{11}} e^{-\tilde{u}_2(\theta_9+\theta_7+\theta_5)} e^{-\tilde{u}_1\theta_3}\overline{u}_2\end{aligned} \tag{3.154}$$

$$\begin{aligned}\overline{p}_{G_1} = \overline{p}_{A_{11}} + a_{11}\overline{u}_3 + a_7 e^{-\tilde{u}_1\theta_{11}} e^{-\tilde{u}_2\theta_9}\overline{u}_3 + a_5 e^{-\tilde{u}_1\theta_{11}} e^{-\tilde{u}_2(\theta_9+\theta_7)}\overline{u}_3 \\ + e^{-\tilde{u}_1\theta_{11}} e^{-\tilde{u}_2(\theta_9+\theta_7+\theta_5)} e^{-\tilde{u}_1\theta_3}\left(a_1^r\overline{u}_2 + c_1\overline{u}_3\right)\end{aligned} \tag{3.155}$$

Functions that would be optimized at the position level are

$$\overline{p} = \begin{bmatrix} p_1 \\ p_2 \\ p_3 \\ p_4 \\ p_5 \\ p_6 \end{bmatrix} = \begin{bmatrix} \overline{u}_1^t\overline{p}_{O_1} \\ \overline{u}_2^t\overline{p}_{O_1} \\ \overline{u}_3^t\overline{p}_{O_1} \\ \overline{u}_1^t\overline{p}_{G_1} \\ \overline{u}_2^t\overline{p}_{G_1} \\ \overline{u}_3^t\overline{p}_{G_1} \end{bmatrix} \tag{3.156}$$

The Jacobian matrix $\hat{J}$ is represented as

$$\hat{J} = \begin{bmatrix} \frac{\partial\overline{p}_{O_1}}{\partial\theta_{11}} & \frac{\partial\overline{p}_{O_1}}{\partial\theta_9} & \frac{\partial\overline{p}_{O_1}}{\partial\theta_7} & \frac{\partial\overline{p}_{O_1}}{\partial\theta_5} & \frac{\partial\overline{p}_{O_1}}{\partial\theta_3} \\ \frac{\partial\overline{p}_{G_1}}{\partial\theta_{11}} & \frac{\partial\overline{p}_{G_1}}{\partial\theta_9} & \frac{\partial\overline{p}_{G_1}}{\partial\theta_7} & \frac{\partial\overline{p}_{G_1}}{\partial\theta_5} & \frac{\partial\overline{p}_{G_1}}{\partial\theta_3} \end{bmatrix}$$

where

$$\frac{\partial \overline{p}_{O_1}}{\partial \theta_{11}} = -a_7 e^{-\tilde{u}_1\theta_{11}} \tilde{u}_1 e^{-\tilde{u}_2\theta_9} \overline{u}_3 - a_5 e^{-\tilde{u}_1\theta_{11}} \tilde{u}_1 e^{-\tilde{u}_2(\theta_9+\theta_7)} \overline{u}_3 - a_1^r e^{-\tilde{u}_1\theta_{11}} \tilde{u}_1 e^{-\tilde{u}_2(\theta_9+\theta_7+\theta_5)} e^{-\tilde{u}_1\theta_3} \overline{u}_2$$

$$\frac{\partial \overline{p}_{O_1}}{\partial \theta_9} = -a_7 e^{-\tilde{u}_1\theta_{11}} e^{-\tilde{u}_2\theta_9} \tilde{u}_2 \overline{u}_3 - a_5 e^{-\tilde{u}_1\theta_{11}} e^{-\tilde{u}_2(\theta_9+\theta_7)} \tilde{u}_2 \overline{u}_3 - a_1^r e^{-\tilde{u}_1\theta_{11}} e^{-\tilde{u}_2(\theta_9+\theta_7+\theta_5)} \tilde{u}_2 e^{-\tilde{u}_1\theta_3} \overline{u}_2$$

$$\frac{\partial \overline{p}_{O_1}}{\partial \theta_7} = -a_5 e^{-\tilde{u}_1\theta_{11}} e^{-\tilde{u}_2(\theta_9+\theta_7)} \tilde{u}_2 \overline{u}_3 - a_1^r e^{-\tilde{u}_1\theta_{11}} e^{-\tilde{u}_2(\theta_9+\theta_7+\theta_5)} \tilde{u}_2 e^{-\tilde{u}_1\theta_3} \overline{u}_2$$

$$\frac{\partial \overline{p}_{O_1}}{\partial \theta_5} = -a_1^r e^{-\tilde{u}_1\theta_{11}} e^{-\tilde{u}_2(\theta_9+\theta_7+\theta_5)} \tilde{u}_2 e^{-\tilde{u}_1\theta_3} \overline{u}_2$$

$$\frac{\partial \overline{p}_{O_1}}{\partial \theta_3} = -a_1^r e^{-\tilde{u}_1\theta_{11}} e^{-\tilde{u}_2(\theta_9+\theta_7+\theta_5)} e^{-\tilde{u}_1\theta_3} \tilde{u}_1 \overline{u}_2$$

$$\frac{\partial \overline{p}_{G_1}}{\partial \theta_{11}} = -a_7 e^{-\tilde{u}_1\theta_{11}} \tilde{u}_1 e^{-\tilde{u}_2\theta_9} \overline{u}_3 - a_5 e^{-\tilde{u}_1\theta_{11}} \tilde{u}_1 e^{-\tilde{u}_2(\theta_9+\theta_7)} \overline{u}_3 - e^{-\tilde{u}_1\theta_{11}} \tilde{u}_1 e^{-\tilde{u}_2(\theta_9+\theta_7+\theta_5)} e^{-\tilde{u}_1\theta_3} \left(a_1^r \overline{u}_2 + c_1 \overline{u}_3 \right)$$

$$\frac{\partial \overline{p}_{G_1}}{\partial \theta_9} = -a_7 e^{-\tilde{u}_1\theta_{11}} e^{-\tilde{u}_2\theta_9} \tilde{u}_2 \overline{u}_3 - a_5 e^{-\tilde{u}_1\theta_{11}} e^{-\tilde{u}_2(\theta_9+\theta_7)} \tilde{u}_2 \overline{u}_3$$
$$- e^{-\tilde{u}_1\theta_{11}} e^{-\tilde{u}_2(\theta_9+\theta_7+\theta_5)} \tilde{u}_2 e^{-\tilde{u}_1\theta_3} \overline{u}_2 \left(a_1^r \overline{u}_2 + c_1 \overline{u}_3 \right)$$

$$\frac{\partial \overline{p}_{G_1}}{\partial \theta_7} = -a_5 e^{-\tilde{u}_1\theta_{11}} e^{-\tilde{u}_2(\theta_9+\theta_7)} \tilde{u}_2 \overline{u}_3 - e^{-\tilde{u}_1\theta_{11}} e^{-\tilde{u}_2(\theta_9+\theta_7+\theta_5)} \tilde{u}_2 e^{-\tilde{u}_1\theta_3} \overline{u}_2 \left(a_1^r \overline{u}_2 + c_1 \overline{u}_3 \right)$$

$$\frac{\partial \overline{p}_{G_1}}{\partial \theta_5} = -e^{-\tilde{u}_1\theta_{11}} e^{-\tilde{u}_2(\theta_9+\theta_7+\theta_5)} \tilde{u}_2 e^{-\tilde{u}_1\theta_3} \overline{u}_2 \left(a_1^r \overline{u}_2 + c_1 \overline{u}_3 \right)$$

$$\frac{\partial \overline{p}_{G_1}}{\partial \theta_3} = -e^{-\tilde{u}_1\theta_{11}} e^{-\tilde{u}_2(\theta_9+\theta_7+\theta_5)} e^{-\tilde{u}_1\theta_3} \tilde{u}_1 \overline{u}_2 \left(a_1^r \overline{u}_2 + c_1 \overline{u}_3 \right)$$

The weighting matrices used in the double support phase models are

$$\hat{H} = diag\left[h_1, h_2, h_3, h_4, h_5, h_6\right]$$

$$\hat{R} = \Delta t^2 diag\left[r_1, r_2, r_3, r_4, r_5, r_6\right]$$

$$\hat{S} = 4\Delta t^4 diag\left[s_1, s_2, s_3, s_4, s_5\right]$$

As the result of the proposed algorithm, five command accelerations, belong to the right leg joints, are generated minimizing the performance measure. These joint accelerations are $\ddot{\theta}_{11}, \ddot{\theta}_9, \ddot{\theta}_7, \ddot{\theta}_5, \ddot{\theta}_3$ for the "right foot flat double support phase and $\ddot{\theta}_{10}, \ddot{\theta}_8, \ddot{\theta}_6, \ddot{\theta}_4, \ddot{\theta}_2$ for "the left foot flat double support phase". Different than the single support phase, six command accelerations remain unknown. In the

double support phase models, the six scalar constraint equations of the acceleration level provide these unknown accelerations. At the end, total of eleven acceleration commands happen to be computed and available for use in the computed torque control block.

The Matlab® codes, developed for the optimal predictive control algorithm are written in four separate m-files for each of the four models.

3.5 Inverse Kinematics

As it may have been noticed, there are many distinctions between the single support and the double support models. Mainly, the double support model is a closed linkage while the single support model is an open linkage. Naturally, the motion of the double support model is constrained as a result of the closed linkage. This means the double support model may be unable to achieve every motion which is possible for the single support model. This causes a major difficulty in the transition from the single support phase to the double support phase. Neither the joint variables nor the joint velocities of the single support model can be carried on as the initial joint variables of the double support model. Another reason of this event is the immediate flattening of the landing foot just after the heel strike. Because of these two subjects, the initial joint variables of the double support model must be determined again.

Obviously, it is unnatural to define a single posture which is assigned as the initial state of every double support phase. In this study, it is aimed to maintain a natural gait as far as possible. For this purpose, the deviation of the joint variables during the transition is reduced by utilizing an inverse kinematic solution. Since two double support models are incorporated in the simulation, there are two similar inverse kinematic solutions; one for the left foot flat double support model and one for the right foot flat double support model. Only the expressions corresponding to one of these solutions are presented because the procedures are identical. Hence, the right foot double support model has been selected for the presentation of the inverse kinematic analysis.

For the inverse position analysis, the position of the origin of body-1 with respect to the heel points are taken from the past single support model. However, the orientation of body-1 cannot be carried on because the right leg has only 5 joints to maintain that orientation. Because of this deficiency, the inverse kinematic solution gives inexact results. If there were a joint for yaw motion at the hip, this would not be a problem. In order to overcome this problem, the orientation of body-1 about y-axis is neglected. Therefore, the orientation matrix is defined as

$$\hat{C} = e^{\tilde{u}_1(\theta_2+\theta_{10})} \tag{3.157}$$

and the position vector from the point A_{11} to O_1 becomes

$$\overline{r} = \overline{p}_{O_1} - \overline{p}_{A_{11}} - a_{11}\overline{u}_3 - a_1^r \hat{C}\overline{u}_2 \tag{3.158}$$

Using these known values, the joint angles of the right leg are obtained as described below.

$$\overline{r} = a_7 \hat{C}^{(11,7)}\overline{u}_3 + a_5 \hat{C}^{(11,5)}\overline{u}_3 \tag{3.159}$$

multiplying both sides by $e^{u_1\theta_{11}}$ from the left

$$e^{\tilde{u}_1\theta_{11}}\overline{r} = a_7 e^{-\tilde{u}_2\theta_9}\overline{u}_3 + a_5 e^{-\tilde{u}_2(\theta_9+\theta_7)}\overline{u}_3 \tag{3.160}$$

multiplying both sides by $\overline{u}_2^t$ from the left

$$\overline{u}_2^t e^{\tilde{u}_1\theta_{11}}\overline{r} = \overline{0} \tag{3.161}$$

$$\left(\overline{u}_2^t \mathbf{cos}\,\theta_{11} - \overline{u}_3^t \mathbf{sin}\,\theta_{11}\right)\overline{r} = \overline{0} \tag{3.162}$$

$$\mathbf{cos}\,\theta_{11} r_2 = \mathbf{sin}\,\theta_{11} r_3 \tag{3.163}$$

Hence

$$\theta_{11} = \text{atan2}\left(\sigma_{11} r_2, \sigma_{11} r_3\right) \quad , \quad \sigma_{11} = \mp 1 \tag{3.164}$$

Then, going back to orientation matrix

$$e^{-\tilde{u}_2(\theta_9+\theta_7+\theta_5)} e^{-\tilde{u}_1\theta_3} = e^{\tilde{u}_1\theta_{11}}\hat{C} = \hat{C}^* \tag{3.165}$$

Pre-multiplying by $\overline{u}_2^t$

$$\overline{u}_2^t e^{-\tilde{u}_1\theta_3} = \overline{u}_2^t \hat{C}^* \tag{3.166}$$

$$\overline{u}_2^t \mathbf{cos}\,\theta_3 + \overline{u}_3^t \mathbf{sin}\,\theta_3 = \overline{u}_2^t \hat{C}^* \tag{3.167}$$

$$\mathbf{cos}\,\theta_3 = \hat{C}_{22}^* \tag{3.168}$$

$$\mathbf{sin}\,\theta_3 = \hat{C}_{23}^* \tag{3.169}$$

Hence

$$\theta_3 = \text{atan}2\left(C_{23}^*, C_{22}^*\right) \tag{3.170}$$

Since,

$$\theta_9 + \theta_7 + \theta_5 = \phi_9 \tag{3.171}$$

multiplying Equation (3.165) by $\overline{u}_1$ from the right

$$e^{-\tilde{u}_2\phi_9}\overline{u}_1 = \hat{C}^*\overline{u}_1 \tag{3.172}$$

$$\overline{u}_1 \mathbf{cos}\,\phi_9 + \overline{u}_3 \mathbf{sin}\,\phi_9 = \hat{C}^*\overline{u}_1 \tag{3.173}$$

$$\mathbf{cos}\,\phi_9 = \hat{C}_{11}^* \tag{3.174}$$

$$\mathbf{sin}\,\phi_9 = \hat{C}_{31}^* \tag{3.175}$$

Hence

$$\phi_9 = \text{atan}2\left(C_{31}^*, C_{11}^*\right) \tag{3.176}$$

Going back to Equation (3.160)

$$\overline{r}^* = e^{\tilde{u}_1\theta_{11}}\overline{r} \tag{3.177}$$

$$\overline{r}^* = a_7 e^{-\tilde{u}_2\theta_9}\overline{u}_3 + a_5 e^{-\tilde{u}_2(\theta_9+\theta_7)}\overline{u}_3 \tag{3.178}$$

$$r_1^* = a_7\overline{u}_1^t e^{-\tilde{u}_2\theta_9}\overline{u}_3 + a_5\overline{u}_1^t e^{-\tilde{u}_2(\theta_9+\theta_7)}\overline{u}_3 \tag{3.179}$$

$$r_1^* = -a_7 \sin\theta_9 - a_5 \sin\left(\theta_9 + \theta_7\right) \tag{3.180}$$

and

$$r_3^* = a_7 \bar{u}_3^t e^{-\tilde{u}_2\theta_9}\bar{u}_3 + a_5 \bar{u}_3^t e^{-\tilde{u}_2(\theta_9+\theta_7)}\bar{u}_3 \tag{3.181}$$

$$r_3^* = a_7 \cos\theta_9 + a_5 \cos\left(\theta_9 + \theta_7\right) \tag{3.182}$$

Square the equations (3.180), (3.182) and adding them

$$r_1^{*2} = a_7^2 \sin^2\theta_9 + 2a_5 a_7 \sin\theta_9 \sin\left(\theta_9 + \theta_7\right) + a_5^2 \sin^2\left(\theta_9 + \theta_7\right) \tag{3.183}$$

$$r_3^{*2} = a_7^2 \cos^2\theta_9 + 2a_5 a_7 \cos\theta_9 \cos\left(\theta_9 + \theta_7\right) + a_5^2 \cos^2\left(\theta_9 + \theta_7\right) \tag{3.184}$$

$$r_1^{*2} + r_3^{*2} = a_7^2 + a_5^2 + 2a_5 a_7 \cos\theta_7 \tag{3.185}$$

$$\cos\theta_7 = \frac{r_1^{*2} + r_3^{*2} - a_7^2 - a_5^2}{2a_5 a_7} = \xi_7 \tag{3.186}$$

$$\sin\theta_7 = \sigma_7\sqrt{1-\xi_7^2} \quad , \quad \sigma_7 = \mp 1 \tag{3.187}$$

Hence

$$\theta_7 = \operatorname{atan2}\left(\sigma_7\sqrt{1-\xi_7^2}, \xi_7\right) \tag{3.188}$$

Re-arranging the equations (3.180) and (3.182)

$$a_7 \sin\theta_9 + a_5 \sin\theta_9 \cos\theta_7 + a_5 \cos\theta_9 \sin\theta_7 = -r_1^* \tag{3.189}$$

$$a_7 \cos\theta_9 + a_5 \cos\theta_9 \cos\theta_7 - a_5 \sin\theta_9 \sin\theta_7 = r_3^* \tag{3.190}$$

Treating $\sin\theta_9$ & $\cos\theta_9$ as if independent and solving as linear equations

$$\begin{bmatrix} \left(a_7 + a_5\cos\theta_7\right) & -a_5\sin\theta_7 \\ a_5\sin\theta_7 & \left(a_7 + a_5\cos\theta_7\right) \end{bmatrix} \begin{bmatrix} \cos\theta_9 \\ \sin\theta_9 \end{bmatrix} = \begin{bmatrix} r_3^* \\ -r_1^* \end{bmatrix}$$

Determinant of the coefficient matrix is

$$\Delta = \left(a_7 + a_5\cos\theta_7\right)^2 + \left(a_5\sin\theta_7\right)^2 \tag{3.191}$$

If $\Delta \neq 0$;

$$\mathbf{sin}\,\theta_9 = \frac{-\left(a_7 + a_5\,\mathbf{cos}\,\theta_7\right) r_1^* - a_5\,\mathbf{sin}\,\theta_7 r_3^*}{\Delta} = \xi_9 \tag{3.192}$$

$$\mathbf{cos}\,\theta_9 = \frac{\left(a_7 + a_5\,\mathbf{cos}\,\theta_7\right) r_3^* - a_5\,\mathbf{sin}\,\theta_7 r_1^*}{\Delta} = \eta_9 \tag{3.193}$$

Hence

$$\theta_9 = \text{atan}2\left(\eta_9, \xi_9\right) \tag{3.194}$$

and

$$\theta_5 = \phi_9 - \left(\theta_9 + \theta_7\right) \tag{3.195}$$

Thus, the joint angles $\theta_{11}, \theta_9, \theta_7, \theta_5, \theta_3$ are obtained to maintain a similar posture of the past left foot flat single support model. The joint angles of the left leg ($\theta_{10}, \theta_8, \theta_6, \theta_4, \theta_2$) are obtained using the same procedure. The orientation matrix is equal to the one, given in Equation (3.157). However, the position vector is from the point A_{10} to O_1.

$$\overline{r} = \overline{p}_{O_1} - \overline{p}_{A_{10}} - a_{11}\overline{u}_3 + a_1^l \hat{C}\overline{u}_2 \tag{3.196}$$

The sign ambiguities in the inverse solution are specified as shown below to attain the desired configuration.

$$\sigma_{11} = \sigma_7 = \sigma_{10} = \sigma_6 = 1$$

After the joint angles are obtained by the inverse position analysis, the joint velocities are to be found. The solution procedure starts with the derivation of the Jacobian matrix. It is built to get the right leg joint velocities as described below.

$$\overline{V} = \hat{J}\dot{\overline{q}} \tag{3.197}$$

where

$\overline{V}$ is the 6x1 column matrix which includes the components of the linear and angular velocity of body-1,

$\hat{J}$ is the 6x5 Jacobian matrix,

$\dot{\bar{q}}$ is the column matrix including $\dot{\theta}_{11}, \dot{\theta}_9, \dot{\theta}_7, \dot{\theta}_5, \dot{\theta}_3$

$$\begin{bmatrix} J_{11} \\ J_{21} \\ J_{31} \end{bmatrix} = -a_7 \hat{C}^{(11,09)} \tilde{u}_1 \hat{C}^{(09,07)} \bar{u}_3 - a_5 \hat{C}^{(11,09)} \tilde{u}_1 \hat{C}^{(09,05)} \bar{u}_3 - a_1^r \hat{C}^{(11,09)} \tilde{u}_1 \hat{C}^{(09,01)} \bar{u}_2$$

$$\begin{bmatrix} J_{12} \\ J_{22} \\ J_{32} \end{bmatrix} = -a_7 \hat{C}^{(11,07)} \bar{u}_1 - a_5 \hat{C}^{(11,05)} \bar{u}_1 - a_1^r \hat{C}^{(11,03)} \tilde{u}_2 \hat{C}^{(03,01)} \bar{u}_2$$

$$\begin{bmatrix} J_{13} \\ J_{23} \\ J_{33} \end{bmatrix} = -a_5 \hat{C}^{(11,05)} \bar{u}_1 - a_1^r \hat{C}^{(11,03)} \tilde{u}_2 \hat{C}^{(03,01)} \bar{u}_2$$

$$\begin{bmatrix} J_{14} \\ J_{24} \\ J_{34} \end{bmatrix} = -a_1^r \hat{C}^{(11,03)} \tilde{u}_2 \hat{C}^{(03,01)} \bar{u}_2$$

$$\begin{bmatrix} J_{15} \\ J_{25} \\ J_{35} \end{bmatrix} = -a_1^r \hat{C}^{(11,01)} \bar{u}_3$$

$$\begin{bmatrix} J_{41} \\ J_{51} \\ J_{61} \end{bmatrix} = -\bar{u}_1$$

$$\begin{bmatrix} J_{42} \\ J_{52} \\ J_{62} \end{bmatrix} = -\hat{C}^{(11,09)} \bar{u}_2$$

$$\begin{bmatrix} J_{43} \\ J_{53} \\ J_{63} \end{bmatrix} = -\hat{C}^{(11,07)} \bar{u}_2$$

$$\begin{bmatrix} J_{44} \\ J_{54} \\ J_{64} \end{bmatrix} = -\hat{C}^{(11,05)} \bar{u}_2$$

$$\begin{bmatrix} J_{45} \\ J_{55} \\ J_{65} \end{bmatrix} = -\hat{C}^{(11,03)} \bar{u}_1$$

Since, the number of the right leg joints is deficient, equation (3.197) is solved by using the pseudo-inverse of the Jacobian matrix.

$$\dot{\bar{q}} = \hat{J}^{-1}\bar{V} \tag{3.198}$$

Thus; $\dot{\theta}_{11}, \dot{\theta}_9, \dot{\theta}_7, \dot{\theta}_5, \dot{\theta}_3$ are obtained. The left leg joint velocities $\dot{\theta}_{12}, \dot{\theta}_{10}, \dot{\theta}_8, \dot{\theta}_6, \dot{\theta}_4, \dot{\theta}_2$ are acquired by the constraint equations (3.48) and (3.51) which have been derived in section 3.1.4.

As a result, the deviation of the joint variables during the transition from the single support phase to the double support phase is reduced as far as possible by utilizing this inverse kinematic solution.

CHAPTER 4

SIMULATION ENVIRONMENT

The physical and mathematical models, the resultant expressions of the applied methods for both direct and inverse dynamic solutions and also the control algorithm used in the simulation were introduced in the previous chapters. After this analysis, in order to simulate the gait of a humanoid walker, the mathematical expressions are to be translated into a programming code and they must be computed effectively. For this purpose, Matlab® software and one of its add-in tools, Simulink® were preferred because of their superior features.

Matlab® is a high-performance language for technical computing. It integrates computation, visualization, and programming in an easy-to-use environment where problems and solutions are expressed in familiar mathematical notation. Simulink® is a software package for modeling, simulating, and analyzing dynamic systems [30].

Employing these tools in the thesis study provided many benefits. First of all, such a programming environment permits the user to gain full control over the simulation. The restrictions which must be admitted are at a minimum number. Therefore, the user becomes able to edit every part of the simulation freely. In this connection, each part of the presented humanoid gait simulation is accessible and re-configurable. For instance, another researcher can upgrade the control algorithm partially while keeping the rest of the simulation the same.

The detailed usage of Matlab® and Simulink® will be described in the following sections. Also, in this chapter, the main structure and the subsystems of the Simulink® model will be presented. Moreover, the simulation configuration parameters will be discussed in a detailed manner.

The Simulink® models built for this study are hierarchical. They are organized using the bottom-up approach. In this approach, many blocks constitute a subsystem and at a higher layer, these subsystems are collected in a larger subsystem. At the top layer, the main system model includes all the subsystems and the Simulink® blocks. By this way, the organization of the simulation becomes comfortable and compact block diagrams are attained. This feature also makes the simulation structure more realizable.

As it happens in every simulation platform, some parameters are to be determined before the program runs. These parameters refer to two different types of parameters in this study. The first one is the configuration parameters of Simulink® software. These are determined according to the characteristics of the simulated dynamic system. The second type of parameters is directly related to the built model. For this study, the mass and height of the humanoid walker, the weighting factors used in the optimization, the prediction time range (Δt) and similar internal constants like gravitational acceleration are this kind of parameters.

In the proposed simulation model, “fixed-step” type, “ode1” continuous solver is used because the model has continuous states. By this solver, numerical integration is performed to compute the values of these continuous states. The integration technique preferred is Euler’s method (ode1). The integration techniques used by the fixed-step continuous solvers trade accuracy for computational effort. Since, the accuracy is satisfied by the effective control algorithm, the shortest computation time is aimed in this study. Therefore, the least complex integration method was chosen. Furthermore, this “fixed-step” type solver computes the simulation's next time by adding a fixed-size time step to the current time. The fixed step size was chosen as 0.01 seconds after a lot of trials. Although, the computation time increases with smaller step sizes than 0.01, no valuable enhancement occurs in the simulation. Besides, the stop time of simulation is not critical. It may run forever for the proposed model. Of course, a minimum period is needed to complete a full gait cycle.

For the simulation presented in the thesis, the mass and height of the humanoid walker were taken as 56 kg and 1.60 m. The gravitational acceleration (g) is indicated as 9.81 m/s^2 in the necessary m-files of the model. The rest of this kind of configuration parameters will be mentioned in the relevant sections.

4.1 The Main System of the Simulink® Model

As it may have been remembered, the full gait cycle was divided into four successive phases. The model of each phase is constructed in a subsystem and the integrity of these four models is achieved in the main system. At this top-layer, the phase selector subsystem provides the transitions from the model of one phase to the model of another phase. In Figure 4.1, the main system and its subsystems are illustrated.

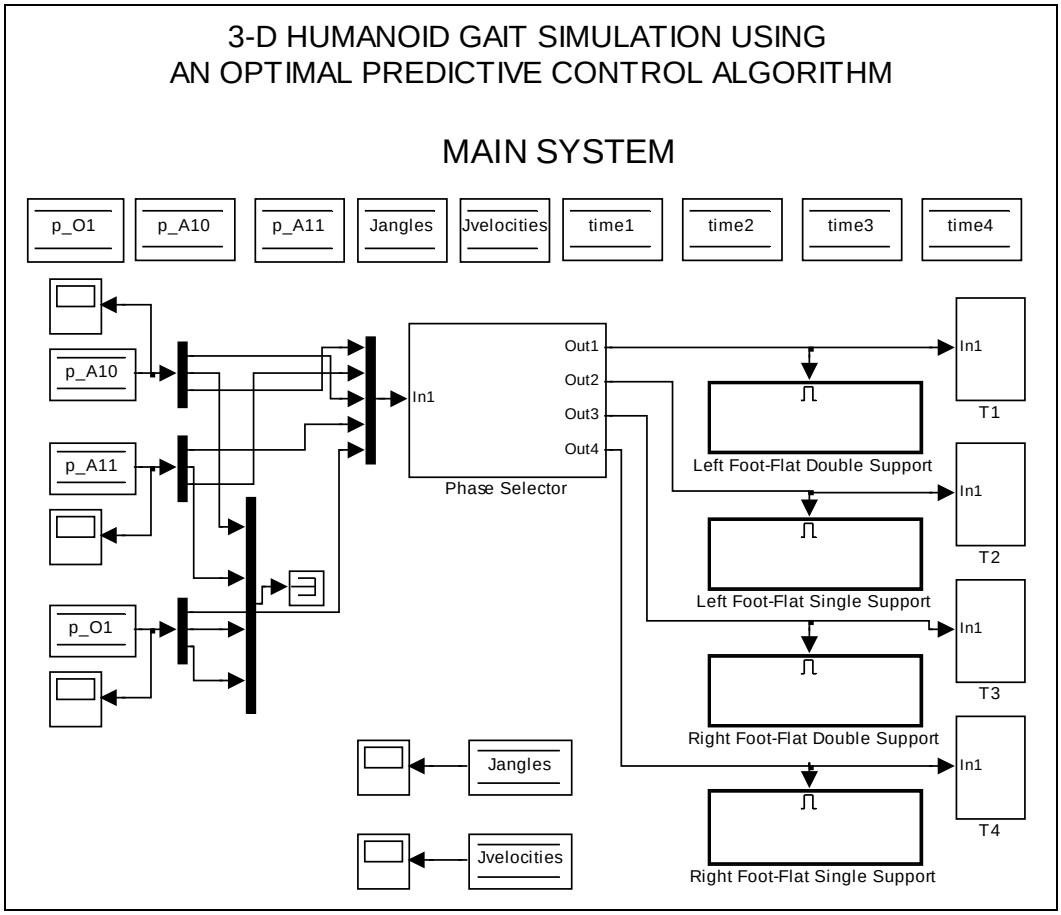

Figure 4.1 The main system (top-layer) of the Simulink® model

In the main system, the phase selector subsystem has a critical importance for the proper operation of the simulation model. It decides the current phase of gait comparing the positions of the origin O_1 (body-1's frame origin), A_{10} and A_{11} (the heel points of the left and the right foot). Internal structure of the phase selector subsystem is shown in Figure 4.2.

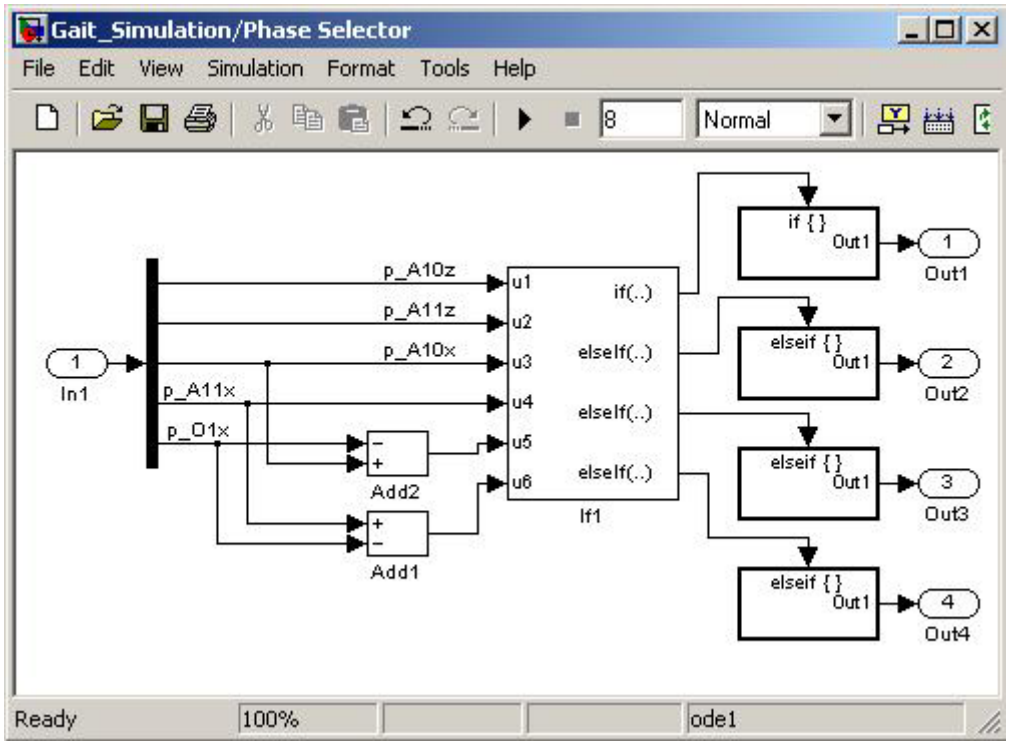

Figure 4.2 The phase selector subsystem

In the conditional block (If1), there are four "if expressions" employing 6 inputs. These inputs are as defined below:

u1 is the z component of A_{10}

u2 is the z component of A_{11}

u3 is the x component of A_{10}

u4 is the x component of A_{11}

u5 is u3 minus the x component of O_1

u6 is u4 minus the x component of O_1

The four conditional statements are as follows:

1. If u1 <= 0.001 & u3 > u4 & u5 > 0.02 then Out1.
2. If u5 <= 0.02 & u2 > 0.001 then Out2.
3. If u2 <= 0.001 & u4 > u3 & u6 > 0.02 then Out3.
4. If u6 <= 0.02 & u1 > 0.001 then Out4.

The explanation of the first statement is that IF the left heel is above the ground 0.001 m or less AND it is in front of the right heel AND the distance between A_{10} and O_1 in the x-direction is greater than 0.02 m THEN the “left foot flat double support phase” is the current phase. Similarly, in the third expression, it is stated that IF the right heel is above the ground 0.001 m or less AND it is in front of the left heel AND the distance between A_{11} and O_1 in the x-direction is greater than 0.02 m THEN the “right foot flat double support phase” is the current phase. The second statement expresses that IF the distance between A_{10} and O_1 in the x-direction is less than or equal to 0.02 m AND the right heel is above the ground more than 0.001 m THEN the “left foot flat single support phase” is the current phase. Similarly, the fourth expression states that IF the distance between A_{11} and O_1 in the x-direction is less than or equal to 0.02 m AND the left heel is above the ground more than 0.001 m THEN the “right foot flat single support phase” is the current phase. By this way, the transitions from one phase model to another one are achieved successfully. As every part of the simulation, these statements can also be modified for different desired walking patterns.

The main system includes four more subsystems. Each one of these subsystems includes the blocks of four separate phases. During the simulation process, they are enabled one after the other by the phase selector subsystem. These four subsystems take the name of the phase which they simulate. These are:

1. The left foot flat double support subsystem
2. The left foot flat single support subsystem
3. The right foot flat double support subsystem
4. The right foot flat single support subsystem

The internal structure, the running procedure and other properties of these subsystems will be explained in separate sections.

Moreover, in the main system, there are nine “data store memory blocks”. They are used to store some variables. These are the coordinates of the points O_1, A_{10} and A_{11}, the joint angles, the joint velocities and the timer data. The “data store read blocks”, at any layer, access the “data store memory blocks” and transmit data to the relevant block. In a similar manner, the “data store write blocks”, send data from any layer to the “data store memory blocks” at the top-layer. Hence, the continuity is provided in the simulation. Four timer memory blocks are placed in the main system. Each one of them is associated to a single phase model. For instance, when the “left foot flat single support phase” subsystem is enabled, “time2” memory block starts to store the phase time of this subsystem from zero to the end of the phase and at the end, it resets to zero by the subsystem “T2”. The internal view of the “T2” subsystem is shown in Figure 4.3. This procedure runs independent of the simulation time and it is required to set the initial values of the starting phase.

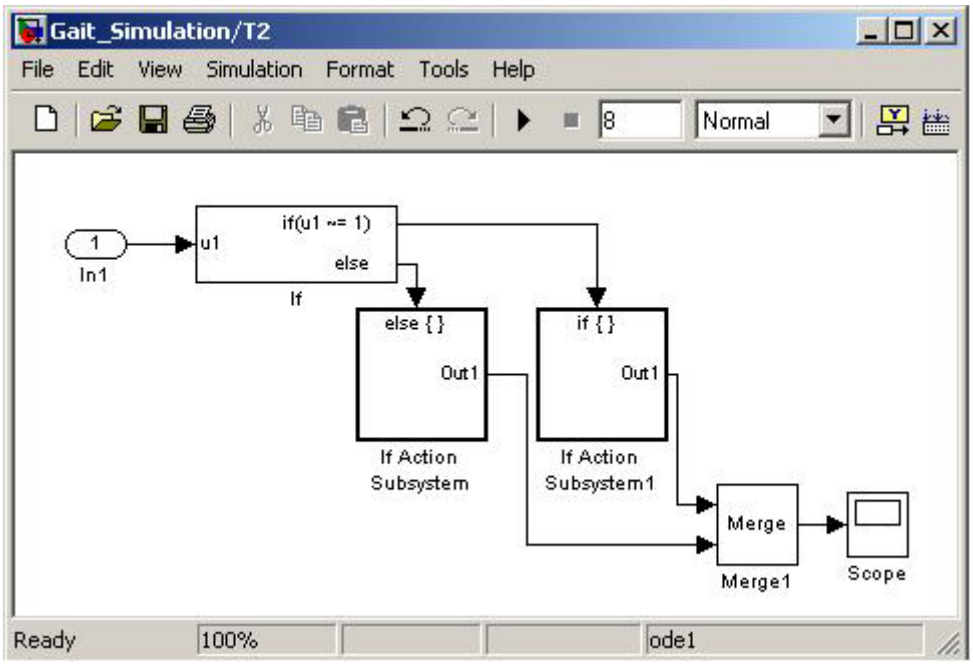

Figure 4.3 The “T2” phase time reset subsystem

Furthermore, some common subsystems are present both in the double support phase subsystems and in the single support phase subsystems. These are the integration subsystem, the trigger subsystem and the timer subsystem.

The integration subsystem contains many integration blocks. The function of this subsystem is to compute the joint velocities and the joint angles by integrating the joint accelerations at each step due to the specified solver. Also, the initial values of these variables are assigned in the integration subsystem by external signals. In order to follow the signal lines in this subsystem easily, several multiplexer and de-multiplexer blocks are used and the integration blocks belonging to a joint are grouped together. In Figure 4.4, the internal structure of these groups can be examined. Here the input port 1 is the joint acceleration, 2 is the initial joint velocity and 3 is the initial joint angle. The output port 1 is the angular displacement and 2 is the angular velocity. Besides, a trigger signal (input port 4) is generated to reset the initial values of the integration blocks at the beginning of each phase. One of the four integration subsystems is shown in Figure 4.5.

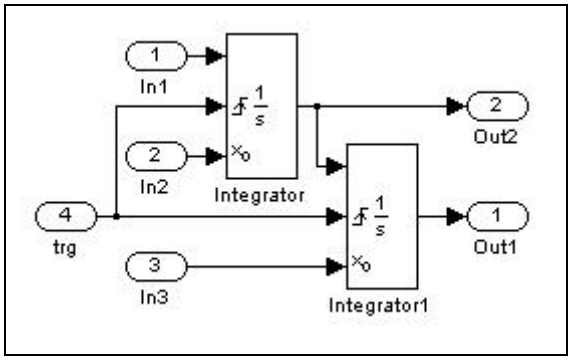

Figure 4.4 Internal structure of a joint's integration subsystem

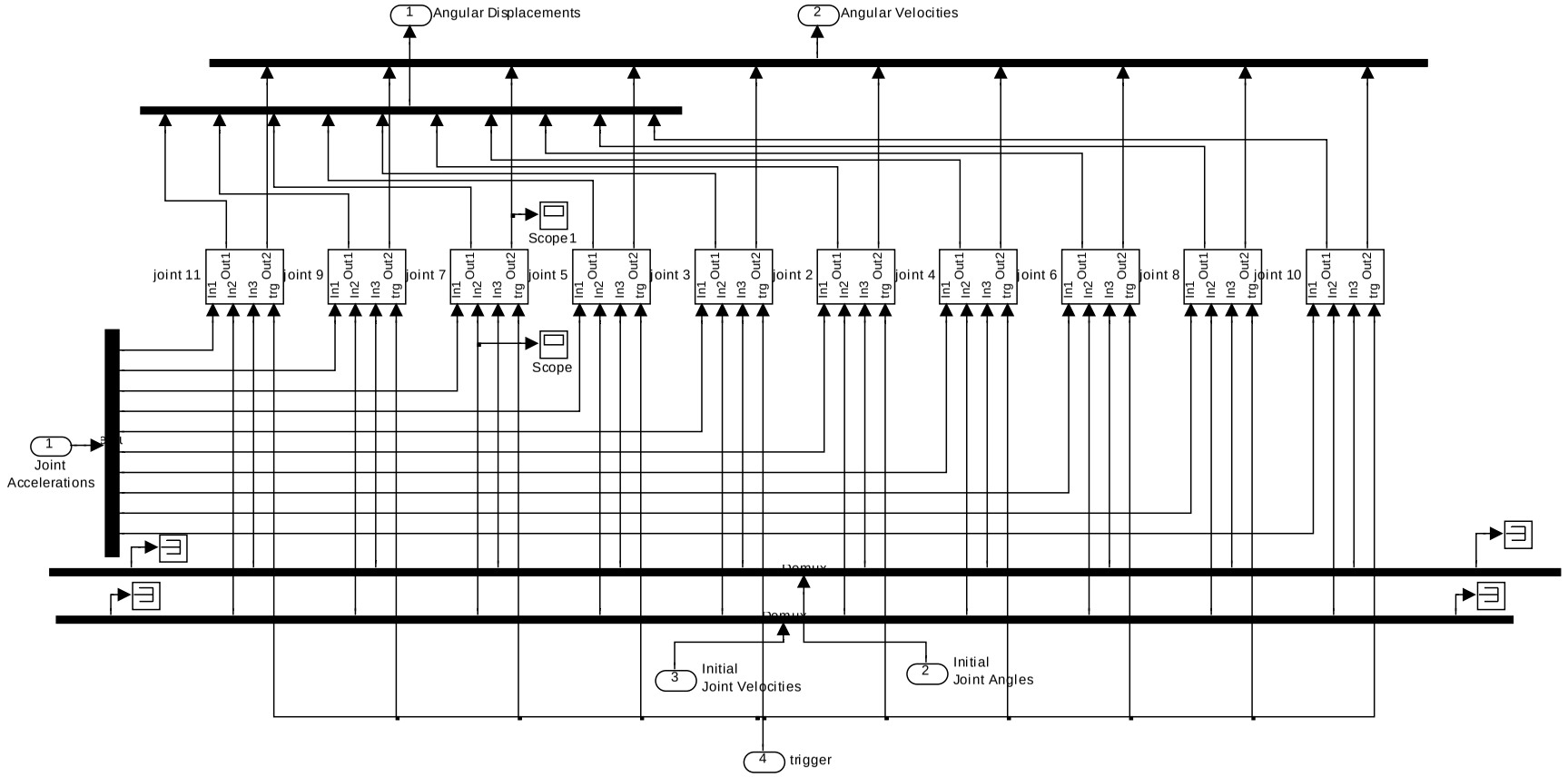

Figure 4.5 The integration subsystem

The trigger subsystem, shown in Figure 4.6, generates the trigger signal at the beginning of the phase. Hence, the integration process starts with the latest joint variables. Without this subsystem, the values at the beginning of the simulation would be initialized at every run of a phase model. Therefore, a proper gait could not be carried out. In this subsystem, if the phase time (not the simulation time) is zero, the output signal is “1”; else it is “0”.

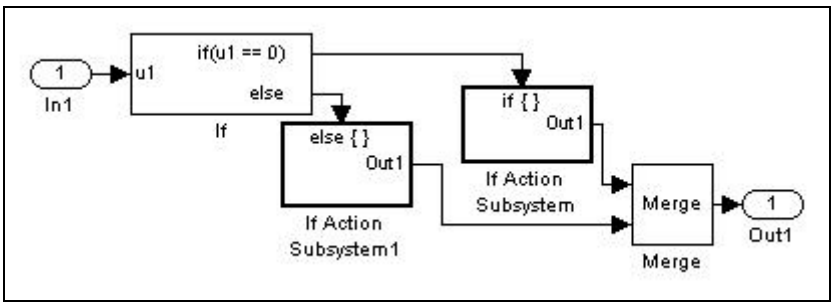

Figure 4.6 The trigger subsystem

The timer subsystem is an essential subsystem. Since, the simulation is performed phase by phase; the instants of start and stop of a phase acquire very much importance. At the beginning of a phase (i.e. when the phase time is zero), the last position values of O_1, A_{10} and A_{11} points are sent from the previous phase model to the current one as the initial values. Also, at the end of the phase, the phase time must be reset for a next run. For this reason, a particular timer other than the default clock block which shows the simulation time was built. By this subsystem, it becomes also possible to operate the trigger subsystem and the reference input subsystems of both the double and single support phase models. In Figure 4.7, the timer subsystem is illustrated.

After the explanation of these common subsystems of the simulation, the four subsystems of the single and the double support phases are presented in the following sections.

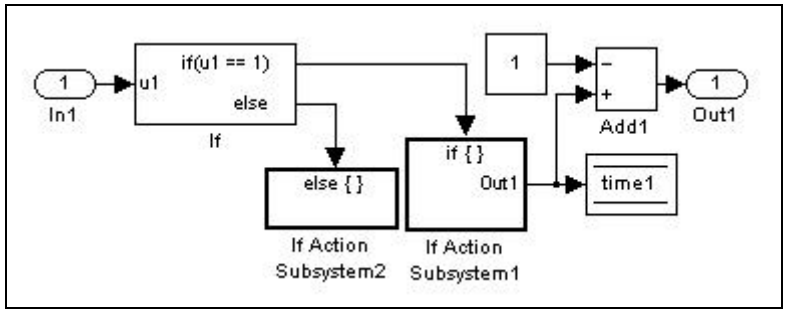

Figure 4.7 The timer subsystem

4.2 The Single Support Phase Subsystems

The main system of the simulation model includes two single support phase subsystems. One of them contains the "left foot flat single support phase" model and the other one contains the "right foot flat single support phase" model. The only difference between these subsystems is in the contents; otherwise their structures are the same. In the Figure 4.8 and 4.9, these Simulink subsystems are illustrated.

These subsystems are enabled when the phase selector subsystem sends them a signal of "1". Then, the timer subsystem starts to count the phase time. At the first step, when the phase time is zero, the trigger subsystem resets the initial values in the integration subsystem and the initials of the model are assigned from the data store memory blocks of p_O1, p_A10, p_A11 in the top layer. Meanwhile, the reference input subsystem of the single support phase model starts running using the phase time data.

The reference input subsystem contains the position and velocity components of point O_1 (origin of body-1's frame) and the heel point of the swinging foot. It is possible to change these reference values according to the desired gait. In this subsystem, the prediction time range (Δt) is specified and the desired future values of the references happen to be obtained in this manner. The reference input subsystem is illustrated in Figure 4.10.

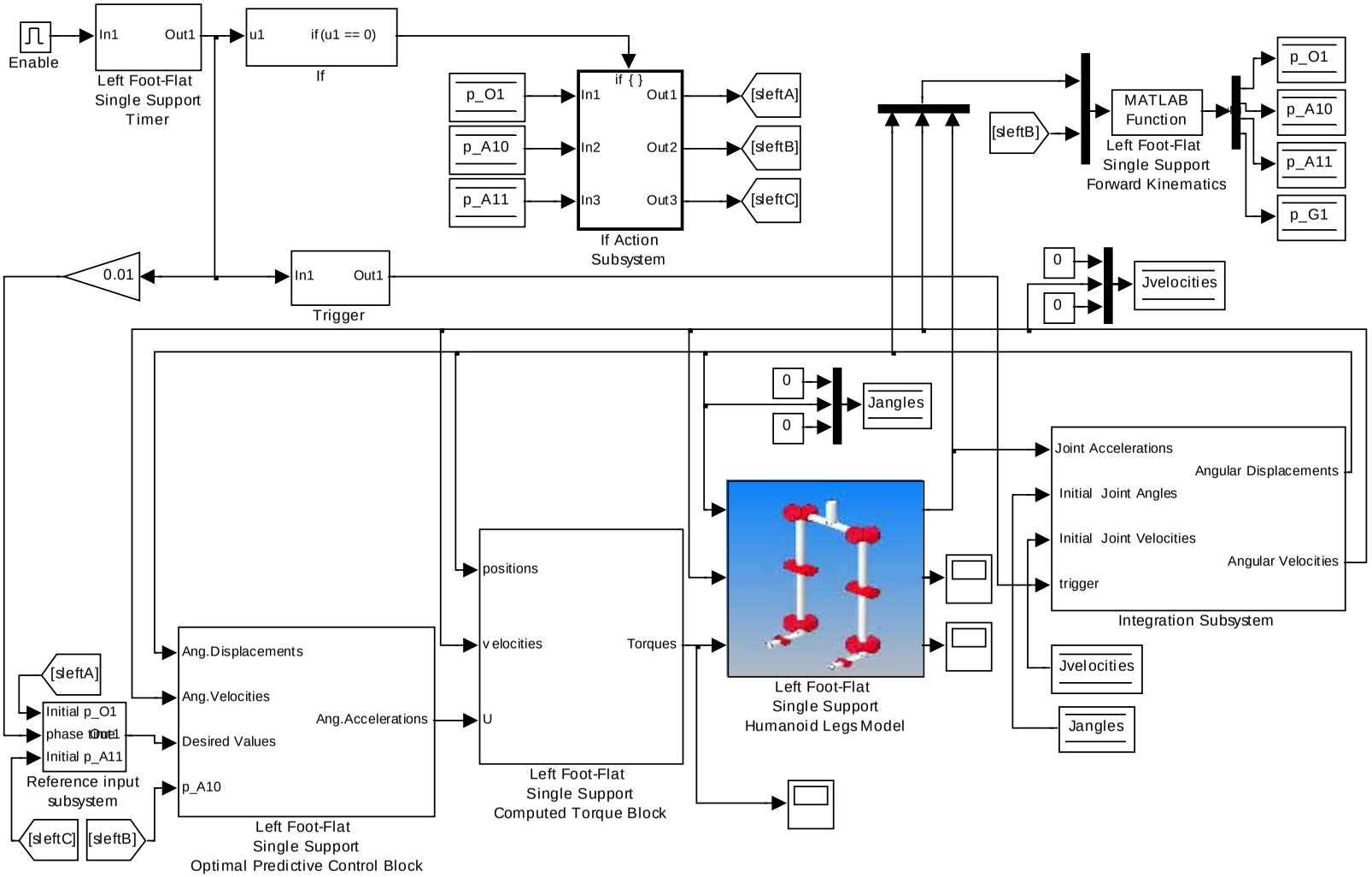

Figure 4.8 The left foot flat single support phase subsystem

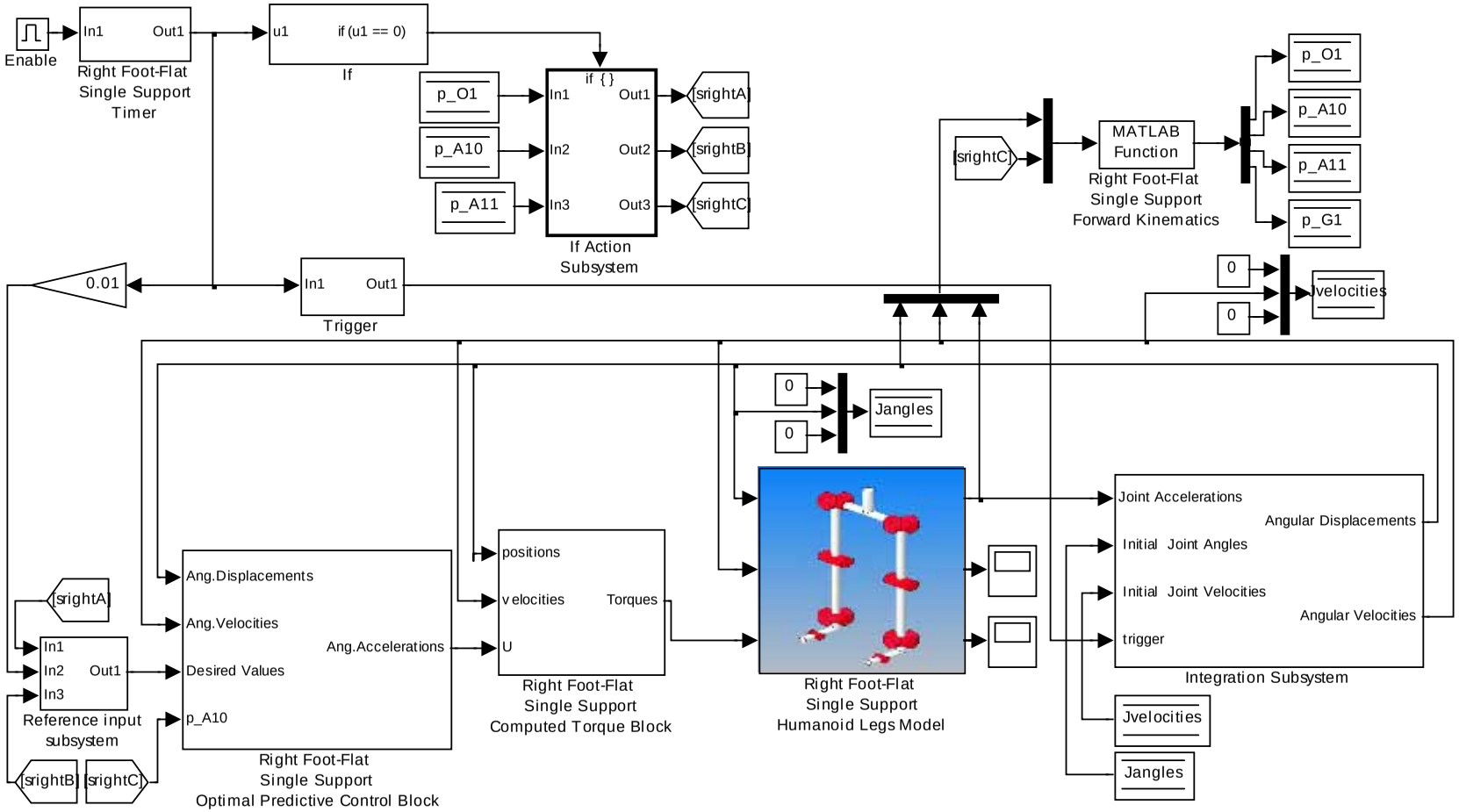

Figure 4.9 The right foot flat single support phase subsystem

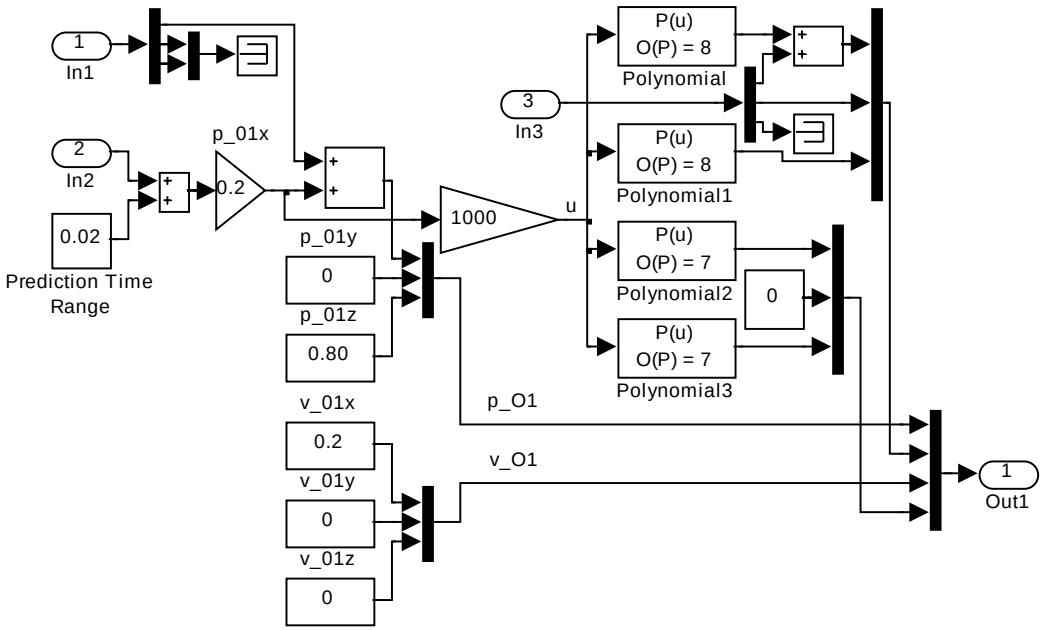

Figure 4.10 The reference input subsystem of the single support model

It may have been noticed in Figure 4.10 that a straight line, 80 cm above the ground is described as the desired path of origin O_1. The desired velocity is specified as 0.2 m/s in this direction and the prediction time range is specified as 0.02 seconds. The desired paths of the left heel point (A_{10}) in the "right foot flat single support phase" and the right heel point (A_{11}) in the "left foot flat single support phase" are the same. These paths are determined by the eigth order polynomials given by the following equations:

$$\begin{aligned} P_x(u) = & -5.69535e11u^8 + 1.49367e110u^7 - 1.60087e10u^6 \\ & + 8.91429e8u^5 - 2.67406e7u^4 + 0.00039e9u^3 \\ & - 0.00165e6u^2 + 4.83u \end{aligned} \tag{4.1}$$

$$\begin{aligned} P_z(u) = & -1.39834e11u^8 + 3.37575e10u^7 - 3.21689e9u^6 \\ & + 1.51404e8u^5 - 3.59123e6u^4 + 4.15695e4u^3 \\ & - 390u^2 + 4.43u + 35.45 \end{aligned} \tag{4.2}$$

These polynomials depend on the position of O_1 point in the x-direction, not on time. Hence, a synchronous motion between the HAT and the swinging foot is

achieved. Since, the desired velocity of O_1 point is constant during the single support phase; it becomes easy to specify the relation between the phase time (t) and the independent variable of the polynomials (u). This relation is expressed as:

$$u = \mathrm{X}_{O_1} = v_{O_1}^{x} t \tag{4.3}$$

The reference paths of the heel points are defined according to some criteria. Firstly, the path should be smooth and differentiable. So, the swinging foot becomes able to perform a continuous motion. Secondly, the maximum height of the foot from the ground is adjusted for a normal gait. In the determination of these desired paths, an extra attention was paid to the heel contact of the swinging foot. It is aimed to generate the least possible impact during the landing of foot. Hence, the desired paths are designed to achieve a soft touch on the ground. In the optimal predictive control algorithms of the single support phase models, the desired velocity components of the heel points are also required together with the desired position components. Therefore, the desired velocity values of the heel points are obtained by differentiating the above polynomials once. The polynomials representing the velocities are given below:

$$\begin{aligned} P_x'(u) = {} & -4.5563e9u^7 + 1.0456e9u^6 - 9.6052e7u^5 + 4.4571e6u^4 \\ & - 0.10696e6u^3 + 1164.9u^2 - 3.3059u + 4.8294 \end{aligned} \tag{4.4}$$

$$\begin{aligned} P_z'(u) = {} & -1.1187e9u^7 + 2.363e8u^6 - 1.9301e7u^5 + 7.5702e5u^4 \\ & - 1.4365e4u^3 + 124.71u^2 - 0.77474u + 4.4318 \end{aligned} \tag{4.5}$$

During the simulation, total of twelve desired values enter the optimal predictive control (OPC) subsystem, in this phase. This subsystem generates the ten command accelerations of the joints. In the OPC subsystem, a Matlab function block is placed and an m-file which contains the algorithm described in Chapter 3 is embedded in this block. The optimization weighting factors used in this subsystem have a great influence on the humanoid gait. These factors were decided by the trial-and-error procedure. During this procedure, the minimization of the heel point position error was kept prior to the minimization of the position

error of body-1. Also, having lower actuating torques was another emphasized criterion.

After that, all the command accelerations enter the computed torque subsystem. The computation algorithm for the required single support phase actuating torques was introduced in Chapter 3. This algorithm is employed by the m-file in the Matlab function block of the computed torque subsystem. As the output of this subsystem, ten actuating torque values are obtained and they are sent to the humanoid model subsystem (the plant). Similar to the previous subsystems, an m-file is embedded in the Matlab function block of the plant. The m-file representing 36 Newton – Euler equations produces the joint accelerations using 3 input vectors: the actuating torques, the angular displacements and the angular velocities. Moreover, the reaction forces and the reaction moments are obtained as the other outputs of this subsystem.

The joint angles and the joint velocities become available, after the integration of the joint accelerations. Then, the cascaded loops are closed and the simulation runs another step. This cycle continues until the condition of the next phase is satisfied.

The forward kinematics subsystems of the single support phases compute the kinematic expressions given in Chapter 3 using the joint variables. Hence, all the kinematic information about each link of the humanoid walker comes out. Also, this subsystem visualizes the humanoid walker by generating a 3D plot.

The initial values of the joint variables in the integration subsystem of the single support phase models are assigned directly from the memory blocks. Hence, the values of the last double support phase joint variables can be used as the initials of the new single support phase. This property assures the continuity of the humanoid gait when passing from the double support phase to the single support phase.

Up to here, the common features of the two single support phase subsystems are explained. However, there are some distinctions between the two. Firstly, separate m-files are utilized in the Matlab function blocks of the left foot flat and

the right foot flat single support subsystems. For instance, the m-file, “Torquer_SS_right.m” is used in the computed torque control subsystem of the “right foot flat double support phase”, while; the m-file, “Torquer_SS_left.m” is used in the computed torque control subsystem of the “left foot flat double support phase”. Secondly, the Goto/From blocks exchange for the left foot flat and the right foot flat periods. While; the initial position data of the right heel point (A_{11}) are used in the OPC subsystem of the “right foot flat double support phase”, in the left foot flat one, the initial position data of the left heel point (A_{10}) are used.

4.3 The Double Support Phase Subsystems

Two double support phase subsystems are built for the simulation. One of them contains the “left foot flat double support phase” model and the other one contains the “right foot flat double support phase” model. The structure of these subsystems is identical, but their contents are different. The common features of these two subsystems are presented over one of them and the distinctions are emphasized. The subsystems of the left and the right foot flat double support phases can be examined in Figure 4.11 and 4.12.

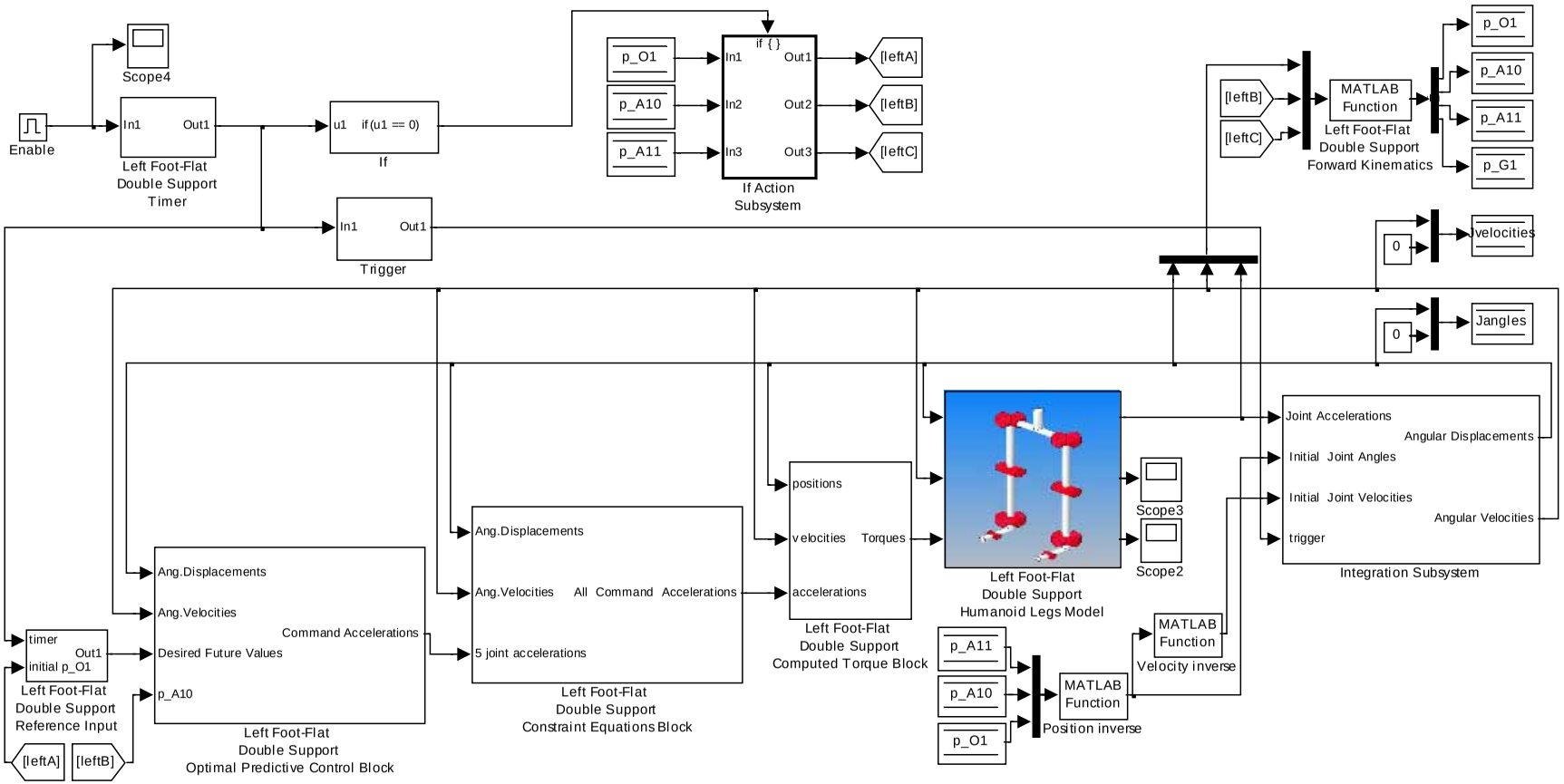

Figure 4.11 The left foot flat double support phase subsystem

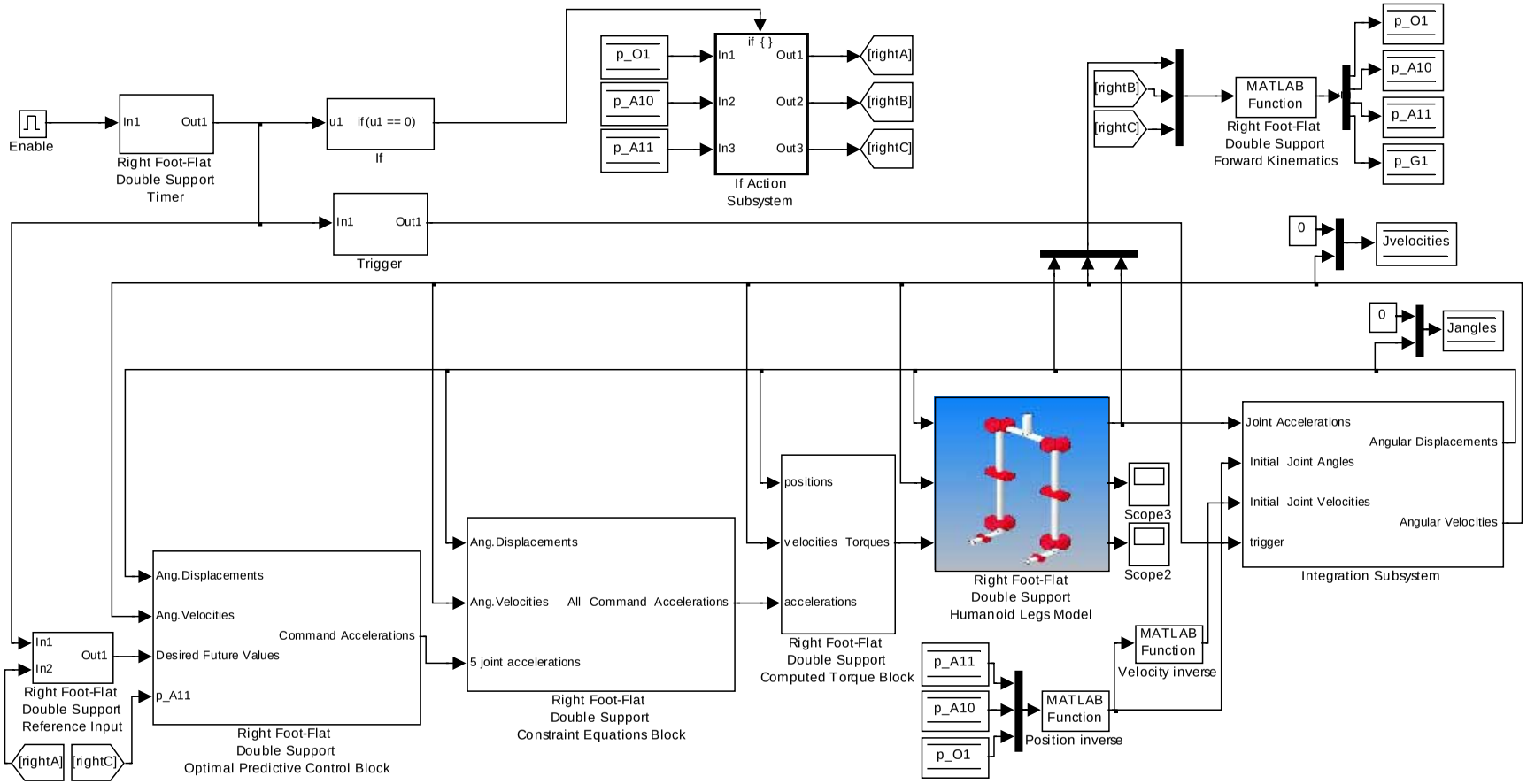

Figure 4.12 The right foot flat double support phase subsystem

Similar to the single support phase models, these subsystems are enabled by the phase selector subsystem. Firstly, the timer subsystem starts to count the phase time. The trigger subsystem resets the initial values in the integration subsystem at the first step and the initials of the model are assigned. In the meantime, the reference input subsystem of the double support phase model starts running using the phase time data.

These parts of the double support phase subsystems are identical with the single support phase subsystems. But, the difference comes to place at the reference input subsystem. The reference input subsystems contain only the position and velocity components of point O_1 (origin of body-1's frame) in this phase. It is possible to change these reference values according to the desired gait. In this subsystem, the desired future values of the references are obtained by providing the sum of the phase time and the prediction time range (Δt). The reference input subsystem of the double support phase subsystems is illustrated in Figure 4.13.

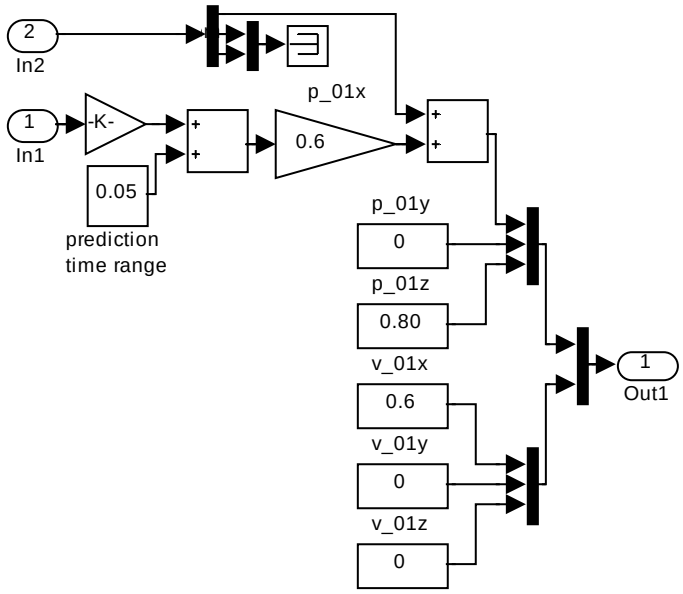

Figure 4.13 The reference input subsystem of the double support model

While, the desired height of the origin O_1 from the ground is same as it was in the single support phase (80 cm), the desired velocity in the x-direction is increased

to 0.6 m/s. Also, the prediction time range is increased and specified as 0.05 seconds. The reason of these changes is the desire to have a faster walking. By altering these parameters, the walking speed and the control stiffness can be adjusted. However, these changes effect the next single support phase and certainly the parameters of that phase must be updated together with the optimization factors.

During the simulation, the desired values are handled by the optimal predictive control (OPC) subsystem. This subsystem generates the five command accelerations of the joints at the flat foot side. In the OPC subsystem, a Matlab function block is placed and an m-file (Optimal_DS_left.m or Optimal_DS_right.m) which contains the algorithm described in Chapter 3 is embedded in that block. After that, the remaining six command accelerations are calculated from the six scalar constraint equations and added to the preceding five command accelerations. So, total of eleven command accelerations are acquired to drive eleven joints.

Then, all the command accelerations enter the computed torque subsystem. The algorithm of the computation of required double support phase actuating torques was introduced in Chapter 3. The weighting factors in the optimization procedure of computed torque algorithm are carried out by trial-and-error method. The main goal of these trials was to reduce the ankle joint accelerations while keeping the tracking error tolerable. However, in order to realize different goals, one can select different weightings. This algorithm is employed by the m-file in Matlab function block of the computed torque subsystem. As the output of this subsystem eleven actuating torque values are obtained and they are sent to the humanoid legs model subsystem (the plant). Similar to the previous subsystems, an m-file is embedded in the Matlab function block. The m-file representing 36 Newton – Euler equations and 6 scalar constraint equations produces the joint accelerations using the vector of the actuating torque, the angular displacement and the angular velocity inputs. Moreover, the reaction forces and the reaction moments are obtained as the bi-products of this formulation as in the single support phase.

After the integration of the joint accelerations, the simulation runs the next step. This cycle continues until the condition of the next phase is satisfied.

The forward kinematics subsystems of the double support phases compute the kinematic expressions given in Chapter 3. As a result, the positions, velocities and accelerations of each link of the humanoid walker become available. As a second task of this subsystem, the humanoid walker is visualized by a 3D plot.

The last subsystems of the double support phases are the inverse kinematics subsystems. In the single support phase subsystems, there is no need for such an inverse kinematics effort. However, the transition from the single support phase to the double support phase arises a vital problem at the beginning of the new phase. Since, the double support models are closed linkage systems; they cannot accomplish every motion generated by the single support models. For this reason, the last joint variables produced by a single support model cannot be used as the initial joint variables in the integration subsystem of a double support model. In addition to this, just after the heel of the swinging foot touches the ground at the end of a single support phase, the sole of that foot flattens immediately. This also makes the initial joint variables of a double support phase different than the last values of the ended single support phase. However, this deviation is minimized by finding the initial joint variables from the inverse kinematics solution. According to the last position and velocity of points O_1, A_{10} and A_{11}, the necessary joint variables are computed by both the constraint equations and the inverse kinematic equations. This subsystem takes the required inputs directly from the relevant top-layer data store memory blocks. By this way, although a discontinuity occurs at the joint variables, they deviate a little during the transition.

The differences between the two double support phase subsystems are the same as in the single support phase subsystems. The m-files utilized in the Matlab function blocks of the left foot flat and the right foot flat double support subsystems are different. Also, the Goto/From blocks shift for the left foot flat and the right foot flat periods.

CHAPTER 5

RESULTS AND DISCUSSION

The results of gait simulation using the humanoid model which imitates a subject of 56 kg mass and 1.60 m height is presented in this chapter. The initial posture of the humanoid walker is specified in such a manner that the simulation starts with the left foot flat double support model. Actually, the initial kinematic parameters are not so critical. The simulation is able to start from any non-singular configuration employing the suitable one of four models corresponding to four phases of gait.

The desired gait pattern for the humanoid model is established by defining the trajectories of 4 points: O_1 (the origin of body-1), G_1 (the mass center of body-1), A_{10} (the left heel point) and A_{11} (the right heel point). In this study, the desired trajectories of O_1 and G_1 are given as two straight lines parallel to each other along x-direction. By the optimal control algorithm, the model generates *natural* oscillations about these lines like a human being without any enforcement. Also, the desired orientation of HAT is determined as a result of this method.

In the presented study, body-1 has two different velocities on these lines in the single and double support phases. As in ideal gait of human, it is faster during the double support phase. The desired velocities of both O_1 and G_1 points are 0.6 m/s in the double support phase and 0.2 m/s in the single support phase. These velocities are specified after so many trials to reach an optimum value with lower actuating torques.

In the single support phases, the desired paths of A_{10} and A_{11} points are specified by the polynomials presented in chapter 4. Thus, for the swinging foot, it is aimed to realize a step of 0.4 m length and a maximum height of 6 cm over the ground. These desired paths are also designed giving serious attention to reduce the impact which occurs when the heel strike.

These reference values can be modified due to desired humanoid gait. As an improvement, instead of the pre-defined paths, it is possible to use a high-level controller which generates appropriate paths for walking.

With these reference values, two successive full gait cycles are simulated. This motion takes 1.77 seconds and each of the four phases occurs twice. The reference and actual position values of point O_1 in x, y and z diections are plotted in figure 5.1. Then, the reference and actual position values of point G_1 can be investigated in figure 5.2. the oscillations from the desired paths can be reduced by tuning the optimization weighting factors. The elapsed time for this run of simulation is 12.67 seconds on a desktop computer with 1.6 MHz processor and 512 Mb RAM. This value is quite good for such a complicated simulation. In figure 5.3, the side view of the humanoid model during the gait is illustrated as snapshots. Also, the front view can be examined in figure 5.4.

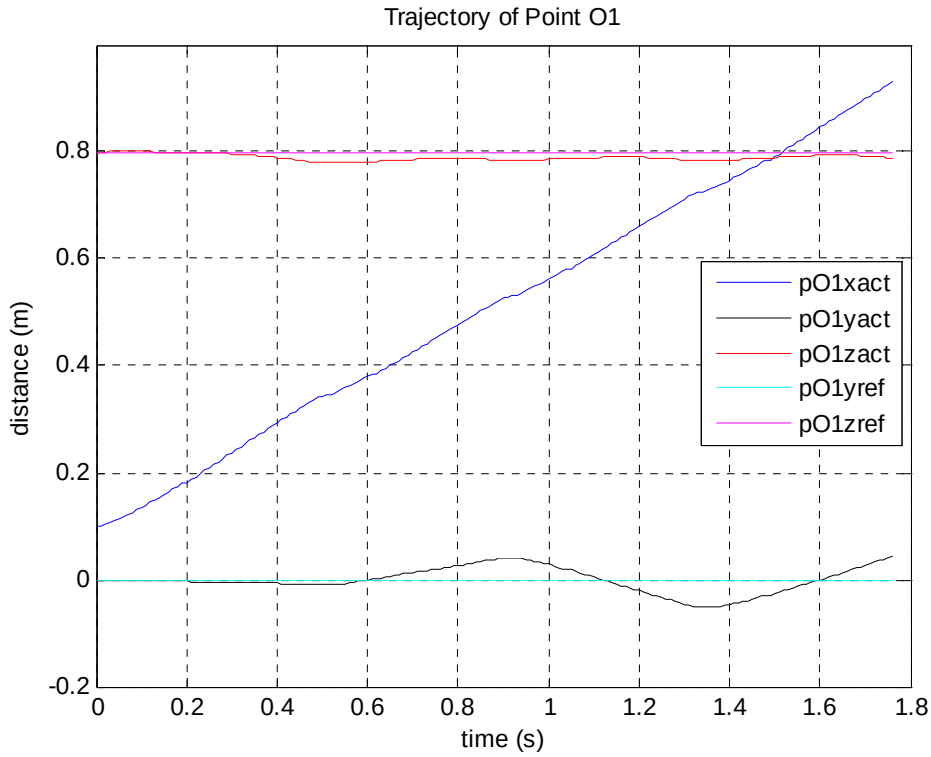

Figure 5.1 Trajectory of point O_1

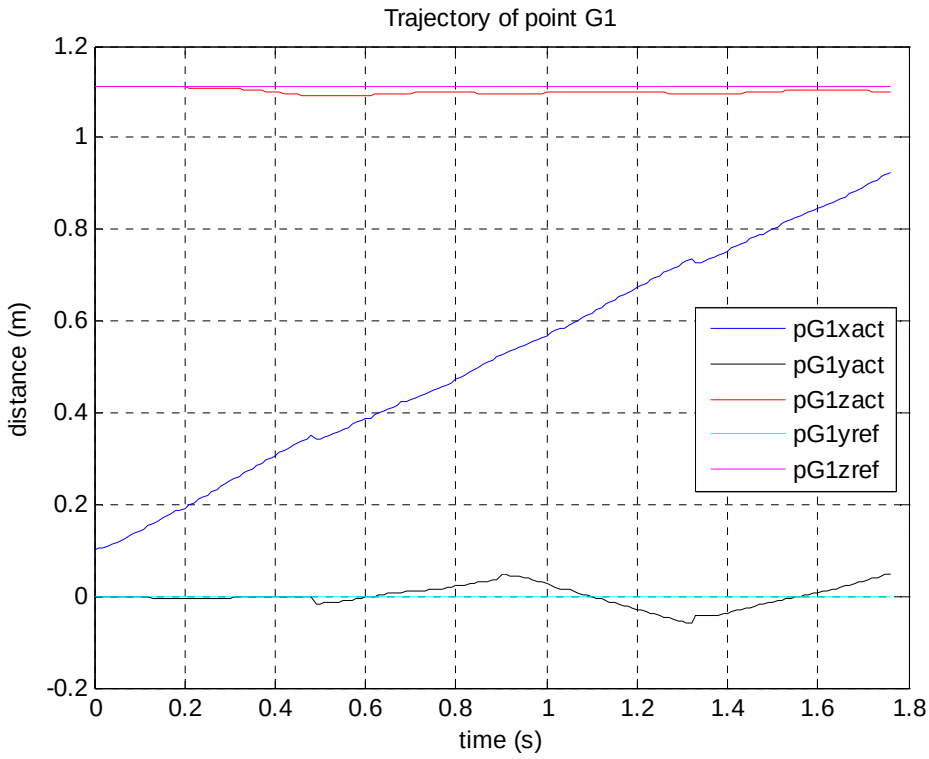

Figure 5.2 Trajectory of point G_1

The resultant joint angles of the simulation are presented in the figures 5.5 and 5.6. The continuity of the joint angles during the transition from the double support phase to the single support phase may be noticed in these figures. However, some unavoidable deviations occur at the end of the single support phases. This phenomena has been explained in section 3.5.

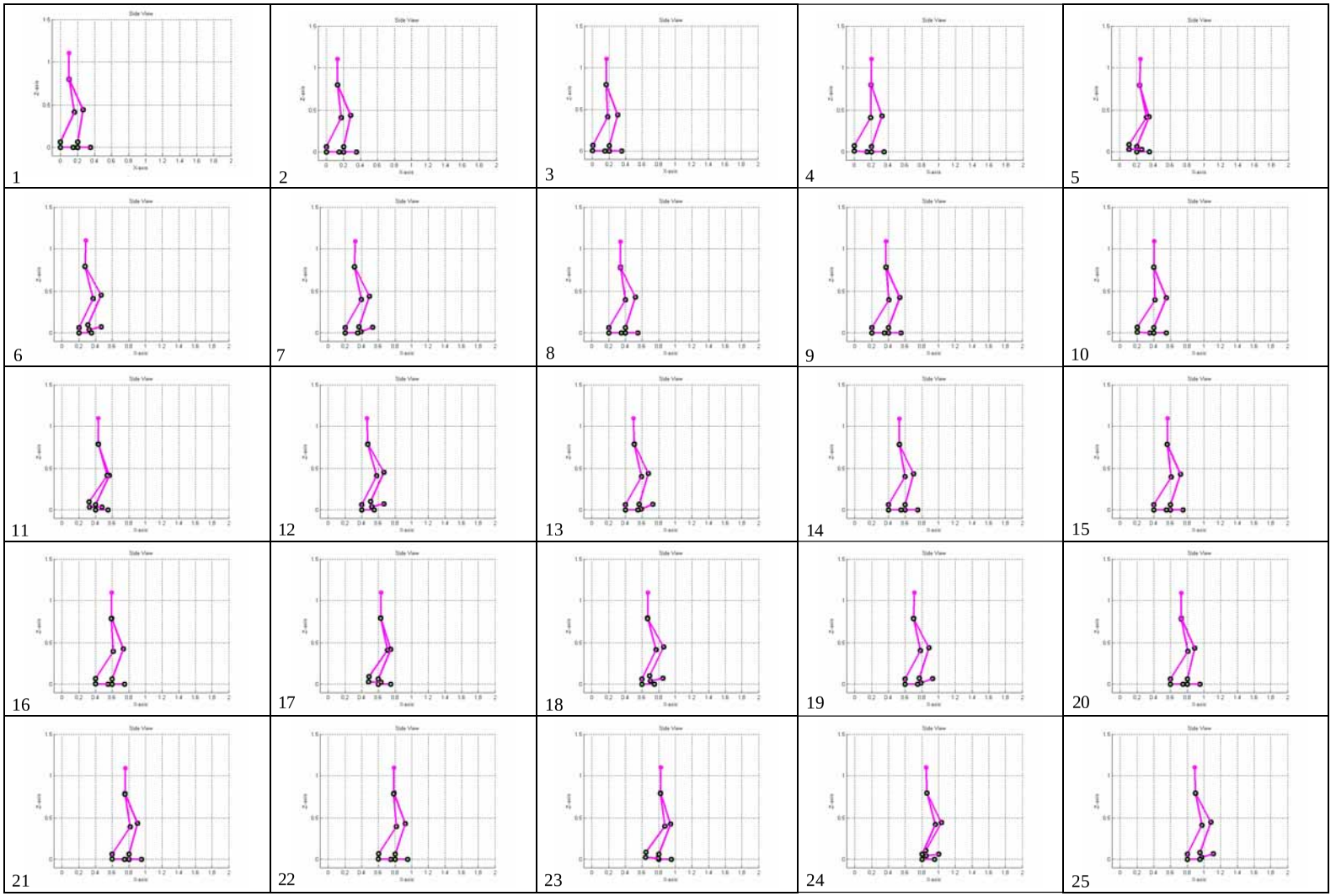

Figure 5.3 Side view of the humanoid walker performing two gait cycles

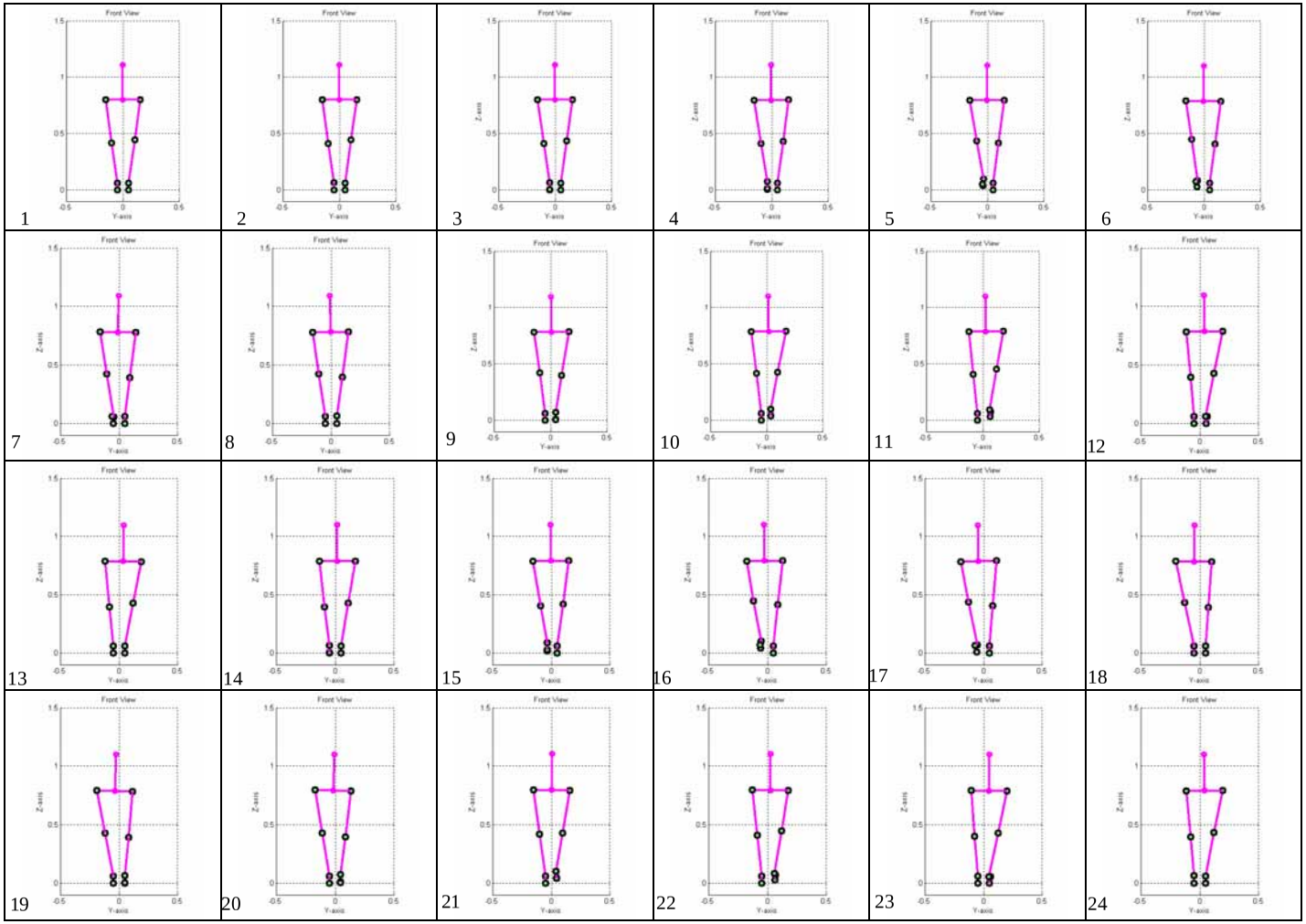

Figure 5.4 Front view of the humanoid walker performing two gait cycles

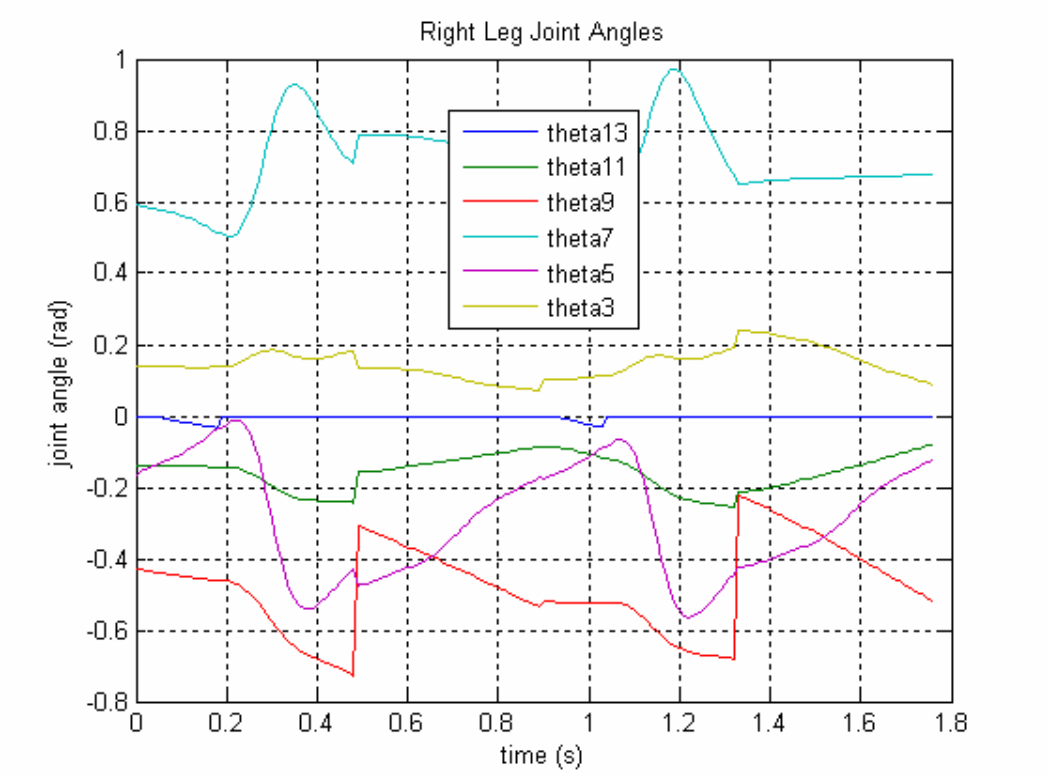

Figure 5.5 Right leg joint angles

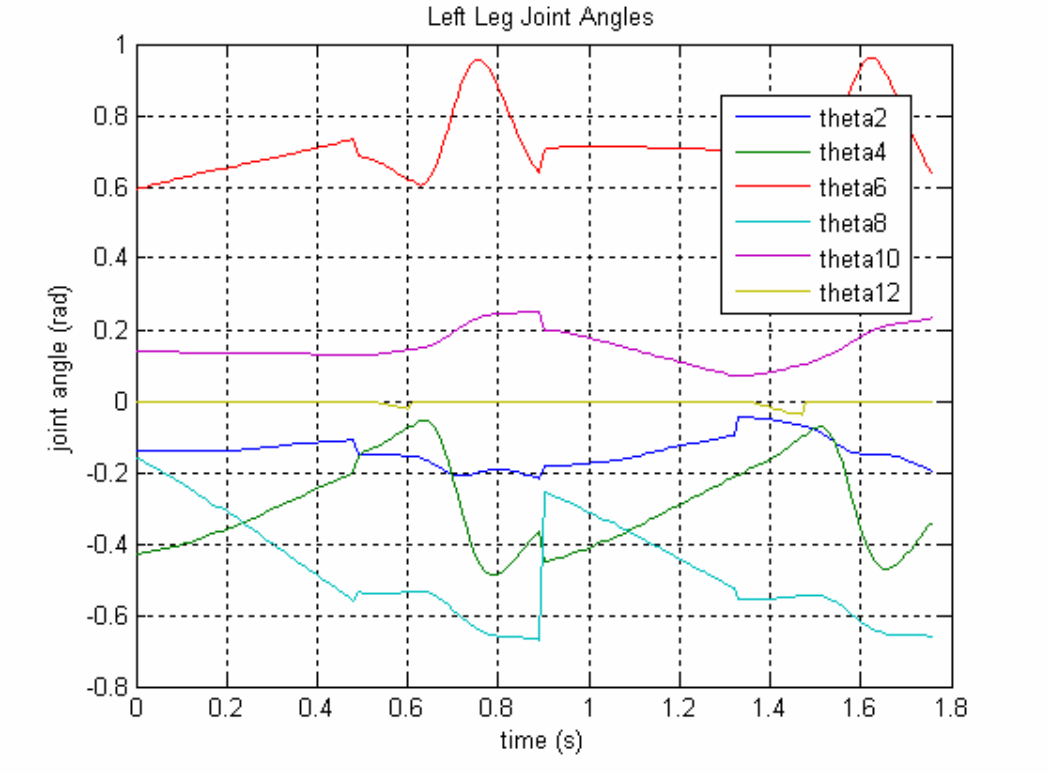

Figure 5.6 Left leg joint angles

The actuating torques necessary to accomplish the desired gait are presented in the figures 5.7 through 5.14. These torques are associated with the second gait cycle because in the first gait cycle, the humanoid model is at rest initially. This makes the starting torques higher. However, in the second gait cycle, the inertial effects are included. Obviously, the joint torques generated in the double support phases are smaller than the single support torques. The reason of this is the sharing of HAT's weight between two legs. In the single support phase, whole load is on one leg and naturally this requires higher actuating torques at the joints of this leg.

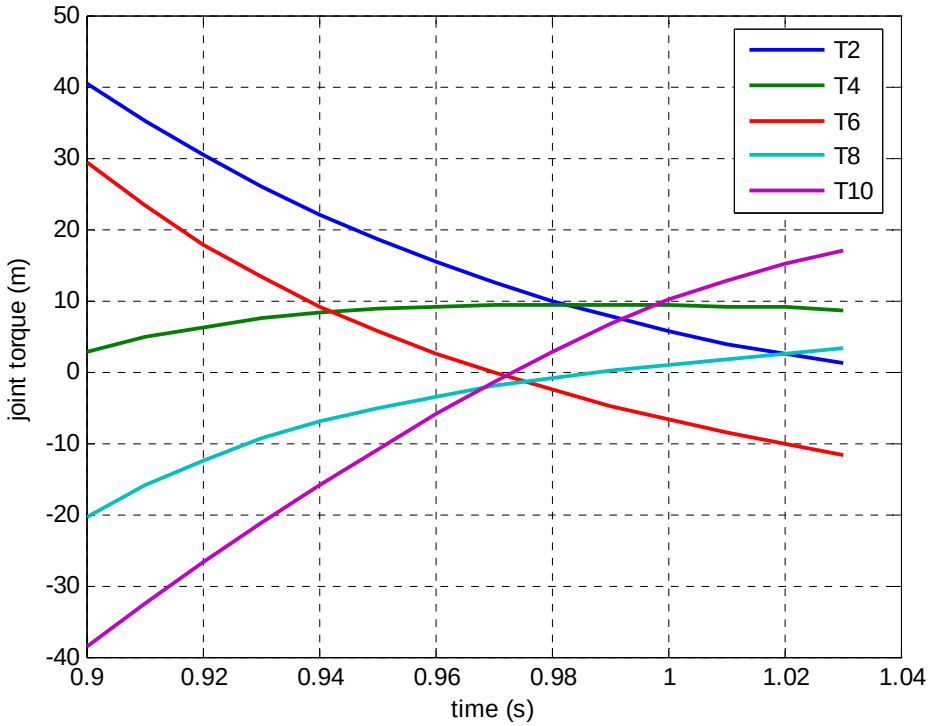

Figure 5.7 Left leg joint torques in the left foot flat double support phase

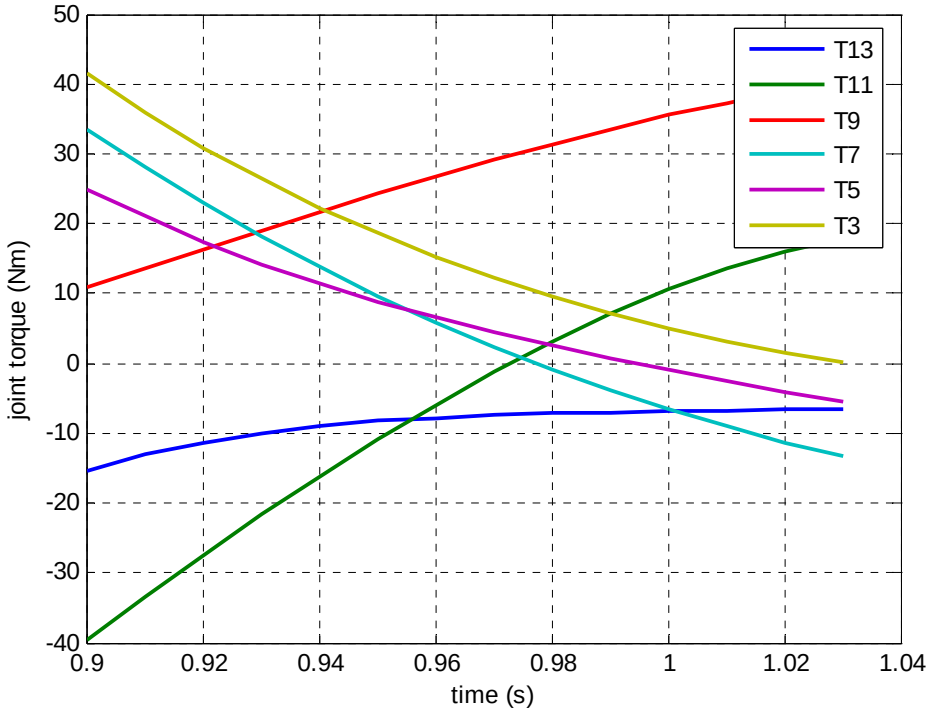

Figure 5.8 Right leg joint torques in the left foot flat double support phase

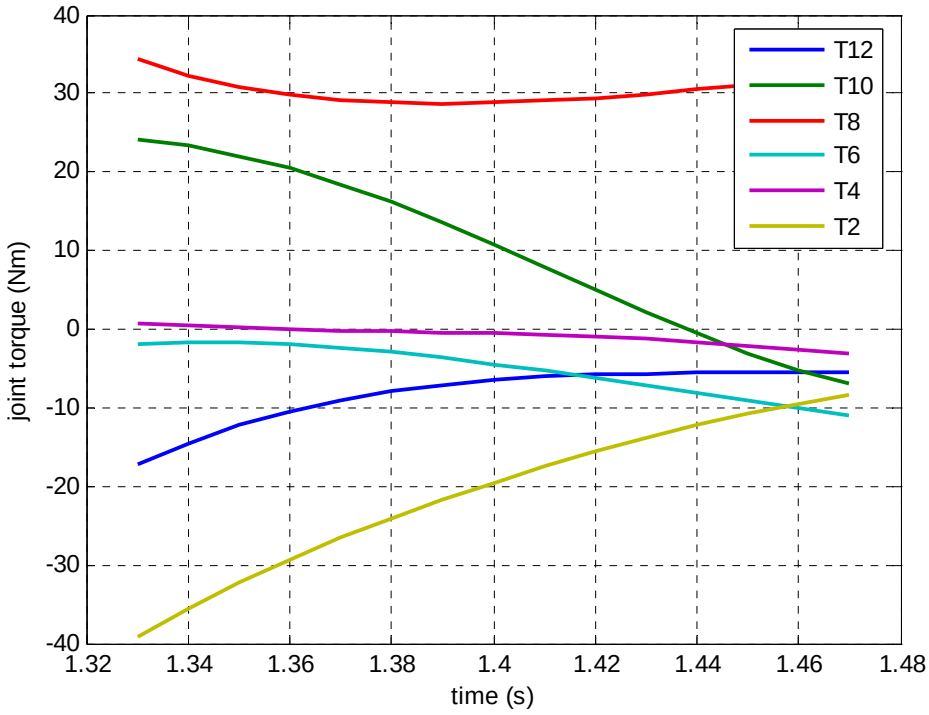

Figure 5.9 Left leg joint torques in the right foot flat double support phase

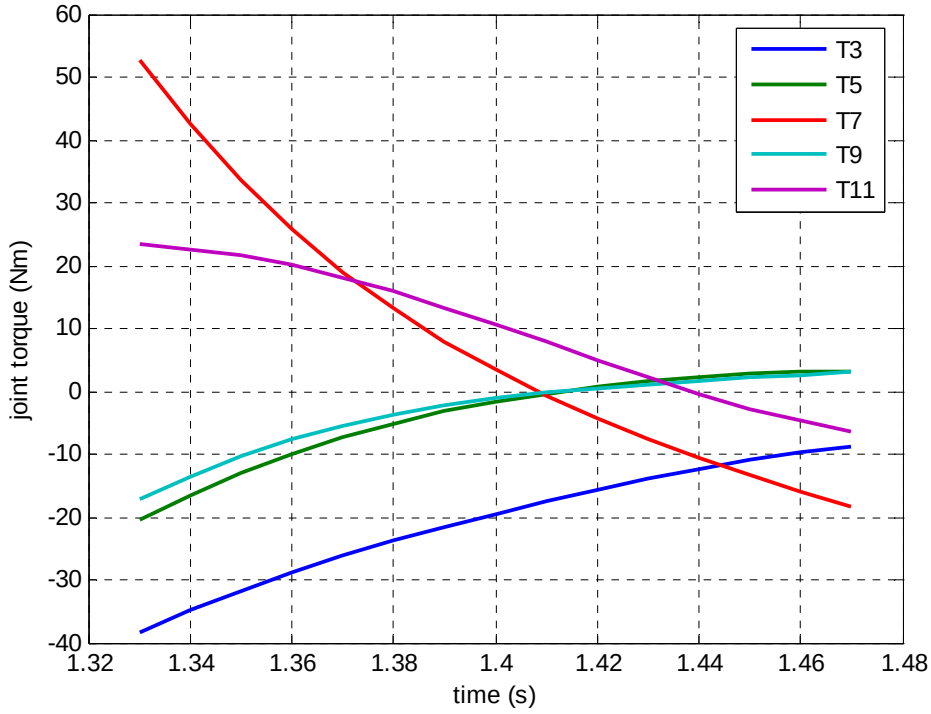

Figure 5.10 Right leg joint torques in the right foot flat double support phase

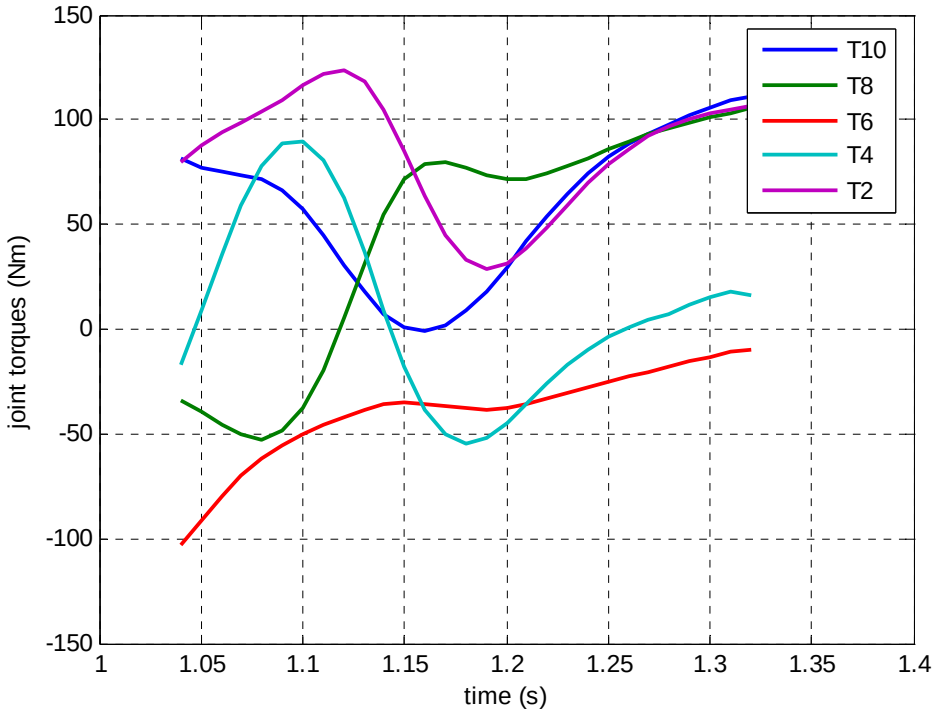

Figure 5.11 Left leg joint torques in the left foot flat single support phase

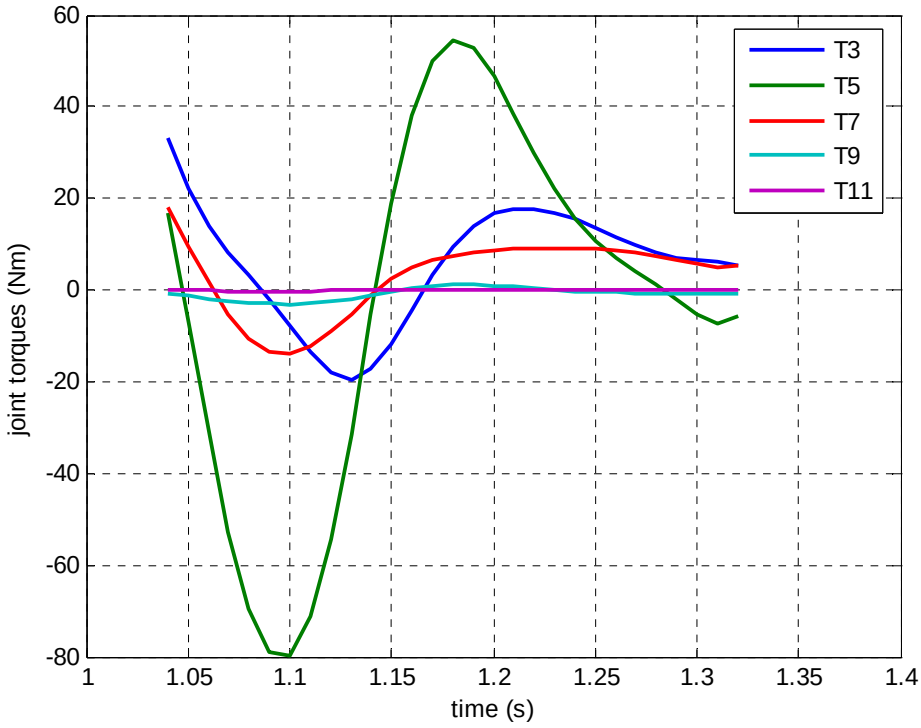

Figure 5.12 Right leg joint torques in the left foot flat single support phase

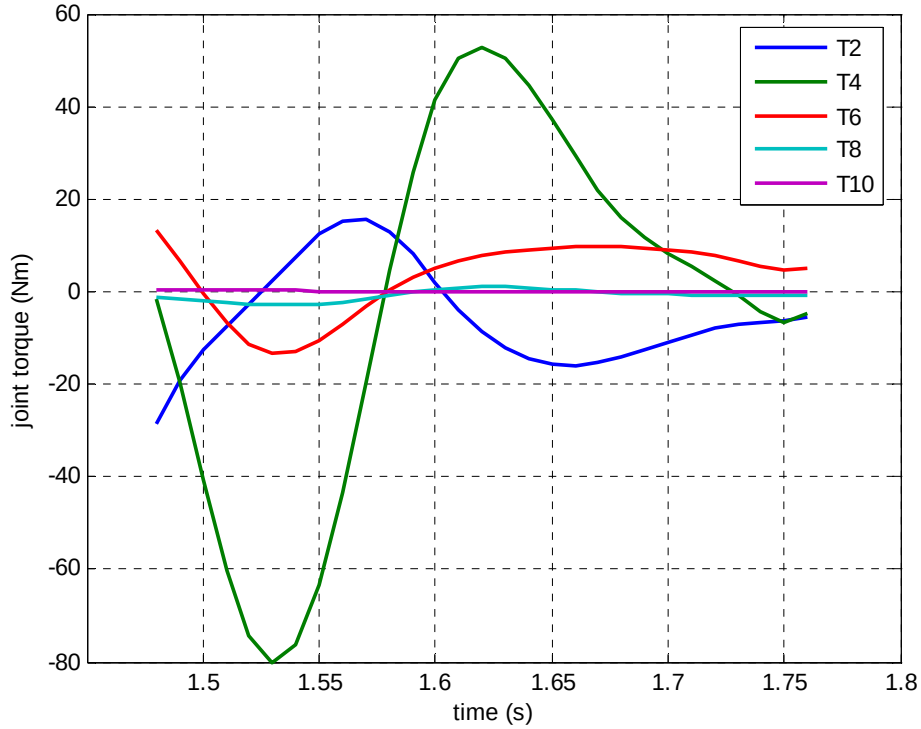

Figure 5.13 Left leg joint torques in the right foot flat single support phase

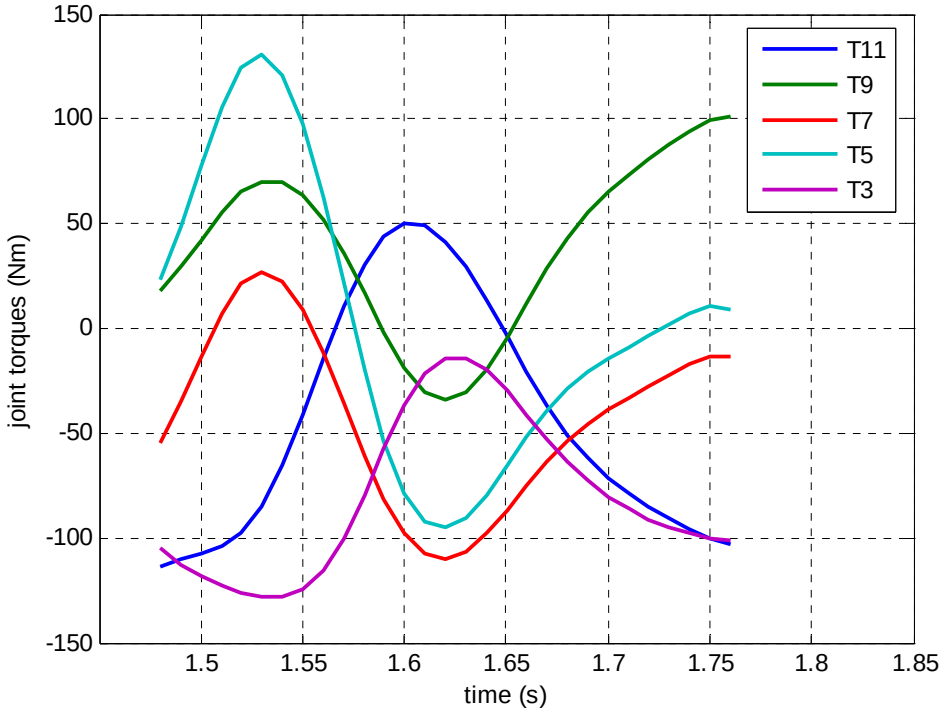

Figure 5.14 Right leg joint torques in the right foot flat single support phase

These torque values are effected by the desired walking speed, the prediction time range and the optimization weighting factors. It is possible to obtain lower actuating torques or smaller tracking errors using different values for these parameters. Adding structural elements like springs and dampers into the models may reduce these actuating torques. Furthermore, specifying the desired paths in such a manner that makes use of the inertial effects for the benefit of humanoid model, lower torques may be required to sustain the gait.

Although, the simulation is capable of producing all reactions which occur at the joints, only the ground reaction forces are presented. For instance, the knee joint or the hip joint of a humanoid walker can easily be designed using the joint reactions in the strength analysis. In figures 5.15 through 5.18, the ground reaction forces of four models in the second gait cycle of simulation are illustrated.

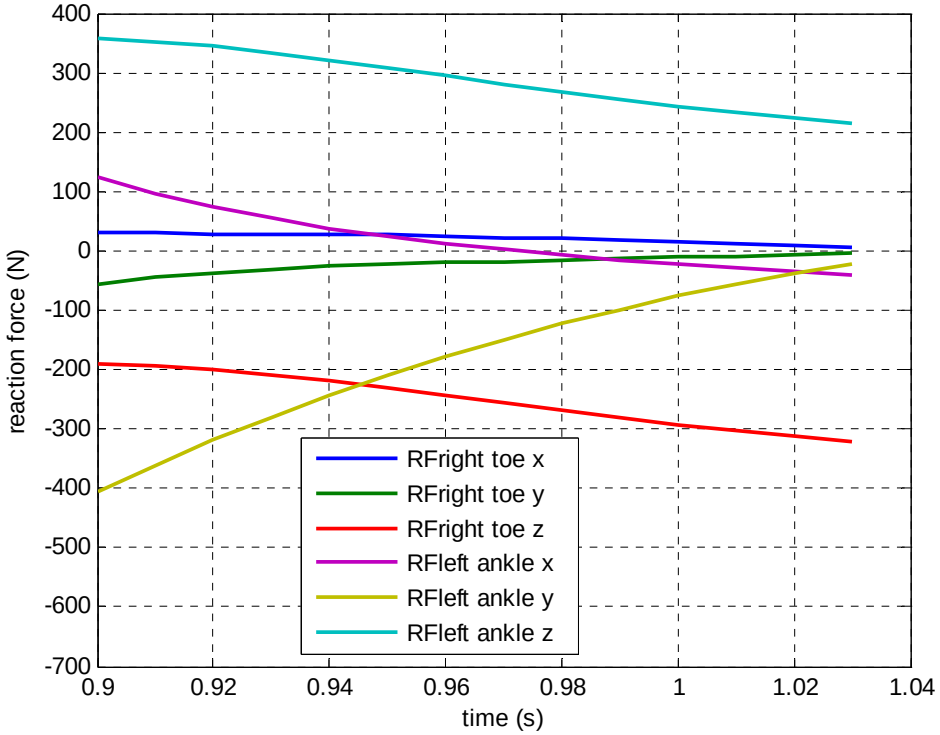

Figure 5.15 Ground reaction forces in the left foot flat double support phase

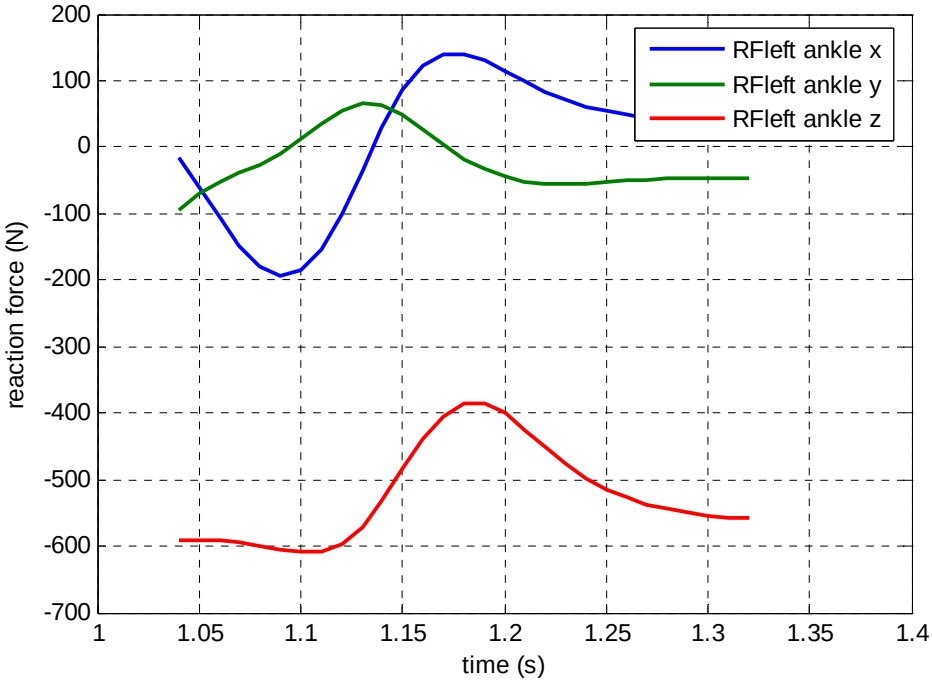

Figure 5.16 Ground reaction forces in the left foot flat single support phase

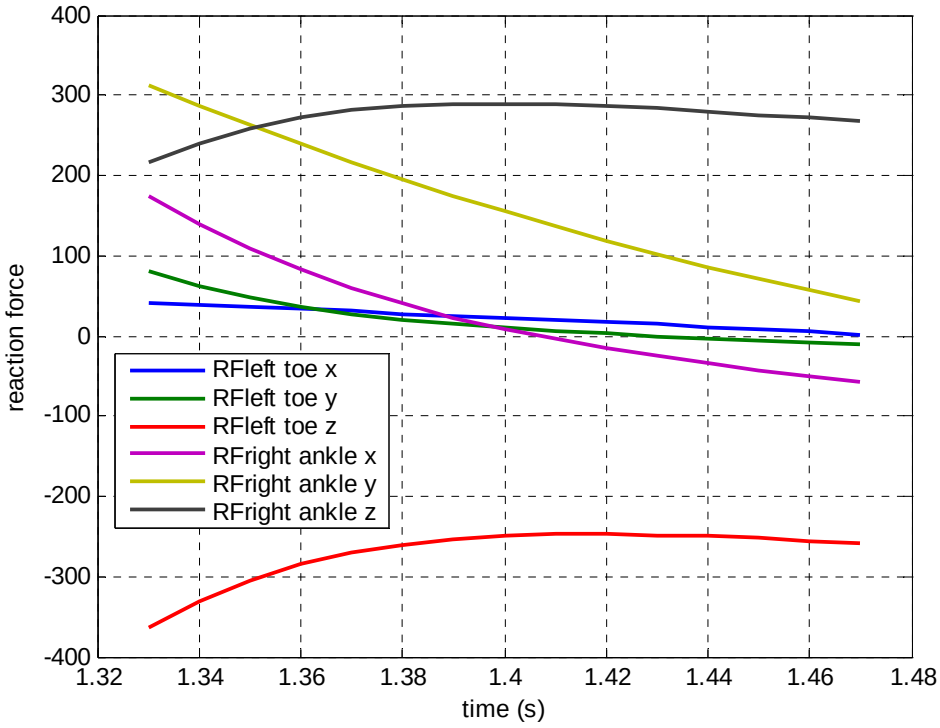

Figure 5.17 Ground reaction forces in the right footflat double support phase

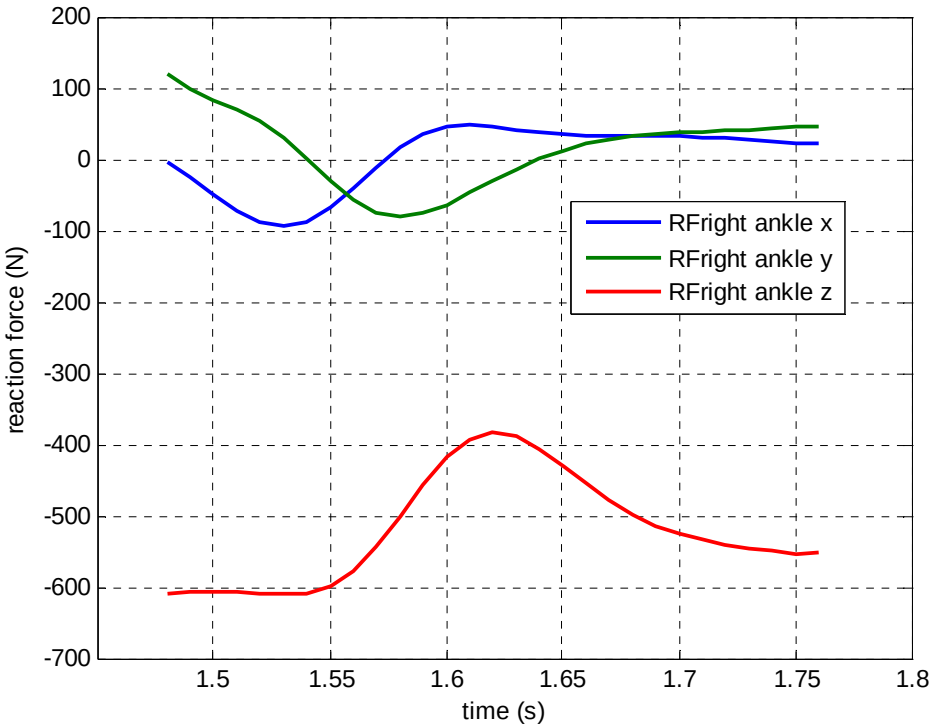

Figure 5.18 Ground reaction forces in the right foot flat single support phase

CHAPTER 6

SUMMARY AND CONCLUSION

In this study, a 3-dimensional computer simulation of a humanoid walking system was developed and the optimal predictive control algorithm was applied on this system. Matlab and Simulink softwares were used for the computations.

Firstly, the physical models were designed with the aim of imitating a humanoid system. Four different models were used in the simulations; two models for the single support phase and two models for the double support phase. These phases were divided into two as the left foot flat single/double support phase and the right foot flat single/double support phase. Each of these models was composed of six rigid bodies. The masses and the lengths of these bodies were determined according to the anthropometric data. Thus, it was tried to obtain a mechanical system which resembles the human being. However, it was well known that a realistic simulation of walking of the human being requires more complicated models. The inertia tensors of the bodies were calculated by the help of Solidworks software. In the double support phase models, the foot was designed including a toe joint which enhances the transition from the double support phase to the single support phase. However, the transition from the single support phase to the double support phase was modeled neglecting the rotation of the landing foot around the heel. Also, the foot sole of the stance leg was assumed to be fixed on the ground. Ten revolute joints in the single support phase models and eleven revolute joints in the double support phase models connected the rigid bodies.

Secondly, the kinematic equations were derived recursively and the dynamic equations of four models were obtained using the Newton – Euler formulation. All the coefficients of the unknown terms in these equations were separated and arranged in the coefficient matrices due to the solution procedure of the required unknowns.

The closed loop control system which was used in the simulations was composed of two parts: The computed torque control part and the optimal predictive control part. Although, the Lagrange formulation is suitable to employ with the computed torque control method, using some simple matrix manipulations, the Newton – Euler equations were converted into the same suitable form for the computed torque control method. Also, in the computed torque algorithm of the double support phases, a torque optimization was realized because of the redundancy. As the second part of the control system, a novel application of optimal and predictive control algorithms on the bipedal locomotion was introduced. By the optimal predictive control algorithm, the humanoid gait was sustained in a stable and re-configurable manner. Different desired humanoid gaits can be achieved by modifying the optimization weighting factors and the prediction time ranges. This property of the present study creates many alternatives for future work.

After that, all the mathematical expressions, solution methods and the control algorithms were imposed in user-defined Matlab functions in m-files. The Simulink model of the system was built and the m-files were incorporated in the subsystems of this simulation model. As the result of many trials, the optimization weighting factors were specified according to the desired gait.

At the end, the simulated humanoid gait of the proposed mechanical system was investigated by the actuating torque curves and other plots. In addition, an animation of the gait was generated.

Although, this study covers quite a lot of problems in the simulation of humanoid gait, in order to improve it the following future works are recommended. These works can also be considered as the suggestions to achieve a gait which is more similar to the gait of a human being.

1. The hip joint assemblies can be made spherical by adding a revolute joint along z-direction to each hip. Thus, the humanoid system attains a cornering ability and the yaw motion of the HAT becomes possible.
2. In the performance measures used in the optimal control parts, some other optimization functions corresponding to the mechanical energy can be

employed in addition to the present optimization functions. Hence, taking the advantage of gravity and inertial effects, an energy efficient locomotion can be accomplished.

3. The desired paths of the pelvis, the left and the right foot can be determined by an additional high level controller. This controller can be designed using neural networks and fuzzy logic. During the gait, this control system can make decisions of correct movements. The knowledge base can be built using the gait analysis data of a human being.
4. The HAT and the pelvis can be connected by an actuated two DOF joint at the waist. Thus, the unbalance can be compensated by appropriate motions of torso. This can also improve the stability and reduce excessive torque values.
5. A further model can be added to the present ones to examine the short interval just after the initial contact of the heel. For this purpose, a foot model which can rotates around the contact point under its heel can be designed.
6. Elasticity can be added to the joints in order to increase walking efficiency.

REFERENCES

1. Shannon, R.E. “Introduction to the Art and Science of Simulation”, Proceedings of the 1998 Winter Simulation Conference
2. Goldstein, J. and Regele, R., “Pro-Robot: Paving the Road for Humanoid Robots”, Technological State of the Art, March 2003, Version 1.4.
3. LaBarca, R.S., “Towards Robotic Bipedal Walking: An Experimental System for Designing Control Software for Dynamically Stable Robots”, Senior Thesis, Carnegie Mellon University, May 1998.
4. Sudarsky L., “Geriatrics: Gait Disorders in the Elderly”, The New England Journal of Medicine, No. 20, 1990, pp. 1441-1445.
5. Molson Medical Informatics Project, “Normal Gait”, http://sprojects.mmi.mcgill.ca/gait/normal/intro.asp (Last modified 15.05.1999).
6. Skelly, M.M. and Chizeck, H.J., “Simulation of Bipedal Walking”, UWEE Technical Report, Number 2001-0001, October 3, 2001.
7. Gilchrist, L.A. and Winter, D.A., “A Multisegment Computer Simulation of Normal Human Gait”, IEEE Transactions on Rehabilitation Engineering, Vol. 5, No. 4, December 1997, pp. 290-299.
8. Wojtyra, M., “Dynamical Analysis of Human Walking”, 15th European ADAMS Users' Conference Technical Papers, Rome, Italy, 2000.
9. Onyshko, S.and Winter, D.A., “A Mathematical Model for the Dynamics of Human Locomotion”, Journal of Biomechanics, Vol.13, 1980, pp.361-8.
10. Ju, M. and Mansour, J.M., “Simulation of the Double Limb Support Phase of Human Gait”, Vol. 110, 1988, pp. 223–229.
11. Pandy, M.G. and Berme, N., “A Numerical Method for Simulating the Dynamics of Human Walking”, Journal of Biomechanics, Vol. 21, No. 12, 1988, pp. 1043–1051.

12. Latham II., P.W., "A Simulation Study of Bipedal Walking Robots: Modeling, Walking Algorithms, and Neural Network Control", Doctoral Thesis, University of New Hampshire, 1992.

13. Günther, M. and Ruder, H., "Synthesis of Two-Dimensional Human Walking: A Test of the λ – Model", Biological Cybernetics, No.89, pp.89-106, 2003.

14. Anderson, F.C. and Pandy, M.G., "Three-Dimensional Computer Simulation of Gait",

15. Hardt, M. and Von Stryk, O., "Dynamic Modeling in the Simulation, Optimization, and Control of Bipedal and Quadrupedal Robots", Math. Mech. 83, No. 10, 2003, pp.648 – 662.

16. Granata, K.P., Brogan, D.C., Sheth, P.N., "Stable Forward Dynamic Simulation of Bipedal Gait Using Space-Time Analysis", IV World Congress of Biomechanics, 2002.

17. Denk, J. and Schmidt, G., "Synthesis of a Walking Primitive Database for a Humanoid Robot using Optimal Control Techniques", Proceedings of IEEE-RAS International Conference on Humanoid Robots (HUMANOIDS2001) Tokyo, Japan, November 2001, pp. 319–326.

18. Nicholls, E., "Bipedal Dynamic Walking in Robotics", Honours Thesis, The University of Western Australia, October 26, 1998

19. Potkonjak, V. and Vukobratovic, M., "A Generalized Approach to Modeling Dynamics of Human and Humanoid Motion", International Journal of Humanoid Robotics, Vol. 2, No. 1, 2005, pp. 21–45.

20. Kato, J., et al., "Pneumatically Powered Artificial Legs Walking Automatically Under Various Circumstances", In Proc. of 4th Int. Symposium in External Control of Human Extremities, 1972, pp.458-470.

21. Hirai, K., Hirose, M., Haikawa, Y., Takenaka, T., "The Development of Honda Humanoid Robot", Proceedings of the 1998 IEEE International Conference on Robotics & Automation, Leuven, Belgium, May 1998

22. Hirukawa, H., Kanehiro, F., Kajita, S., "Experimental Evaluation of the Dynamic Simulation of Biped Walking of Humanoid Robots", Proceedings of the 2003 IEEE ICRA, Taipei, Taiwan, September 14-19, 2003, pp. 3105-3110.

23. Pratt, J.E. and Pratt, G.A., "Exploiting Natural Dynamics in the Control of a Planar Bipedal Walking Robot", Proceedings of the Thirty-Sixth Annual Allerton Conference on Communication, Control, and Computing, Monticello, Illinois, September 1998.

24. Nishiwakiz, K. and Kagamiy, S., "Toe Joints that Enhance Bipedal and Fullbody Motion of Humanoid Robots", Proceedings of the 2002 IEEE ICRA, Washington DC, May, 2002.

25. Borelli, G. A. 1680. "De Motu Animalium" (English) Translated by P. Maquet, Springer-Verlag, Berlin, Heidelberg, 1989.

26. Vukobratovic, M. and Juricic, D., "Contributions to the synthesis of biped gait", IEEE Transactions on Biomedical Engineering, BME-16, 1969,pp.1-6.

27. Goswami, A., "Postural Stability of Biped Robots and the Foot-Rotation Indicator (FRI) Point", International Journal of Robotics Research, 1999, 18(6): 523-533.

28. Özgören, M.K., "Topological Analysis of 6-joint Serial Manipulators and Their Inverse Kinematic Solutions", Mechanisms and Machine Theory, 37, 2002, pp.511-547.

29. Human Anthropometric Data, http://www.personal.usyd.edu.au/~mslee/ESSwww/lee/zygal/glossary/anthropometry/winter.html, (Last modified 02.04.2003)

30. The Mathworks Inc., "Matlab Simulink User's Guide", The Mathworks Inc., 1999.

APPENDIX A

COEFFICIENT MATRIX OF THE RIGHT FOOT FLAT SINGLE SUPPORT PHASE

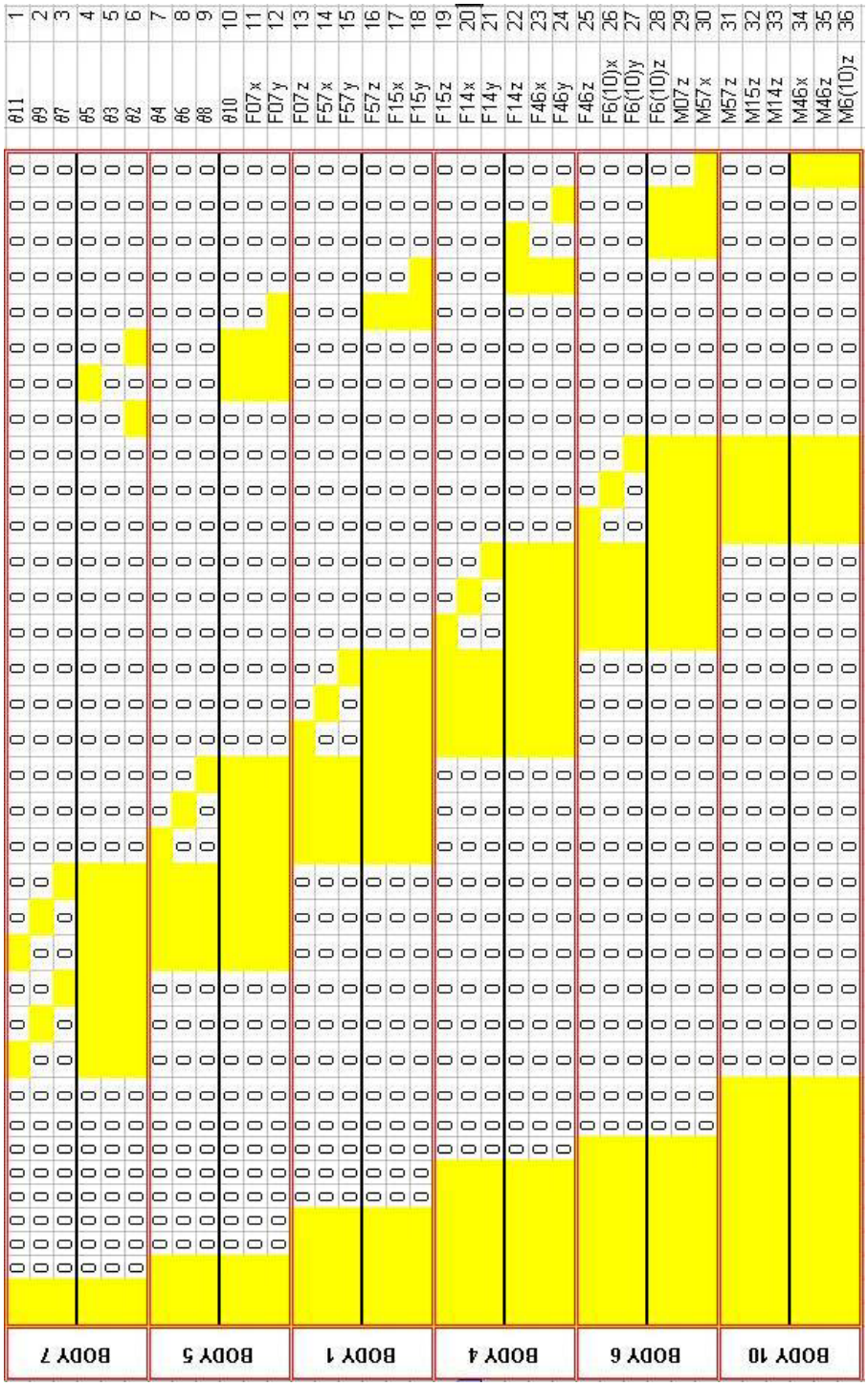

APPENDIX B

COEFFICIENT MATRIX OF THE RIGHT FOOT FLAT SINGLE SUPPORT PHASE (AFTER ROW SHIFTING)

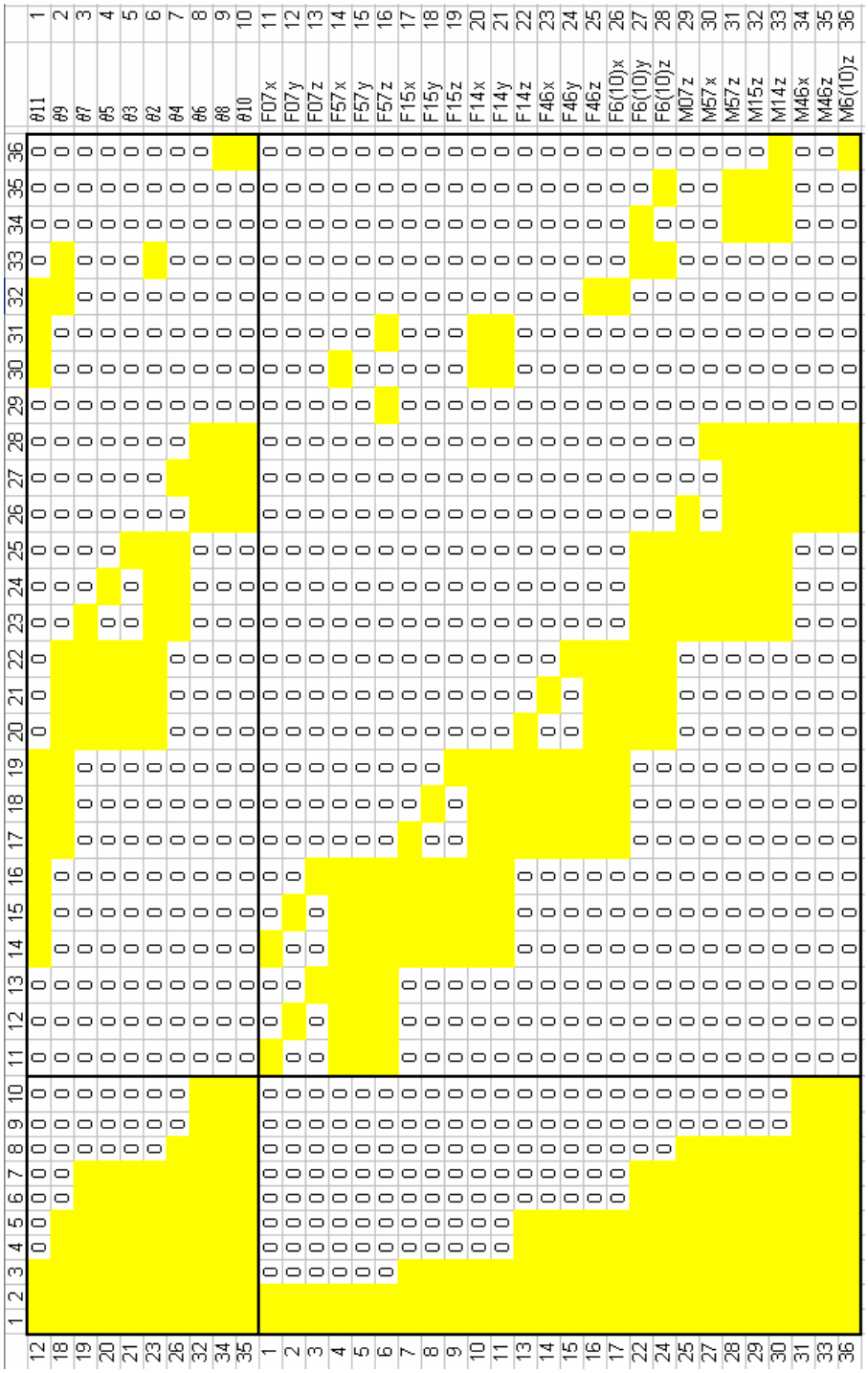

APPENDIX C

COEFFICIENT MATRIX OF THE LEFT FOOT FLAT DOUBLE SUPPORT PHASE